

**LIGHTWEIGHT STRUCTURAL DESIGN OF A UAV  
WING THROUGH THE USE OF CORELESS  
COMPOSITE MATERIALS EMPLOYING NOVEL  
CONSTRUCTION TECHNIQUES**

by

**Neill N. Moore**

A dissertation submitted in fulfilment of the  
academic requirements for the degree

**Master of Science**

in Engineering

School of Mechanical Engineering

College of Agriculture, Engineering and Science

University of Kwazulu-Natal

Pietermaritzburg

South Africa

October 2017

# Preface

The research contained in this thesis was completed by the candidate while based in the Discipline of Mechanical Engineering, School of Agricultural, Earth and Environmental Sciences of the College of Agriculture, Engineering and Science, University of KwaZulu-Natal, Pietermaritzburg South Africa. The research was financially supported by the CSIR Defence Peace, Safety and Security Aeronautics Systems Competency.

The contents of this work have not been submitted in any form to another university and, except where the work of others is acknowledged in the text, the results reported are due to investigations by the candidate.

---

Signed: Dr. Clinton Bemont

Date:

# Declaration 1: Plagiarism

I, Neall Neville Moore, declare that:

- (i) the research reported in this dissertation, except where otherwise indicated or acknowledged, is my original work;
- (ii) this dissertation has not been submitted in full or in part for any degree or examination to any other university;
- (iii) this dissertation does not contain other persons' data, pictures, graphs or other information, unless specifically acknowledged as being sourced from other persons;
- (iv) this dissertation does not contain other persons' writing, unless specifically acknowledged as being sourced from other researchers. Where other written sources have been quoted, then:
  - a) their words have been re-written but the general information attributed to them has been referenced;
  - b) where their exact words have been used, their writing has been placed inside quotation marks, and referenced;
- (v) where I have used material for which publications followed, I have indicated in detail my role in the work;
- (vi) this dissertation is primarily a collection of material, prepared by myself, published as journal articles or presented as a poster and oral presentations at conferences. In some cases, additional material has been included;
- (vii) this dissertation does not contain text, graphics or tables copied and pasted from the Internet, unless specifically acknowledged, and the source being detailed in the dissertation and in the References sections.

---

Signed: Neall Neville Moore

Date:

## Declaration 2: Publications

My role in each paper and presentation is indicated. The \* indicates corresponding author.

1. Moore, N. N,\* Bemont C.P. and Thomson V.A. Lightweight structural design of a UAV wing through the use of coreless composite materials. Article submitted for review to *Aerospace Science and Technology*, Elsevier.

I wrote the article based on the work that I did for this MSc thesis, and was supervised by Dr Bemont and Mr Thomson.

---

Signed: Neall Neville Moore

Date:

## Abstract

A new structural layout was designed for an existing UAV wing with the aims of lightening the wing by eliminating the use of cored composite construction and reducing the manufacturing time of the wing by making use of waterjet-cut internal frames while satisfying strength and stiffness requirements. Two layouts, a traditional metal wing layout and a tri-directional rib lattice layout, were selected for consideration based on the literature surveyed. In order to present a valid comparison with the previous wing design the same composite materials were used in the design of the new wing layout and material tests were performed according to ASTM testing standards to obtain the mechanical properties of these materials. Load cases for the wing in flight were calculated according to FAR-23 standards and the loads on the wing were found using XFLR5 vortex-lattice methods. An empirical, spreadsheet-based initial sizing tool was developed to obtain initial layouts for an iterative FEA-based optimisation process that employed the SolidWorks Simulation Premium software package and made use of the Tsai-Wu composite material failure criterion and empirical buckling equations. The iterative optimisation resulted in the traditional metal wing layout being selected and predicted a weight saving of 14% over the original wing design. A full scale prototype wing was constructed in the CSIR UAS Laboratory using wet layup techniques and laser cut internal frames as it was found that the waterjet cutting of thin composite frames was not practical as a result of the high working pressure of the waterjet cutter. The prototype wing showed an actual weight saving of 14% but took considerably longer to manufacture due to the necessity of constructing specialised jigs to aid in the bonding and alignment of the internal frames. The prototype wing was tested using a custom set-up whiffle tree rig up to its maximum limit load of 4.9 g and showed an average of 4% error between measured and predicted deflections thereby validating the FEA models. It was concluded that a UAV wing can be significantly lightened through a coreless structural design, but at the expense of an increase in construction time. It is hoped that this study will contribute towards a changed design philosophy in an industry where cored construction is the norm. It is recommended that the methods developed during this project be applied to the rest of the aircraft components in order to obtain a lighter overall structure.

# Acknowledgements

I would like to thank the following people for their contributions and support:

- My supervisor, Dr Clinton Bemont, from the University of Kwazulu-Natal. I am extremely grateful to have had the privilege of working with you and appreciate all the time and effort that you invested throughout the duration of my project. Your expert advice and guidance have helped me immeasurably.
- My co-supervisor, Mr Vaughan Thomson, from Graven Designs. Thank you for our meaningful conversations, your expert inputs and especially your help and advice with my FEA models and constraints.
- Mr John Monk, from the CSIR Aeronautic Systems Competency. Thank you for your generous financial support of this project, for the use of the UAS Lab facilities and equipment and for entrusting me with both.
- Mr Chris McDuling and Mr Erich Guldenpfennig from the CSIR Materials Science and Manufacturing unit. Thank you for teaching and mentoring me through the materials testing process.
- Mrs Laura Moore, my wife. Thank you for your patience, love and support that you have given so unselfishly, and for the time that you spent helping me build my material testing coupons and test wing. Your sore feet have paid off.
- Mr Albert Dall and Mrs Anita Dall, my parents. Thank you for keeping me motivated, encouraging me, praying for me, and helping me with my testing.
- All those that have helped me with various stages of constructing my test piece, Mr Kgaugelo Mabeko, Mr Matthew Titus, and Mrs Katherine Barker: your help was much appreciated.
- My Father in heaven: without You, none of this is possible.

# Contents

Preface .....	ii
Declaration 1: Plagiarism.....	ii
Declaration 2: Publications .....	iii
Abstract.....	iv
Acknowledgements .....	v
Contents .....	vi
List of Figures .....	xi
List of Tables .....	xv
Nomenclature.....	xvi
1. Introduction and Dissertation Overview .....	1
1.1. Introduction .....	1
1.1.1. The Kwadira UAV .....	1
1.1.2. Current Wing Structural Design.....	1
1.1.3. Problems Arising From Cored FRP Construction.....	3
1.2. Research Hypothesis .....	3
1.3. Research Objectives .....	3
1.4. Research Methodology and Scope.....	3
1.5. Research Significance and Novelty.....	4
1.6. Dissertation Overview.....	4
2. Literature Review and Theory.....	5
2.1. Literature Review.....	5
2.1.1. Aircraft Flight Loads and Flight Envelope .....	5
2.1.2. Wing Loading / Lift Distribution .....	5
2.1.3. Wing Structural Layout Schemes.....	5
2.1.4. FRP Design and Construction.....	6
2.1.5. FEA of FRP Materials .....	7
2.1.6. Static Wing Testing .....	7
2.1.7. Summary of Literature Reviewed .....	8
2.2. Theory: Wing Loading / Lift Distribution.....	9
2.2.1. Maximum Load Cases and Flight Envelope .....	9
2.2.2. XFRL5 and Vortex Lattice Methods .....	9
2.2.3. Span-wise Lift Distribution.....	9
2.2.4. Chord-Wise Lift Distribution.....	9
2.3. Theory: FRPs.....	10
2.3.1. A Brief Description of Composites .....	10

2.3.2.	Laminate Shorthand.....	10
2.3.3.	Classical Laminate Theory .....	10
2.3.4.	Failure Theories .....	11
2.3.5.	Grid Structures .....	12
2.4.	Theory: Aircraft Wing Structural Design.....	12
2.4.1.	Popular FRP Structural Layouts.....	12
2.4.2.	Fully Monocoque Layout with Stressed Skin .....	12
2.4.3.	Fully Monocoque Layout with Isogrid Lattice Structures .....	12
2.4.4.	Semi-Monocoque Layout with Cored Skin .....	12
2.4.5.	Semi-Monocoque Layout with Stiffened Skin.....	12
2.4.6.	Buckling.....	13
2.5.	Theory: FRP Construction.....	14
2.5.1.	Construction Techniques .....	14
2.5.2.	Wet Layup and Vacuum Bagging .....	14
2.5.3.	CNC Waterjet Cutting .....	14
2.6.	Theory: FEA of Composite Materials .....	15
2.6.1.	SolidWorks Simulation Premium.....	15
2.6.2.	Shell Elements.....	15
2.6.3.	Ply/Laminate Properties.....	15
2.6.4.	Surface Contact .....	15
2.7.	Theory: Wing Structural Testing .....	16
2.7.1.	Whiffle Tree Testing .....	16
2.7.2.	Sandbag Testing .....	16
2.8.	Chapter Summary .....	16
3.	Material Properties.....	17
3.1.	Selected Materials .....	17
3.2.	Material Testing.....	17
3.2.1.	Previous Tests .....	17
3.2.2.	Tests Performed for This Research .....	17
3.2.3.	Testing Methodology.....	18
3.2.4.	Limitations of Testing Methodology and Proposed Solutions .....	22
3.3.	Properties of Selected Materials .....	22
3.3.1.	86GSM Glass Fibre Plain Weave with Ampreg 21 Epoxy Resin .....	22
3.3.2.	106GSM Glass Fibre Plain Weave with Ampreg 21 Epoxy Resin .....	23
3.3.3.	200GSM Carbon Fibre Twill Weave with Ampreg 21 Epoxy Resin .....	23

3.3.4.	343GSM Carbon UD Tape with Ampreg 21 Epoxy Resin.....	24
3.3.5.	Ampreg 21 Epoxy Resin.....	24
3.3.6.	DC Wort NEMA G11 Prepared Glass Fibre Sheet .....	24
3.4.	Chapter Summary .....	25
4.	Loads, Structural Layout and Initial Sizing Model.....	26
4.1.	Loads on the Kwadira Wing.....	26
4.1.1.	V-n Diagram and Selected Load Cases .....	26
4.1.2.	XFLR5 Analyses and Lift Distribution .....	28
4.1.3.	Tail Boom Loads.....	31
4.1.4.	Safety and Build Factors, Ultimate Loads .....	31
4.1.5.	Shear Force, Bending Moment and Torque Diagrams .....	32
4.2.	Proposed New Structural Layout.....	35
4.2.1.	Description of Structural Components .....	35
4.2.2.	Proposed New Structural Layouts.....	35
4.2.3.	Structural Component Interactions.....	37
4.3.	Initial Sizing Model.....	38
4.3.1.	Spar Caps.....	38
4.3.2.	Shear Flow .....	39
4.3.3.	Wing Skins.....	41
4.3.4.	Shear Webs .....	42
4.3.5.	Ribs.....	43
4.3.6.	Shear Pins .....	43
4.3.7.	Initial Predicted Mass Reduction vs Current Wing.....	43
4.4.	Chapter Summary .....	43
5.	FEA Analysis and Optimisation.....	44
5.1.	SolidWorks CAD Model.....	44
5.1.1.	Surface Modelling .....	44
5.1.2.	Split Lines .....	45
5.2.	Material Property Input .....	45
5.3.	Laminate Property Assignment.....	45
5.3.1.	Spar Caps.....	45
5.3.2.	Wing Skins.....	46
5.3.3.	Webs and Ribs.....	46
5.4.	Loads and Boundary Conditions.....	47
5.4.1.	Load Cases.....	47

5.4.2.	Boundary Conditions.....	48
5.5.	Shell Mesh, Component Contact and Solver .....	50
5.5.1.	2-D Shell Meshing.....	50
5.5.2.	Contact Entities .....	51
5.5.3.	Solver Selection .....	51
5.5.4.	Mesh Convergence Study .....	51
5.6.	FEA Results.....	52
5.6.1.	Tsai-Wu Failure Criterion and Safety Factor.....	52
5.6.2.	Strains and Displacements .....	53
5.6.3.	Inter-Laminate Shear Stresses.....	54
5.7.	Iterative Layout Optimisation.....	55
5.7.1.	Iteration Procedure .....	55
5.7.2.	Chosen New Structural Layout .....	55
5.8.	Iterative Layup Optimisation.....	55
5.8.1.	Iteration Procedure .....	55
5.8.2.	Buckling Considerations.....	56
5.8.3.	Final Layups.....	56
5.8.4.	Final FEA Results .....	57
5.8.5.	Weight Estimation.....	63
5.9.	Chapter Summary .....	63
6.	Wing Manufacture.....	66
6.1.	Kwadira Wing Moulds .....	66
6.1.1.	Mould Preparation.....	66
6.1.2.	Release Agent .....	66
6.2.	Wing Skin and Spar Cap Layup.....	66
6.2.1.	Material Preparation .....	66
6.2.2.	Layup and Vacuum Bagging.....	67
6.2.3.	Leading/Trailing Edge Trimming and Lip Layup .....	68
6.3.	Web and Rib Construction .....	69
6.3.1.	GFRP/CFRP Sheets.....	69
6.3.2.	Laser / CNC Router Cutting.....	69
6.3.3.	Web and Rib Lattice Assembly.....	70
6.3.4.	Cleating of Lattice to Top Skin .....	71
6.4.	Wing Closing and De-Moulding.....	72
6.4.1.	Joining Lines .....	72

6.4.2.	De-Moulding.....	73
6.4.3.	Hardpoints.....	75
6.4.4.	Final Weight.....	75
6.5.	Chapter Summary .....	76
7.	Experimental Setup, Testing and Results.....	77
7.1.	Experimental Setup .....	77
7.1.1.	CSIR Wing Structural Test Rig.....	77
7.1.2.	Whiffle Tree Loads and Set Up.....	78
7.1.3.	Test Rig and Wing Setup.....	79
7.2.	Test Procedure and Results.....	82
7.3.	Chapter Summary .....	84
8.	Discussion .....	85
8.1.	Discussion of Literature Review.....	85
8.2.	Discussion of Material Properties and Testing .....	85
8.3.	Discussion of Analytical Wing Loadings, Structural Layouts and Initial Sizing Model.....	86
8.4.	Discussion of the FEA Models .....	86
8.5.	Discussion of the Construction and Testing .....	87
8.6.	Validation of FEA with Test Results .....	87
9.	Conclusions and Recommendations .....	89
9.1.	Summary of Objectives .....	89
9.2.	Synopsis of Research Conducted and Findings .....	89
9.3.	Hypothesis .....	90
9.4.	Recommendations for Future Work.....	90
	References.....	91
	Appendix A – Kwadira Wing Dimensions .....	94
	Appendix B – Layout and Layup Iteration Results .....	95
	Appendix C – Journal Paper Submitted For Review.....	102

# List of Figures

Figure 1 - A SolidWorks CAD rendering of the Kwadira UAV.....	1
Figure 2 - A SolidWorks rendering showing an internal view of the current Kwadira wing design with structural components numbered.....	2
Figure 3 - Buckling coefficient $K_c$ for a flat plate subjected to compressive loading (Niu, Airframe Stress Analysis And Sizing, 1997).....	13
Figure 4 - Composite test coupons with strain gauges and lead wires attached.....	18
Figure 5 - Failure of a $45^\circ \times 45^\circ$ coupon in CSIR MSM's Instron tensile testing machine.....	19
Figure 6 - Plot of laminated 86GSM $0^\circ \times 90^\circ$ GFRP tensile stress versus longitudinal strain.....	20
Figure 7 - Plot of laminated 86GSM $45^\circ \times 45^\circ$ GFRP shear stress versus longitudinal strain.....	20
Figure 8 - Plot of laminated 106GSM $0^\circ \times 90^\circ$ GFRP tensile stress versus longitudinal strain.....	21
Figure 9 - Plot of laminated 106GSM $45^\circ \times 45^\circ$ GFRP shear stress versus longitudinal strain.....	21
Figure 10 - V-n Diagram for the Kwadira UAV.....	27
Figure 11 - SD7062 and SD7062_Flap as plotted by XFLR5.....	28
Figure 12 - Vortex-Lattice panels as plotted by XFLR5.....	29
Figure 13 – XFLR5 plots of $C_l-F_z$ and $C_l$ -Alpha for the Kwadira wing.....	29
Figure 14 – XFLR5 plot of $c_l$ -Wingspan for the Kwadira wing at $15^\circ$ angle of attack for the 4.9 g, 40 m/s load case.....	30
Figure 15- Shear force diagram of the Kwadira UAV for the Point B load case (40 m/s, 4.9 g).....	33
Figure 16- Bending moment diagram of the Kwadira UAV for the Point B load case (40 m/s, 4.9 g)	33
Figure 17- Torque diagram of the Kwadira UAV for the Point B load case (40 m/s, 4.9 g).....	33
Figure 18- Shear force diagram of the Kwadira UAV for the Point D load case (50 m/s, -1.75 g).....	34
Figure 19- Bending moment diagram of the Kwadira UAV for the Point D load case (50 m/s, -1.75 g).....	34
Figure 20- Torque diagram of the Kwadira UAV for the Point D load case (50 m/s, -1.75 g).....	34
Figure 21 - The first proposed structural layout consisting of a traditional metal wing layout with a rear web and several chord-wise ribs. Colour key: Spar caps – black, front shear webs – purple, rear shear web – orange, chord-wise ribs – green.....	36
Figure 22 - The second proposed structural layout consisting of an angle-grid rib lattice inside the wing.....	37
Figure 23 - Diagram showing the closed cells 12 and 1234 and shear flows $q_1$ and $q_2$ that were used to find the shear flow in the wing components.....	40
Figure 24 - The locations at which the wing skins' shear flow was calculated.....	41
Figure 25 - SolidWorks image showing how the lengths and areas of the shear flow sections were obtained.....	41
Figure 26 - SolidWorks CAD model showing the surface modelling of the Kwadira wing skins and internal structure. Note the separate spar cap sections (highlighted in blue).....	44

Figure 27 - SolidWorks Simulation image showing the orientation of the Carbon unidirectional tape fibres in the top spar caps. ....	45
Figure 28 - SolidWorks Simulation image showing the orientation of the 45° ply in the wing skin laminate. ....	46
Figure 29 - SolidWorks Simulation image showing the orientation of the 45 plies in the internal rib laminates. ....	46
Figure 30 - SolidWorks Simulation image showing the distributed pressure loading applied to the wing surfaces to simulate the lift generated by the wing skins. ....	47
Figure 31 - SolidWorks Simulation image showing the application of the torsional loads to the outboard wing ribs. ....	47
Figure 32 - SolidWorks Simulation image showing the whiffle tree loads distributed over their surfaces. ....	48
Figure 33- SolidWorks Simulation image showing the simple fuselage fixtures that were used for the optimisation analyses. ....	49
Figure 34 - SolidWorks Simulation image showing the simulated fuselage fixtures that were used for the whiffle tree and final analyses. ....	49
Figure 35- SolidWorks Simulation image showing the mesh generated for the analyses and mesh refinement performed around critical areas of interest. ....	50
Figure 36 - SolidWorks Simulation image showing the lines/areas of bonded (red) and non-penetrating (purple) contact within the model. ....	51
Figure 37 - Von Mises Stress of a point along the top spar versus Max Element Size of the mesh. ...	52
Figure 38 - A SolidWorks Simulation image showing an example of the Tsai-Wu failure index used in the analyses. Note that SolidWorks Simulation reports the inverse of the Tsai-Wu index as a Factor of Safety against failure. ....	53
Figure 39 - A SolidWorks Simulation image showing an example of the displacement results used in the analyses. Note the deflection of the wing top surface under aerodynamic loading (blue, bottom) which changes the aerofoil shape. ....	54
Figure 40 - A SolidWorks Simulation image showing an example of an inter-laminar shear stress plot as was used in the analyses. ....	54
Figure 41 - SolidWorks Simulation image showing the FOS of the wing internal structure at the Point B load case. ....	57
Figure 42 - SolidWorks Simulation image showing the FOS of the wing external structure at the Point B load case. ....	58
Figure 43 - SolidWorks Simulation image showing a close-up of the FOS of the wing ribs at the Point B load case. ....	58
Figure 44 - SolidWorks Simulation image showing the deflection of the wing in the y-direction at the Point B load case. ....	59
Figure 45 - SolidWorks Simulation image showing a close-up of the top skin resultant deflection at the Point B load case. ....	59
Figure 46 - SolidWorks Simulation image showing the areas of highest inter-laminar shear stress in the model for the Point B load case. ....	60

Figure 47 - SolidWorks Simulation image showing the FOS of the wing internal structure at the Point D load case.....	60
Figure 48 - SolidWorks Simulation image showing the FOS of the wing external structure at the Point D load case.....	61
Figure 49 - SolidWorks Simulation image showing the deflection of the wing in the y-direction at the Point D load case.....	61
Figure 50 - SolidWorks Simulation image showing a close-up of the bottom skin resultant deflection at the Point D load case. ....	62
Figure 51 - SolidWorks Simulation image showing the areas of highest inter-laminar shear stress in the model for the Point D load case.....	62
Figure 52 - Layup drawing sheet 1 for the new Kwadira wing structure .....	64
Figure 53- Layup drawing sheet 2 for the new Kwadira wing structure .....	65
Figure 54 - Picture showing the layers of material used to lay up the GFRP components: Glass fibre (white, outside), nylon peelply (striped), perforated release film (orange), breather cloth (white, inside) and vacuum film (purple). ....	67
Figure 55 - Picture showing the bottom wing skin layed up in the mould (blue) and covered with peelply, release film, breather cloth (white) and vacuum film (transparent purple). Note also the vacuum fitting used to pull a vacuum on the materials. ....	68
Figure 56 - Picture of the bottom wing skin with leading edge lip. ....	69
Figure 57 - Picture showing the top wing skin (light blue) in the top skin mould (blue). Note the carbon spar caps and webs (black) and the span-wise ribs (white). ....	70
Figure 58 - Picture showing the cleating of the webs and ribs to the top skin. Also note the right-angled strips of GFRP and CFRP bonded to the webs and ribs to create sufficient surface area for bonding the bottom wing skin.....	71
Figure 59 - Picture showing further detail of the cleating as well as the bonding surfaces bonded to the bottom side of the webs and ribs (the wing is lying inverted). ....	72
Figure 60 - Picture showing the lines of filled epoxy resin that was applied to the bonding surfaces of the webs and ribs and the leading and trailing edges of the wing skins. ....	73
Figure 61 - Picture showing the final wing after leading and trailing edge trimming. Note the spar caps (black) as they appear through the semi-transparent GFRP wing skins. ....	74
Figure 62 - Picture showing the NEMA G11 hardpoint (circled in red) bonded into the wing root rib. ....	75
Figure 63 - Picture showing the Wing Structural Test Rig (yellow), whiffle tree (silver), new wing (dull green), wing saddles (white), dummy wing (red), hydraulic jack and pump (black, bottom). ....	77
Figure 64 – Diagram showing the magnitudes of the forces applied to each discrete point along the wing span.....	78
Figure 65 - Image showing the loads to be applied to the wing using the whiffle tree linkages.....	79
Figure 66 - Picture of the whiffle tree as it was set up for testing of the newly built wing. ....	79
Figure 67 - Wing saddles constructed out of polystyrene and aluminium beams that were used to transfer the loads from the whiffle tree to the wing. ....	80

Figure 68 - Picture of the dummy wing that provides hardpoints (circled in red) to transfer the wing bending loads from the new wing. .... 80

Figure 69 - Picture of the dummy fuselage that was constructed which provided hardpoints (circled in red) for the wing shear/torsion pins to attach to. .... 81

Figure 70 - Picture showing the attachment of the wing and dummy wing to the dummy fuselage. Note the wing shear/torsion pins (circled in yellow) and the spar pins (circled in red). .... 81

Figure 71 - Picture showing the hydraulic jack in the Wing Structural Test Rig. Note the hydraulic line exiting the top of the picture. Also note the pulley around which the wire rope is passed to the whiffle tree (circled in blue) and the attachment of the wire rope (circled in red) that is attached to the dummy wing. Also shown is the load cell attached to the right side of the jack. .... 82

Figure 72 - Plot of the measured tip deflection versus the predicted tip deflection. .... 83

## List of Tables

Table 1 - Material properties of 86GSM plain weave glass fibre woven cloth. Source: material testing, see Section 3.2.....	22
Table 2 - Material properties of 106GSM plain weave glass fibre woven cloth. Source: material testing, see Section 3.2. ....	23
Table 3 - Material Properties of 200GSM twill weave Carbon fibre woven cloth. Source: (Perini, 2012).....	23
Table 4 - Material properties of 343GSM Carbon UD tape. Source: (Perini, 2012).....	24
Table 5 - Material Properties of Ampreg 21 Epoxy Resin. Source: (Advanced Materials Technology, 2014), (Bardella, 2000).....	24
Table 6 - Material Properties of DC Wort 6mm thick prepared glass fibre sheet. Source: (DC Wort, 2016).....	25
Table 7 - Top and bottom spar cap initial layups .....	39
Table 8 - The maximum shear flow, weight of GFRP required and initial layup for the wing skins...	42
Table 9 - The maximum shear flow, weight of GFRP required and initial layup for the shear webs ..	42
Table 10 - Results of the FEA whiffle tree analyses and the physical testing compared side by side.	83

# Nomenclature

Symbol	Description	Units
<b>English Letters</b>		
$b$	Wing span	m
$c$	Local wing chord	m
$c_l$	Local aerofoil lift coefficient	-
$c_D$	Local aerofoil total drag coefficient	-
$c_m$	Local aerofoil pitching moment coefficient	-
$E_i$	Elastic modulus of a material in the subscript $i$ direction	GPa
$F_i$	Force in the subscript direction	N
$G_i$	Shear modulus of a material in the subscript $i$ direction	GPa
$K_c$	Buckling coefficient for thin plate subject to compressive loading	-
$L$	Wing lift force	N
$M$	Wing bending moment	N.m
$S$	Wing surface area	m <sup>2</sup>
$T$	Wing torsion	N.m
$V$	Aircraft velocity	m/s
$V_a$	Manoeuvr speed	m/s
$V_c$	Cruise speed	m/s
$V_d$	Dive speed	m/s

<b>Symbol</b>	<b>Description</b>	<b>Units</b>
<b>Greek Letters</b>		
$\alpha$	Wing local incidence angle / Angle of attack	$^{\circ}$
$\beta$	Sideslip angle / Yaw angle	$^{\circ}$
$\gamma_i$	Shear strain in a material in the subscript $i$ direction	-
$\varepsilon_i$	Normal strain in a material in the subscript $i$ direction	-
$\rho$	Air density	$\text{kg/m}^3$
$\sigma_i$	Normal stress in a material in the subscript $i$ direction	MPa
$\tau_i$	Shear stress in a material in the subscript $i$ direction	MPa

<b>Abbreviation</b>	<b>Description</b>
ADC	Analogue to Digital Converter
ASTM	American Society for Testing and Materials
ASC	CSIR Aeronautics Systems Competency
CAD	Computer Aided Design/Drawing
CFRP	Carbon Fibre Reinforced Plastic
CNC	Computer Numerically Controlled
CSIR	Council for Scientific and Industrial Research
DXF	Drawing Exchange Format
EMI	Electro-Magnetic Interference
FEA/FEM	Finite Element Analysis / Finite Element Methods/Modelling
GFRP	Glass Fibre Reinforced Plastic
LLT	Lifting Line Theory
MIT	Massachusetts Institute of Technology
MSM	CSIR Materials Science and Manufacturing
MTOW	Maximum Take-Off Weight
NAFEMS	National Agency for Finite Element Methods and Systems
RTM	Resin Transfer Moulding
TMWL	Traditional Metal Wing Layout
TDRL	Tri-Directional Rib Lattice
UAS	Unmanned Aircraft System
UAV	Unmanned Aerial Vehicle
UD	Uni-Directional
VLM	Vortex Lattice Method
V-n	Velocity-Load Factor
VNE	Velocity Never Exceed (Never Exceed Speed)

# 1. Introduction and Dissertation Overview

## 1.1. Introduction

### 1.1.1. The Kwadira UAV

At the beginning of 2014 Tellumat Avionics Systems contracted the CSIR to design and build a 75kg-class unmanned aircraft according to Tellumat's specifications. The resultant aircraft was titled Kwadira which is the Zulu word for Grey Loerie, a bird traditionally thought to warn of nearby danger. The Kwadira UAV has a maximum take-off weight (MTOW) of 75 kg with a wingspan of just over 5 meters and is capable of flights of up to 5 hours long carrying a 15 kg payload. The aircraft is built entirely using fibre reinforced plastics (FRPs) with minimal use of metals to save weight. The conceptual, aerodynamic, detailed design, structural and manufacturing work was performed at the CSIR and the first prototype was delivered to Tellumat in October 2014. A SolidWorks CAD rendering of the Kwadira UAV can be seen in Figure 1.



Figure 1 - A SolidWorks CAD rendering of the Kwadira UAV.

### 1.1.2. Current Wing Structural Design

The current structural design of the Kwadira wing employs a structural layout popular among UAV manufacturers due to its simplicity. Woven glass, Kevlar or carbon fibres are bonded to each side of a thin core material, typically foam or honeycomb, and are used to form wing skins, webs and ribs. This sandwich construction is strong and resilient to local buckling and is widely used in industry for wings, fuselages, tail booms and internal frames.

The structural layout of the Kwadira wing currently consists of the following components as shown in Figure 2:

1. A woven glass fibre and structural foam sandwich skin which is used to keep the aerofoil shape, resist torsion created by pitching moments and transfer shear loads to the spar caps and shear webs.
2. A main spar in the form of unidirectional carbon fibre spar caps that resist bending moments created by lift and shear forces, assumed to carry all the bending loads.
3. A woven glass fibre and structural foam sandwich vertical main spar shear web that is used to resist the shear created by lift forces, act as a web for the main spar, and create a torsion cell that acts together with the wing skins, assumed to carry most of the shear loads.
4. A glass fibre and structural foam sandwich vertical sub-spar shear web that is used to maintain the aerofoil shape near the trailing edge and close the torsion cell created by the man spar web and skins.
5. Glass fibre and structural foam sandwich root and tip ribs that maintain the shape of the aerofoil and resist/transfer torsion and shear loads through pins or hardpoints.
6. Stainless steel shear pins used to transfer the bending (via shear forces), shear and torsional loads from the outboard to the inboard (fuselage) sections of the wing.

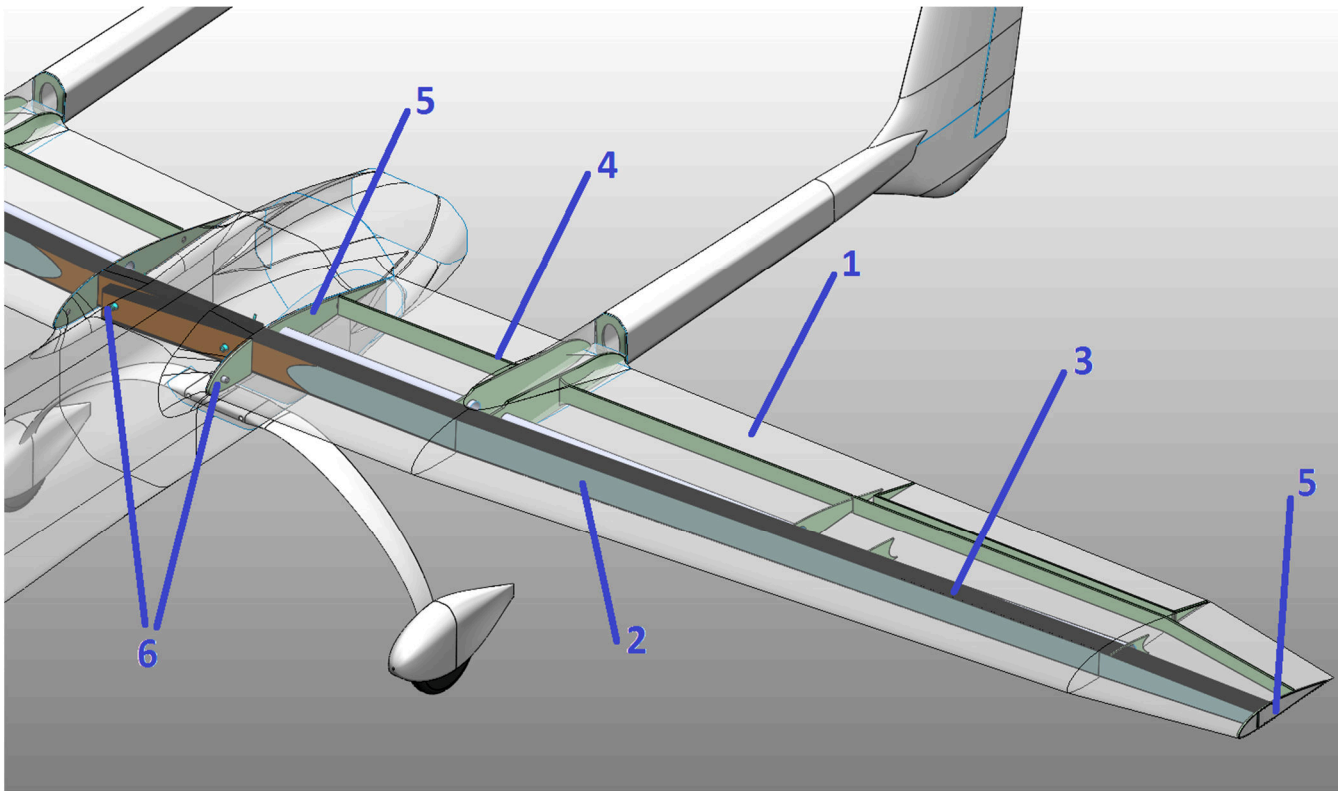


**Figure 2 - A SolidWorks rendering showing an internal view of the current Kwadira wing design with structural components numbered.**

### 1.1.3. Problems Arising From Cored FRP Construction

While cored FRP or sandwich construction has benefits, such as resilience to local buckling and a large strength-to-weight ratio, it also has practical drawbacks inherent in the construction techniques used to manufacture the sandwich panels:

- When constructing moulded parts, an absorbent breather cloth is included as part of the vacuum moulding process which purpose is to distribute the vacuum to all parts of the mould and absorb excess resin. Fibres on the mould side of the core are not exposed to the breather cloth and hence no excess resin can be absorbed from them making the final part heavier than desired.
- Most core materials, even supposedly closed-cell foam types, tend to absorb undesirable amounts of resin. When laying up fibres onto such a core material excess resin is often applied to avoid so-called 'dry spots' where the fibres have not bonded to the core properly. The dry spots lead to skewed fibre/resin ratios and a heavier part.
- In the case of sandwich panel shear webs and ribs, large and thus heavy beads of cotton/resin mixture are often needed to form butted joints to other components.
- The preparation and layup time for a moulded sandwich part is significantly increased by the necessary cutting of the core materials and sanding/finishing of the core edges.

From the points above it can be seen that the main drawbacks of cored FRP construction are added or excessive weight build up and increased preparation time.

## 1.2. Research Hypothesis

I hypothesize that the wing structure of a UAV can be significantly lightened through the use of a coreless structural design employing thin skins and carefully designed internal ribs and frames instead of a sandwich construction, while maintaining strength and rigidity. I further hypothesize that such a structural design will enable quicker construction of the wing by allowing the internal frames and ribs to be cut from prefabricated sheets and assembled in a grid-like fashion.

## 1.3. Research Objectives

The objectives of this research will be to:

1. Reduce the weight of an existing UAV wing through design of a new structural layout that negates the need for sandwich construction while still maintaining adequate strength and rigidity.
2. Reduce the preparation and layup time of the chosen UAV wing using a novel construction technique enabled by objective no. 1

## 1.4. Research Methodology and Scope

The proposed methodology for conducting this research is as follows:

Initially a thorough study of current literature on cored and coreless FRP design, aircraft and wing structures and Finite Element Analysis (FEA) of composite structures will be conducted in order to obtain a deeper understanding of these topics. Once this study has been completed the Kwadira wing will be analysed using a Vortex Lattice Method aerodynamic analysis program such as XFLR5 to determine the loads on the wing during different flight regimes.

A semi-generic spreadsheet-based model for sizing and placement of the coreless composite skins, webs, ribs, frames and spars will be developed using a structural analytical approach. The output from this spreadsheet will be used to build a SolidWorks CAD model and subsequently a SolidWorks Simulation FEA model of the wing. SolidWorks Simulation will then be used to analyse the wing

structure and predict deflections under load at key points along the wing. SolidWorks Simulation will also be used to check for buckling of the composite skins under load.

A test wing will then be constructed according to the layups finalised in the FEA model. The thin wing skins will be constructed using a conventional wet layup process. A CNC router or CNC water jet cutter will be used to cut the ribs and frames from flat prefabricated sheets of FRP. Care will be taken to ensure that the physical FRP parts closely match those of the FEA model. The ribs and frames will then be assembled to form internal lattice structure that will be bonded to the wing skins.

The final mass of the wing will be measured. The wing will then be tested in the CSIR wing structural test rig using a whiffle tree to apply representative loads to the wing. Wing tip deflection will be measured at various load cases. These test results will then be compared to the FEA results obtained from simulation of the Kwadira wing under the whiffle tree loading. The comparison between the simulated results and measured values will be used to validate the analysis model. Finally, the research hypothesis will either be confirmed or rejected based upon the validated analysis results and final measured mass of the wing.

## **1.5. Research Significance and Novelty**

Since the beginning of aviation, aircraft structural designers have sought to make aircraft structures lighter while maintaining the strength required for safe manoeuvring throughout the flight regime. Aircraft mass is an important variable in aircraft design since it affects aircraft speed, range and manoeuvrability. A lighter construction enables an aircraft to fly faster with a given fuel mass, fly further by being able to carry more fuel, carry a larger payload, or be more manoeuvrable. A quicker and thus less labour-intensive construction method will also lower the cost of manufacturing.

There are many local UAV designs that would benefit from a lightweight construction method and it is thus hoped that this work might contribute towards an altered design philosophy in local industry.

The novelty of this research lies in the proposed construction technique tied to the proposed new structural layout. Literature shows that CNC waterjet cutting of prefabricated FRP sheets with grid-like assembly has not yet been performed in South Africa.

## **1.6. Dissertation Overview**

This dissertation has the following structure:

- Chapter 2 – Literature review and Theory
- Chapter 3 – Material Properties
- Chapter 4 – Loads, Structural Layout and Initial Sizing Model
- Chapter 5 – FEA Analysis and Optimisation
- Chapter 6 – Wing Manufacture
- Chapter 7 – Experimental Setup, Testing And results
- Chapter 8 – Discussion
- Chapter 9 – Conclusions and Recommendations

## 2. Literature Review and Theory

### 2.1. Literature Review

#### 2.1.1. Aircraft Flight Loads and Flight Envelope

*Aircraft Structures for Engineering Students* (Megson, 2013) thorough handling of the subject provides great insight into both fundamental and advanced concepts in the field of aircraft structures, dealing with concepts ranging from basic elasticity and thin plate theory to principles of stressed skin construction, airworthiness and airframe loads, and stress analysis of airframe components. Megson provides an overview of flight envelope and critical load factor determination and a detailed analysis of aircraft inertia, manoeuvre and gust loads.

Similar to (Megson, 2013) in its thorough treatment of aircraft structures, *Aircraft Structures* (Peery, 1982) provides a different perspective on many of the same topics centred around analysis of semi-monocoque structures and includes chapters on finite element analysis and thermal stresses. Peery provides another approach to determination of aerodynamic and acceleration loads and the development of a flight envelope.

The *Federal Aviation Regulations Part 23* (United States. Department of Transport., 1965) prescribes airworthiness standards to be used in the design of light, utility and acrobatic aircraft. In particular, FAR23 provides guidelines on the determination of the flight loads required for development of a safe flight envelope. Details on the construction of a velocity-load factor (V-n) diagram that includes gust load cases are given.

Ithurbure (Ithurbure, 1999) and Perini (Perini, 2012) both describe the process of developing a flight envelope based on maximum positive and negative load cases determined from a range of loads as applied to a regional airliner and a large UAV. They also describe how these loads and load cases were used to design the structures of a wing.

#### 2.1.2. Wing Loading / Lift Distribution

*Fundamentals of Aerodynamics* (Anderson, Fundamentals of Aerodynamics, 2007) and *Introduction to Flight* (Anderson, Introduction to Flight, 2008) are valuable resources that deal with basic and advanced concepts in aerodynamics of aerofoils and wings as well as concepts in aircraft stability, performance and design. Anderson explains the Lifting Line Theory (LLT) and Vortex lattice Method (VLM) as applied to subsonic three-dimensional wings and how these methods can be used to obtain an approximation for the local lift, drag and pitching moment coefficients at specific sections along the span of a wing. Anderson then gives a method by which these coefficients can be used to calculate the lift, drag and torsional loadings on a wing.

Unal (Unal, 2013), (Perini, 2012) and (Ithurbure, 1999) all give examples of wing loading and lift distribution calculations as applied to UAV and airliner wings. (Unal, 2013) in particular explains that the pressures on the lower and upper surfaces of a wing differ in magnitude and gives a solution for applying these loads in an FEA environment.

#### 2.1.3. Wing Structural Layout Schemes

(Megson, 2013) and (Peery, 1982) both provide detailed descriptions of traditional and modern metallic aircraft wing construction focussing on the semi-monocoque approach where several spars are utilized to resist bending loads, webs are used to resist vertical shear loads, and the skin is used to resist torsional loads. A large number of usually evenly spaced chord-wise ribs and span-wise stringers are used to stabilise the skin and transfer aerodynamic and concentrated loads to the webs

and spars. (Unal, 2013) gives a good example of a semi-monocoque metallic structure implementation.

Sensmeier & Samareh (Sensmeier & Samareh, 2004) give an overview of aircraft structural layout trends, comparing commercial aircraft to fighter aircraft and Western to Eastern design philosophies. Whilst most commercial and military aircraft today utilise a semi-monocoque construction, the implementation of this layout differs from West to East especially in the number and type of structural elements employed in wing construction. Hassan (Hassan, 2012) concludes that the main driver in modern aircraft structures is the simplification (and hence the decrease in assembly time) of structural components. Deo, Starnes & Holzwarth (Deo, Starnes, & Holzwarth, 2001) give an insightful analysis of FRP usage trends in military and civilian aviation starting from 1965. These references were used to obtain an idea of modern design trends.

Body (Body, 2007) describes the approach that Airbus is taking towards FRPs and gives an overview of both current and future wing structural layouts and mentions that Airbus is moving towards increasing the number of FRP components in its aircraft. The United States Department of Transport (United States. Department of Transport., 2008) gives another example of FRP structural layouts commonly used in light and commercial aircraft.

Collins (Collins, 1985) gives a detailed description of the design methodology for a UAV wing structure employing foam sandwich construction in the wing skins. Collins gives sample calculations for flight envelope, wing loading, stresses and FRP layups of the UAV.

(Unal, 2013), (Perini, 2012), (Ithurbure, 1999) and Sedaghati & Elsayed (Sedaghati & Elsayed, 2006) give detailed descriptions of the design process for ribbed semi-monocoque wing structures and structural elements using FRPs. (Ithurbure, 1999), in particular, compares the weight of stiffened skins with the weight of sandwich structures and concludes that sandwich structures are generally lighter. Arunkumar & Lohith (Arunkumar & Lohith, 2015) details a valuable analysis of the effect of wing rib and stringer spacing on the weight of FRP aircraft structures, an important study point for this research.

Shanygin, Zichenkov and Kondakov (Shanygin, Zichenkov, & Kondakov, 2014) present a fascinating perspective on the modern implementation of FRPs in aircraft structures. They mention that with every new construction material introduced into the field (wood, steel tubing, aluminium) the internal structural layouts of aircraft components has changed. They present a strong case for the implementation of isogrid lattice structures in order to realise the full potential of FRPs. Stavrev and Stavrev (Stavrev & Stavrev, 2014) propose a small manned glider to be dropped from the edge of space with isogrid-reinforced FRP-skinned wings.

Morishima (Morishima, 2011), Xu (Xu, 2012), (Perini, 2012) and (Prinsloo, 2011) give examples of the use of FEA in the analysis and design of FRP aircraft structures.

#### **2.1.4. FRP Design and Construction**

*Theory of Composites Design* (Tsai, 2008) is an invaluable reference on the fundamentals of FRP theory, analysis and design by one of the fathers of modern FRP thinking. Ply stiffness, micro- and macro-mechanics, laminate theory, failure criteria and laminate strength are some of the topics discussed.

The *Composite Materials Handbook* (United States. Department of Defence., 2002) contains a wealth of information on FRPs. Amongst the subjects discussed are materials and construction processes, material property testing and variation, quality control, design and analysis, structural behaviour of joints, damage resistance and durability, structural reliability and environmental management.

The *Crystic Composites Handbook* (Scott Bader Company, 2005) provides detail on FRP materials, layup processes, properties, quality control, mould making and health and safety. Of particular value is its description of open-mould layup processes and quality control section highlighting common faults made during the construction processes.

Gagauz (Gagauz, 2013) gives an overview of FRP sandwich panel design, failure modes and common joining methods. Combining Gagauz with Collins an understanding of the advantages and disadvantages of cored construction was obtained.

Leissa (Leissa, 1985) gives equations for buckling of FRP plates and shells and examines complicating factors such as internal holes. Particular attention is paid to buckling of stiffened plates and the use of FEA is recommended for their analysis. Guo (Guo, 2007) analyses the stress concentration and buckling behaviour of composite panels with reinforced cutouts and makes recommendations as to the most efficient cutout reinforcement.

Huybrechts & Tsai (Huybrechts & Tsai, 1996) give an overview of FRP lattice structures: their behaviour, stiffness, stability and potential for repair and joining. Vasiliev & Razin (Vasiliev & Razin, 2012) present a case for geodesic or anisogrid lattice structures in aircraft and give an example of such a structure implemented in an airliner fuselage. Hicks (Hicks, 2001) proposes a new way of constructing high-strength isogrid structures, making use of both waterjet cutting to cut slots in a sandwich structure and interlacing of unidirectional fibres once the structures have been slotted together.

### 2.1.5. FEA of FRP Materials

*How To Analyse Composites* (Marsden & Irving, 2002) and Ladzinski & Abbey (Ladzinski & Abbey, 2009) provide a detailed overview of FEA of FRPs, dealing with such subjects as material definition, plie specification and material draping, meshing and thickness effects, edge contact, failure prediction theories, inter-laminar stresses, result interpretation and optimisation. Also given are practical design methods and common pitfalls encountered when performing FEA on FRPs.

Nurhaniza (Nurhaniza, 2010), Prinsloo (Prinsloo, 2011), (Perini, 2012), (Morishima, 2011) and (Xu, 2012) all make use of various FEA packages to analyse FRP as applied to aircraft wing structures. The use of different FEA packages by the authors allows for the identification of common simulation practices and procedures which proves valuable in performing FEA in a variety of software packages.

*SolidWorks Help* (Dassault Systemes, 2014) provides useful insight into the operation of the SolidWorks Simulation FEA package meshing, contact constraints and post-processing.

NAFEMS (NAFEMS, 2016) and Comsol (COMSOL, 2016) provide guidance on FEA mesh convergence studies and the different ways mesh refinement can be performed. Differentiation is made between global mesh refinement and local geometrical refinement and the authors recommend plotting a chosen metric, such as Von Mises stress, versus element size to get a clear picture of convergence. (COMSOL, 2016) also highlights the importance of checking for mesh refinement at different points along the model as some areas may converge later than others due to geometrical effects or differing stresses in these areas.

### 2.1.6. Static Wing Testing

Robinson (Robinson, 2004) provided insight into wing sandbag testing, a process by which wings are tested in bending by which calibrated sandbags are placed on the surface of the wing to represent a desired shear force distribution along the wing.

Perini (Perini, 2012) provided an example of the method by which wings might be tested in bending using a whiffle tree: a set of beams and linkages that distribute a single load into multiple points along

a wing that can be used to simulate a shear force distribution along the wing. Juracka et al (Juracka, Jebacek, & Pistek, 2000) and Wright (Wright, 1970) gave further insight into the design and construction of whiffle trees and the process of translating a lift distribution over a wing into a finite number of load points. Review of their work led to the selection of whiffle tree testing for this research (as opposed to sandbag testing) since it was found that whiffle tree testing is more accurate in the application of loads to a wing.

### **2.1.7. Summary of Literature Reviewed**

In order to accomplish the objectives of this research of 1) reducing the weight of the Kwadira UAV wing through use of a new, coreless structural layout and 2) reducing the construction time of the Kwadira UAV wing by using a waterjet cut lattice construction a wide range of literature was reviewed:

1. It was important to gain an understanding of the flight envelope of an aircraft in order to determine the maximum load cases that the Kwadira UAV experiences during flight. This flight envelope was developed according to FAR 23 to ensure that the new structural layout would comply with regulations by which the old structural layout had been designed.
2. Once the maximum load cases had been determined it was necessary to find methods by which these load cases can be converted into aerodynamic lift and drag forces and pitching moments applied to the Kwadira UAV wing. These loadings were then interpreted into shear forces and bending and torsional moments for use in the design of the new structural elements.
3. It was deemed important to gain insight into past, current and future design trends in aircraft structures and commonly used FRP structural layouts in order to supply the research with context and validity. This context, along with an understanding of wing loadings, was used to then better understand the different structural layouts and their associated structural elements which form the basis of this research.
4. In order to design the chosen structural elements effectively, a deeper understanding of FRPs, their properties, analysis, construction methods and design pitfalls was needed. Both cored and coreless composites were studied to obtain a clearer picture of their uses. Particular attention was paid to the buckling of thin plates which will form the majority of the internal wing structure. A study was also done to gain insight into the use of composite lattice structures and their potential applications in aviation.
5. Once the semi-monocoque FRP structural elements had been designed using traditional laminate theory methods it was necessary to gain insight into the FEA of FRPs and the added complexity of modelling anisotropic materials. The chosen FEA package was studied to understand various parameters and controls and an understanding of the importance of mesh convergence was gained.
6. The static strength tests performed on wings by several authors were reviewed and their methods analysed in order to select an appropriate testing method.

Although many examples of coreless, semi-monocoque wing structural design were found, none were found with the explicit goal of reducing the weight of a current cored design. Examples were also found of studies done on FRP lattice structures and their construction using waterjet cutting but none have been found that apply this technique to aircraft wing construction.

## 2.2. Theory: Wing Loading / Lift Distribution

### 2.2.1. Maximum Load Cases and Flight Envelope

Every aircraft to be certified for flight is required to have a flight envelope which specifies manoeuvring limits for the aircraft. The flight envelope is represented by a Velocity-Load Factor or V-n diagram and details limits such as the maximum load factors at manoeuvre, cruise and dive speeds, the Never Exceed Speed (VNE) which is limited by flutter and the positive and negative stall speeds of the aircraft. It is standard practice at the CSIR to develop a V-n diagram according to FAR23 regulations.

Once the V-n diagram is drawn up, critical flight conditions are identified such as a strong upwards gust occurring at manoeuvre speed or a strong downward gust occurring at cruise speed. These critical flight conditions are then used to read off the maximum load factors and their respective velocities for which the structural design calculations will be completed (United States. Department of Transport., 1965).

### 2.2.2. XFLR5 and Vortex Lattice Methods

XFLR5 is a free-to-download aerodynamic analysis program based on XFOIL, an aerofoil analysis tool developed by Mark Drela of MIT. It falls into the category of subsonic, low-order panel codes that do not solve the Navier-Stokes equations but rather make use of the Lifting Line theory (LLT) and Vortex Lattice Methods (VLM) to predict the behaviours of aerodynamic surfaces subjected to flow fields (Anderson, Fundamentals of Aerodynamics, 2007).

The VLM works by assigning horseshoe vortices of varying strengths to panels distributed along the surface of a wing and then solving the resulting system of equations for aerodynamic coefficients (Anderson, Fundamentals of Aerodynamics, 2007). The VLM is considered to be a good first-order approximation and is used extensively in the design of subsonic aircraft but is limited to small wing sweep angles. The bulk of the aerodynamic analysis for this research was done using XFLR5's implementation of the VLM.

### 2.2.3. Span-wise Lift Distribution

Due to the pressure differential between the bottom and top surface of a wing, a vortex is caused at the wingtip due to air flowing from a high pressure zone at the bottom of the wing to a low pressure zone at the top. This so-called wingtip vortex combines with factors such as the span-wise chord distribution, the wing sweep, span-wise and chord-wise flows and span-wise variation of the local wing incidence angle to create a span-wise lift distribution specific to each wing planform (Anderson, Introduction to Flight, 2008).

The VLM uses the wing planform and aerofoil polars to give an approximation for the span-wise lift distribution across the wing represented by a span-wise variation in local lift coefficient for varying angles of incidence. This information can then be used to obtain the span-wise lift force acting on the wing which can be interpreted as a shear force and bending moment for structural calculation purposes (Anderson, Introduction to Flight, 2008).

A similar process is followed to obtain the torsional moment acting on the wing by interpreting the pitching moment coefficient as it varies with the wing span.

### 2.2.4. Chord-Wise Lift Distribution

As the incidence angle of an aerofoil increases the flow across the top of the aerofoil is forced to undergo greater curvature. This has the effect of moving the centre of the low pressure region at the

top of the aerofoil towards the leading edge and places increased demands on the top surface of the aerofoil (Anderson, Introduction to Flight, 2008). For structural calculations it is common practice to represent this chord-wise moving ‘centre of pressure’ as a fixed lifting force and a torsional pitching moment (Megson, 2013). Since the aim of this research was to produce a lightweight wing construction, and thin stressed skins were employed, it was deemed important to evaluate the effect that the moving ‘centre of pressure’ would have on the wing structure.

## 2.3. Theory: FRPs

### 2.3.1. A Brief Description of Composites

By definition, a composite material is a material consisting of more than one distinct constituents (Marsden & Irving, 2002). In the case of FRPs fibre reinforcements are encased inside a polymer resin matrix.

The use of composite materials in aerospace has increased significantly since the early 1960s, starting with non-structural components such as fairings and cabin floors and ending today with main structural components such as wing torsion boxes (Body, 2007) and vertical and horizontal stabilisers. Composite materials are valued for their high strength-to-weight ratios and resistance to fatigue and are therefore ideal for use in aircraft structures (Tsai, 2008).

Designing with composite materials such as FRPs presents unique challenges in the form of material anisotropy by which material strength and stiffness is highly dependent on the orientations of the reinforcement fibres. The designer of FRPs needs to ensure that these unique directional properties are catered for and exploited optimally for a successful design (Tsai, 2008).

### 2.3.2. Laminate Shorthand

It is convention for individual layers of fibres to be referred to as plies and a stack of plies to be referred to as a laminate. Laminate shorthand is a convention by which the orientations of plies in a laminate are described by the angles of the plies relative to the chosen coordinate axis. For example, a laminate described by  $(0/-45/45/90)_s$  would be a laminate consisting of plies angled at  $0^\circ$ ,  $-45^\circ$ ,  $45^\circ$  and  $90^\circ$  and then again at  $90^\circ$ ,  $45^\circ$ ,  $-45^\circ$  and  $0^\circ$ . Such a laminate is said to be symmetric about its midpoint as it has the same ply angles each side of the midpoint.

### 2.3.3. Classical Laminate Theory

Classical laminate theory treats FRPs as orthotropic materials and assumes that laminates can be seen as thin plates loaded only in the axial, transverse and shear directions (United States. Department of Defence., 2002) often denoted by the  $x$ ,  $y$  and  $xy$  directions, respectively. This enables the use of the familiar thin plate theory in the design of aircraft components such as wing skins, webs, stringers, ribs and spars (Megson, 2013).

Classical laminate theory therefore dictates that laminates are represented by the Equations 2.1 to 2.4:

$$\varepsilon_1 = \frac{\sigma_1}{E_1} - \nu_{21} \frac{\sigma_2}{E_2} \quad (2.1)$$

$$\varepsilon_2 = \frac{\sigma_2}{E_2} - \nu_{12} \frac{\sigma_1}{E_1} \quad (2.2)$$

$$\gamma_{12} = \frac{\tau_{12}}{G_{12}} \quad (2.3)$$

$$\nu_{12}E_2 = \nu_{21}E_1 \quad (2.4)$$

This means that the four parameters needed to describe the in-plane elastic behaviour of a laminate are  $E_1$ ,  $E_2$ ,  $G_{12}$  and  $\nu_{12}$  (Marsden & Irving, 2002) which are the elastic moduli of the material in the  $x$  and  $y$  directions, the shear modulus in the  $xy$  direction and the Poisson's ratio in the  $xy$  direction, respectively.

### 2.3.4. Failure Theories

As a result of the orthotropic nature of FRPs conventional failure theories such as the popular Von Mises failure theory cannot be applied directly to an FRP design problem. Instead the Von Mises failure theory has been extended to allow for FRP's differing tensile and compressive strengths in the axial and transverse fibre directions (Tsai, 2008). Failure theories such as the Tsai-Hill, Tsai-Wu and Hashin theories predict First Ply Failure (FPF) of a laminate and take into account complex ply interactions in a multi-axial stress state (Marsden & Irving, 2002).

The Tsai-Wu failure criterion, unlike the Tsai-Hill and Hashin criterion, takes differing ply strengths in tension and compression into account, and as such has been proven to be more representative of real-world laminates (Ladzinski & Abbey, 2009). Based on this the Tsai-Wu criterion was chosen for this study. It is given by Equation 2.5:

$$1 = F_1\sigma_x + F_2\sigma_y + F_6\sigma_{xy} + F_{11}\sigma_x^2 + F_{22}\sigma_y^2 + 2F_{12}\sigma_x\sigma_y + F_{66}\sigma_{xy}^2 \quad (2.5)$$

Where:

$$F_1 = \frac{1}{\sigma_{1uT}} - \frac{1}{\sigma_{1uC}} \quad (2.6)$$

$$F_2 = \frac{1}{\sigma_{2uT}} - \frac{1}{\sigma_{2uC}} \quad (2.7)$$

$$F_6 = \frac{1}{\sigma_{12uT}} - \frac{1}{\sigma_{12uC}} \quad (2.8)$$

$$F_{11} = \frac{1}{\sigma_{1uT} \cdot \sigma_{1uC}} \quad (2.9)$$

$$F_{22} = \frac{1}{\sigma_{2uT} \cdot \sigma_{2uC}} \quad (2.10)$$

$$F_{66} = \frac{1}{\sigma_{12uT} \sigma_{12uC}} \quad (2.11)$$

$$F_{12} = -\frac{\sqrt{F_{11}F_{22}}}{2} \quad (2.12)$$

And:

$\sigma_{1uT}$  = Ultimate tensile strength of the material in the  $x$ -direction

$\sigma_{1uC}$  = Ultimate compressive strength of the material in the  $x$ -direction

$\sigma_{2uT}$  = Ultimate tensile strength of the material in the  $y$ -direction

$\sigma_{2uC}$  = Ultimate compressive strength of the material in the  $y$ -direction

$\sigma_{12uT}$  = Ultimate shear strength of the material

Since FRPs do not exhibit yielding behaviour the ultimate tensile and compressive strengths are used in the failure theory calculations. FPF is predicted to occur when the Tsai-Wu criterion is more than 1.

### **2.3.5. Grid Structures**

International industry has mostly been reluctant to fully exploit the many advantages offered by composite grid lattices (Huybrechts & Tsai, 1996) although there have been a few examples of composite grid lattice structures employed in airliner fuselage construction (Vasiliev & Razin, 2012). Grid lattices are grouped by the directions of the ribs employed in the lattice: quadri-directional have ribs running in four directions, tri-directional lattices have ribs running in three directions and anglegrid lattices have ribs running in two directions.

## **2.4. Theory: Aircraft Wing Structural Design**

### **2.4.1. Popular FRP Structural Layouts**

FRP structural layouts popular with aircraft designers today include the fully monocoque layout with stressed skin, the fully monocoque layout with isogrid lattice structures, the semi-monocoque layout with cored skin and the semi-monocoque layout with stiffened skin (United States. Department of Transport., 2012), (Shanygin, Zichenkov, & Kondakov, 2014).

### **2.4.2. Fully Monocoque Layout with Stressed Skin**

The fully monocoque layout consists of stressed skin that is used to resist shear, axial and torsional loads and hollow frames spaced along the skin to maintain the shape of the skin and increase the buckling resistance of the skin. The fully monocoque layout is popular for fuselage construction.

### **2.4.3. Fully Monocoque Layout with Isogrid Lattice Structures**

While the fully monocoque layout with stressed skin and both the semi-monocoque layouts have their roots in metal aircraft construction (Shanygin, Zichenkov, & Kondakov, 2014), the fully monocoque layout with isogrid lattice structures can be traced back to wooden aircraft construction. This layout replaces the traditional spars, webs, ribs and frames with an isogrid lattice structure that simultaneously resists bending, shear and torsional loading, covered by a thin, non-load-bearing skin.

### **2.4.4. Semi-Monocoque Layout with Cored Skin**

The semi-monocoque layout with cored skin is the layout that is currently employed in the Kwadira UAV and consists of stressed skin that is used to resist torsional loads and webs and spars that are used to resist shear and axial loads respectively. No ribs or stringers are used since the cored construction is used to maintain the shape of the skin.

### **2.4.5. Semi-Monocoque Layout with Stiffened Skin**

The semi-monocoque layout with stiffened skins is similar to the semi-monocoque layout with cored skins but instead of relying on the cored construction to maintain the shape of the skins numerous

chord-wise ribs and span-wise stringers are employed to stabilise the skin. This layout is most popular since the structural elements are taken directly from metal semi-monocoque construction and scale well to larger aircraft (Peery, 1982).

### 2.4.6. Buckling

Thin structural components, such as those employed in aircraft construction, are prone to buckling when subjected to compressive or shear loadings (Niu, Airframe Stress Analysis And Sizing, 1997). Thin skins, webs, spar caps and ribs are often seen to buckle at loads that are lower than those that the material can safely withstand according to conventional failure theories. Buckling is a function of boom or plate stiffness, thickness and geometry. A buckling coefficient  $K_c$  is given as a function of the ratio of a plate's length to its width and is subject to the conditions at the edges of the plate as shown by Figure 3. A generic equation for the buckling of a thin plate due to compressive failure is given by Equation 2.13:

$$F_{c,CR} = EK_c \left(\frac{t}{b}\right)^2 \tag{2.13}$$

Where:

$F_{c,CR}$  = Critical buckling stress of the plate

$K_c$  = Compressive buckling constant

$t$  = Thickness of the plate

$b$  = Length of shorter side of plate

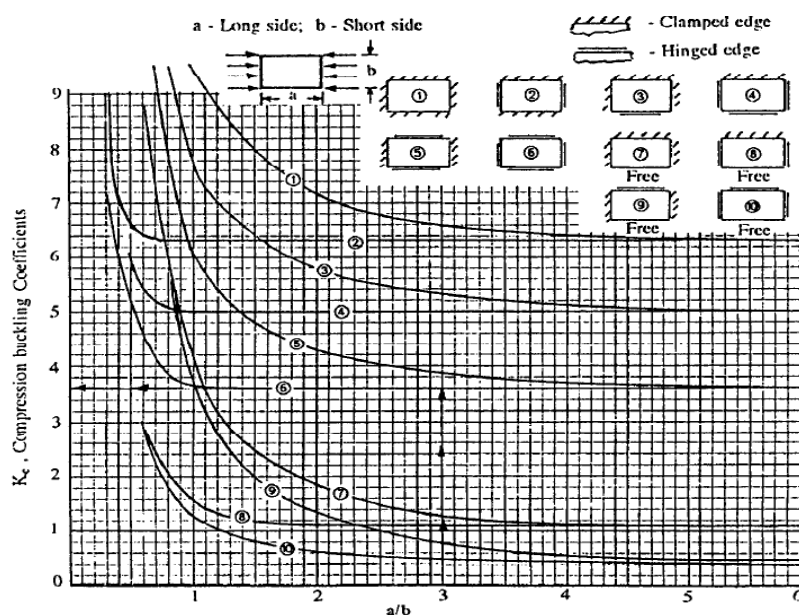


Figure 3 - Buckling coefficient  $K_c$  for a flat plate subjected to compressive loading (Niu, Airframe Stress Analysis And Sizing, 1997).

Each individual component of the aircraft structure needs to be checked for buckling when designing the structure. Thin components are often stiffened by employing cored construction or by attaching stiffeners to the components and these considerations influence the design of the structural layout to a large extent.

## 2.5. Theory: FRP Construction

### 2.5.1. Construction Techniques

At the scale of aircraft such as Kwadira there are several viable FRP construction techniques to consider:

- Vacuum Infusion (VI) is a process by which dry fibres are layed into a mould and covered by a vacuum bag. At one end of the bag a vacuum is drawn while resin is allowed to be drawn into the mould from a reservoir at the opposite end. The resin then wets out the fibres in a controllable manner (United States. Department of Defence., 2002).
- Pre-Pregs: Sheets of fibre area pre-impregnated with resin and cooled in a freezer to retard the curing process. When construction takes place the pre-preg sheets are cut to the correct size and placed in a mould which is then placed in an autoclave to cure. Pre-preg materials produce higher quality and stronger parts but require an autoclave for curing and a freezer for storage (United States. Department of Defence., 2002).
- Wet layup is a process by which fibres are layed into a mould and wet out with resin by hand. The process introduces variation in terms of the final product but is simple and easy to perform (Scott Bader Company, 2005).

### 2.5.2. Wet Layup and Vacuum Bagging

The wet layup of an FRP part consists of the following elements:

- The mould surface which is to be prepared using a release agent
- Paint which becomes chemically bonded with the resin
- The fibres and resin
- Peel ply, a woven nylon cloth which is used to give finished parts a rough surface suitable for bonding to
- Release film, a perforated plastic that separates the part from the breather cloth without bonding to the resin
- Breather cloth, an absorbent fabric that is used to distribute the vacuum throughout the vacuum bag and to absorb excess resin from the fibres
- Vacuum bag, that is used to contain the vacuum, ensure the fibres conform to the shape of the mould and to minimise any air bubbles in the layup that could form voids.

### 2.5.3. CNC Waterjet Cutting

CNC waterjet cutting involves cutting flat sheets of material using a high pressure, focussed stream of water which usually contains abrasive particles such as fine sand. Typical high-pressure cutters can obtain pressures of the order of 300MPa and cut through steel tens of millimetres thick. Waterjet cutting of FRPs is well documented (Hicks, 2001) but certain aspects need to be paid attention to such as the absorption of moisture by the FRP, voids and inclusions in the laid up sheet and the possibility of delamination of plies along the bottom surface of the sheet being cut.

## 2.6. Theory: FEA of Composite Materials

### 2.6.1. SolidWorks Simulation Premium

Simulation Premium is an FEA package fully integrated into the user-friendly SolidWorks environment and has been validated in over 60 NAFEMS benchmarks (Dassault Systemes, 2014). Simulation Premium is capable of, among others: linear static, non-linear, modal, thermal and buckling analyses. It is able to analyse orthotropic composite shells, incorporates powerful material draping features and allows for easy laminate stacking inputs. Simulation Premium calculates the Tsai-Hill, Tsai-Wu and Maximum Stress theory safety factors and reports inter-laminate shear stresses. SolidWorks Simulation Premium was selected as the FEA package for this research.

### 2.6.2. Shell Elements

Since most FEA packages employ orthotropic Classical Laminate Theory (Marsden & Irving, 2002), two-dimensional shell elements are employed. In isotropic analyses a shell thickness is defined; in composite shell analyses the shell thickness and material properties are defined by the number and thickness of the plies used in the laminate. The thickness of the laminates is used to create a theoretical offset from the shell surface which influences the stiffness and contact properties of the elements. SolidWorks Simulation Premium allows for a laminate stack of up to 50 plies and is capable of modelling sandwich plates.

### 2.6.3. Ply/Laminate Properties

The material properties needed to fully define an orthotropic material for FEA analysis are the elastic moduli in the  $x$  and  $y$  directions, the shear modulus in the  $xy$  direction and the Poisson's ratio in the  $xy$  direction. SolidWorks Simulation Premium automatically calculates the stiffness matrix for each laminate according to the plies and ply stacking sequence defined in the property manager of each composite shell.

In order to predict the failure of the laminate the ultimate tensile and compressive strengths in the  $x$  and  $y$  directions and the ultimate shear strength in the  $xy$  direction is required. This first-ply failure prediction is made using the Tsai-Wu failure criterion mentioned in Section 2.3.5. In order to predict delamination failure the maximum shear strength of the resin matrix is required, and this failure prediction is made by evaluating the inter-laminar shear stresses of the laminates.

### 2.6.4. Surface Contact

In SolidWorks Simulation a global bonding option is available that detects surfaces near to each other within a specified tolerance and treats these surfaces as rigidly bonded to each other. The automatic shell mesher then places elements on the surfaces in such a way as to create compatible meshes on each of the bonded surfaces. It is important to note that although SolidWorks Simulation treats these surfaces as rigidly bonded to each other, the program still evaluates the stresses at the bonded joints.

This is representative of the rigid bonding that is employed in FRP construction where high-strength epoxy resins, often mixed with a flocculated cotton filler, are used to bond surfaces together (Prinsloo, 2011). The epoxy resin bonding agent is assumed to be isotropic and thus the shear stress at the surface contact area can be evaluated for a de-bonding failure in the bonding agent.

## **2.7. Theory: Wing Structural Testing**

### **2.7.1. Whiffle Tree Testing**

It is common practice in industry to statically test the strength of an aircraft wing using a whiffle tree assembly. This involves simulating the lift loads that a wing experiences during flight by applying loads at discrete points along the wing span in order to match the shear force and bending moments experienced by the wing (Perini, 2012). A whiffle tree is used to distribute a single load from a hydraulic jack into several loads using an array of beams and linkages. The magnitudes of the final loads applied to the wing are determined by the lengths of the beams used between linkages and are determined using simple geometrical principles.

### **2.7.2. Sandbag Testing**

Sandbag testing works along the same principles as whiffle tree testing in attempting to simulate the primary loads experienced by a wing during flight but with the main difference of using calibrated bags of sand stacked to varying heights along the span of the wing instead of using linkages and discrete loads. Sandbag testing is difficult in practice due to the problem of the sandbags sliding off of the wing at high deflection states and therefore was not considered for this research.

## **2.8. Chapter Summary**

A basic overview is given of some of the underlying theory that was built upon in this research. The components that enable the physical loading of the wing were described and this was followed by a brief description of composite materials and their associated failure theories. The differences between current popular wing structural layouts was highlighted before investigating FRP construction techniques. Lastly, an overview of some of the major functions of SolidWorks Simulation, the FEA package chosen for this research, was given, along with a discussion of common wing structural testing techniques.

## 3. Material Properties

Due to the complex anisotropic nature of composite materials it was required to build up a complete database of material properties that were used in this research.

### 3.1. Selected Materials

In keeping with the research objective of reducing the weight of the Kwadira wing structure it was deemed appropriate to make use of the same materials in the construction of the new lightweight wing structure as were used for the original Kwadira wing. This was done in order to obtain a valid comparison between the old design and the new design stemming from this research. The materials used in this research were:

- 86GSM and 106GSM glass fibre woven cloth for the wing skins, ribs and webs
- 200GSM Carbon fibre woven cloth for the main spar shear webs
- 343GSM unidirectional Carbon fibre tape for the spar caps
- Ampreg 21 Epoxy laminating resin
- DC Wort 6mm thick prepared glass fibre sheet for pin hardpoints

It is acknowledged that the use of CFRP for wing skins, ribs and frames will in all likelihood result in an even lighter wing construction due to the higher strength-to-weight ratio of CFRP compared to GFRP, but in doing so the outcomes of this research would be largely invalidated. Another argument against the use of CFRP for wing skins, ribs and frames for this research is the electro-magnetic opacity of CFRP which causes blanking problems for RF antennae mounted on the top of the aircraft fuselage whereby the CFRP blocks RF signals from reaching the ground station antenna. CFRP was used only for the main spar caps and main spar webs since this was done in the original wing and hence will not cause Electro-Magnetic Interference (EMI) where there previously was none.

### 3.2. Material Testing

#### 3.2.1. Previous Tests

A previous research project saw a re-design of the wing of the CSIR's Modular UAV which involved the creation of a new wing planform and the design of the wing structures using composite materials. Material tests were performed on 343GSM UD Carbon tape and 200GSM Carbon fibre woven cloth combined with Ampreg 21 resin. The tests were conducted by the CSIR Materials Science and Manufacturing (MSM) unit according to international ASTM standards and the results were recorded by Perini (Perini, 2012).

#### 3.2.2. Tests Performed for This Research

In order to design the most efficient structure possible it was deemed prudent to obtain accurate material properties for the 86GSM and 106GSM glass fibre cloth in combination with Ampreg 21 resin. The time frames of the original Kwadira project precluded material testing and so conservative assumptions of the material properties were made based on similar materials. In support of this research the author was granted funding under a Young Researcher's Mentorship fund which made available the opportunity to conduct material tests under the expert guidance of experienced CSIR MSM researchers Mr Chris McDuling and Mr Erich Guldenpfennig.

### 3.2.3. Testing Methodology

For the benefit of later chapters (especially Chapter 5) it is convenient to present here a brief explanation of the methodology employed by MSM (tests conducted for Perini) and the author under MSM's guidance (tests conducted specifically for this research) in the testing of the selected materials:

- Test coupons of a known size given by ASTM standards D3039 (ASTM International, 2002) and D3518 (ASTM International, 2001) were prepared using the selected materials and allowed to cure for 24 hours at room temperature. A total of 20 test coupons were prepared:
  - 5 x 86GSM coupons with 0°x90° fibre orientation. Stress and strain data from these coupons allowed for the determination of ultimate tensile strength, Young's modulus and Poisson's ratio values.
  - 5 x 86GSM coupons with 45°x45° fibre orientation. Stress and strain data from these coupons allowed for the determination of ultimate shear strength and shear modulus values.
  - 5 x 106GSM coupons with 0°x90° fibre orientations.
  - 5 x 106GSM coupons with 45°x45° fibre orientations.
- Pre-wired HBM 1-TM16-6/350GE 350 Ohm T-rosette strain gauges were attached to the specimens in 0° and 90° orientations relative to the fibre directions in order to measure the longitudinal and lateral strain experienced by the coupons as shown in Figure 4.

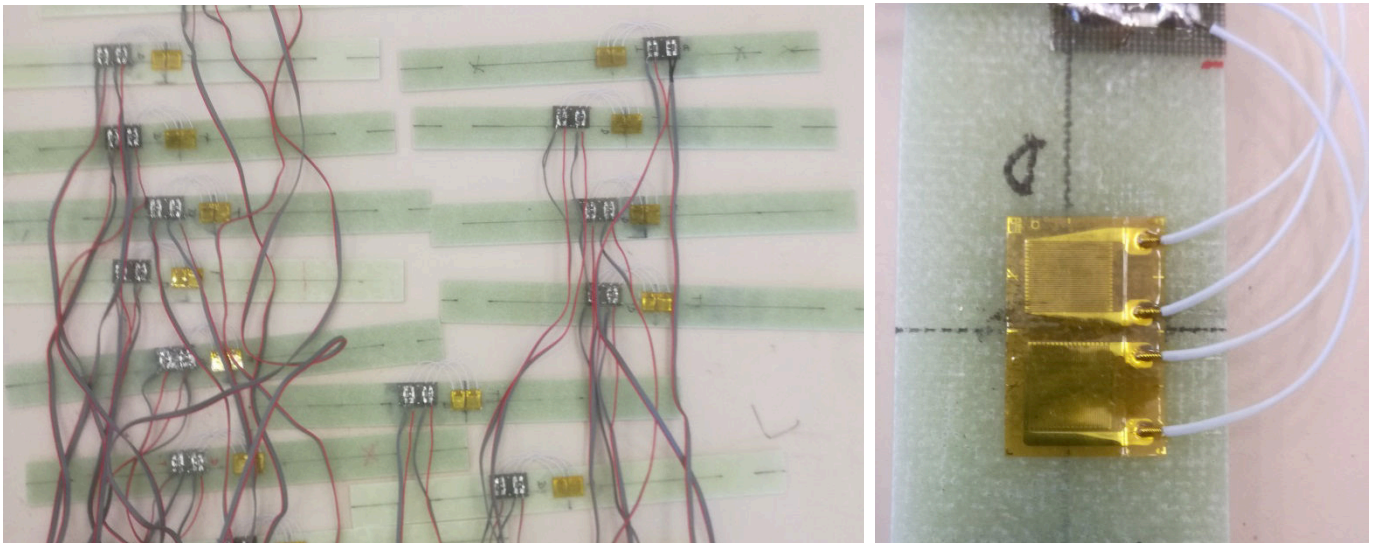
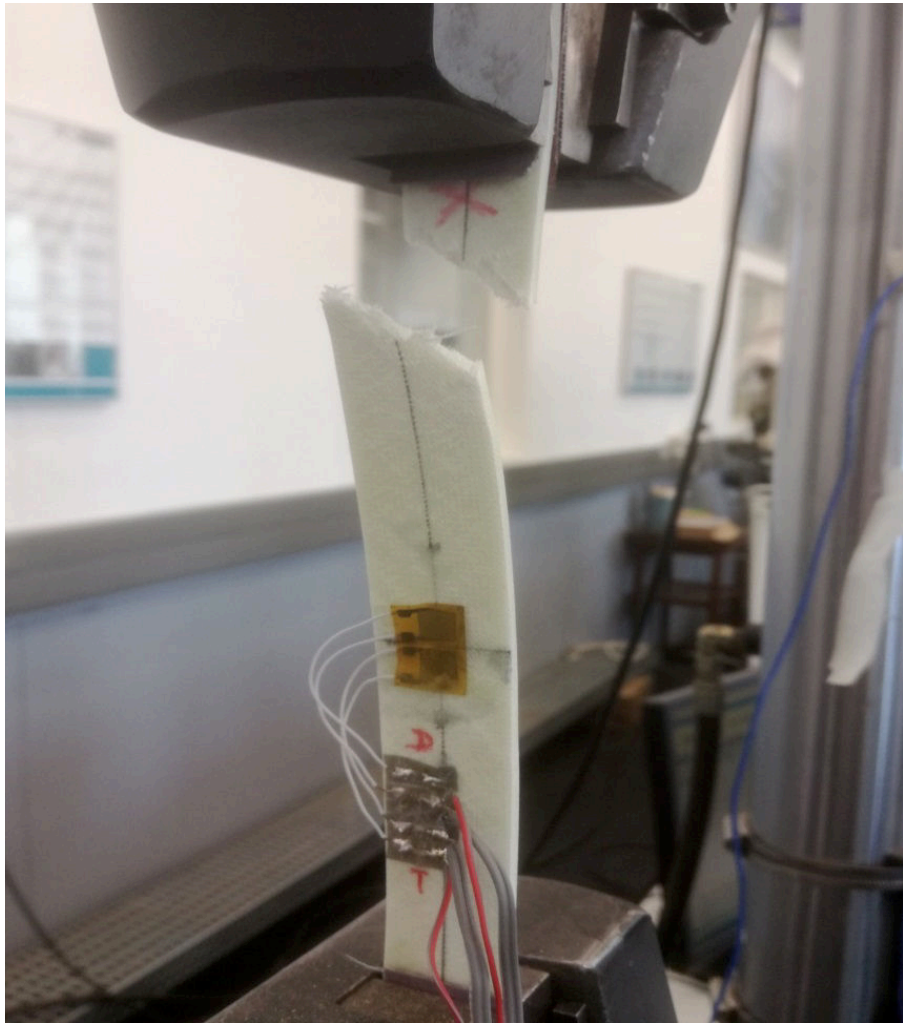


Figure 4 - Composite test coupons with strain gauges and lead wires attached.

- The coupons were stretched to destruction using MSM's Instron tensile testing machines while data was collected from the strain gauges, load cell and extensometer. A typical shear-dominated failure is shown in Figure 5. It must be mentioned that the results for tensile and shear stress were given by the tensile testing machines based on each individual coupon's cross-sectional area.
- Standard engineering equations for stress, strain and stiffness were employed to calculate stiffnesses in the  $x$  and  $y$  directions, maximum tensile and shear stresses, in-plane Poisson's ratios and in-plane shear moduli. Microsoft Excel was used to process the raw strain gauge and load cell data (see Figures 6 to 9) and Young's and shear moduli were calculated in the materials' elastic regions with strain values as prescribed by ASTM D3039 and D3518.



**Figure 5 - Failure of a 45°x45° coupon in CSIR MSM's Instron tensile testing machine.**

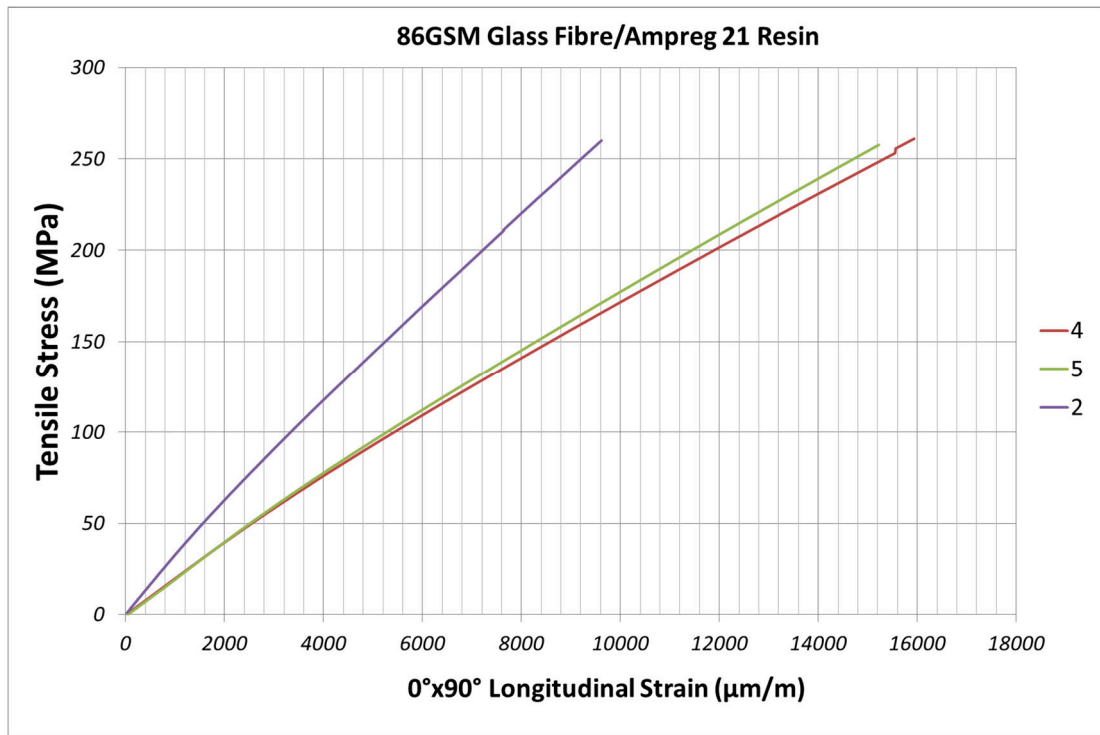


Figure 6 - Plot of laminated 86GSM 0°x90° GFRP tensile stress versus longitudinal strain.

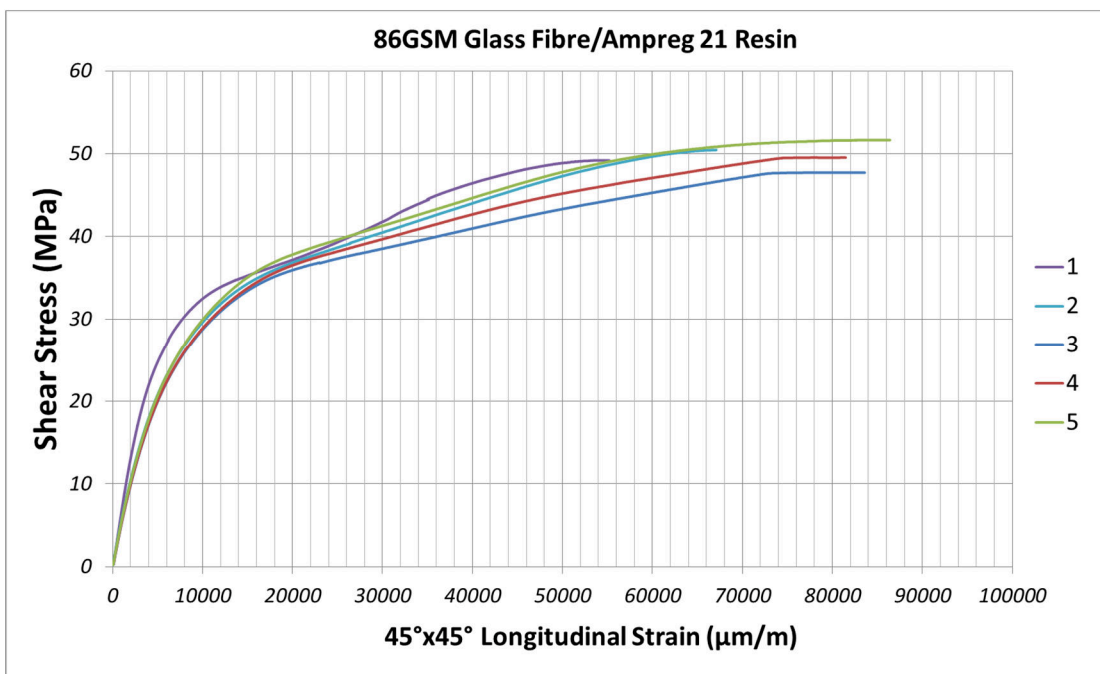


Figure 7 - Plot of laminated 86GSM 45°x45° GFRP shear stress versus longitudinal strain.

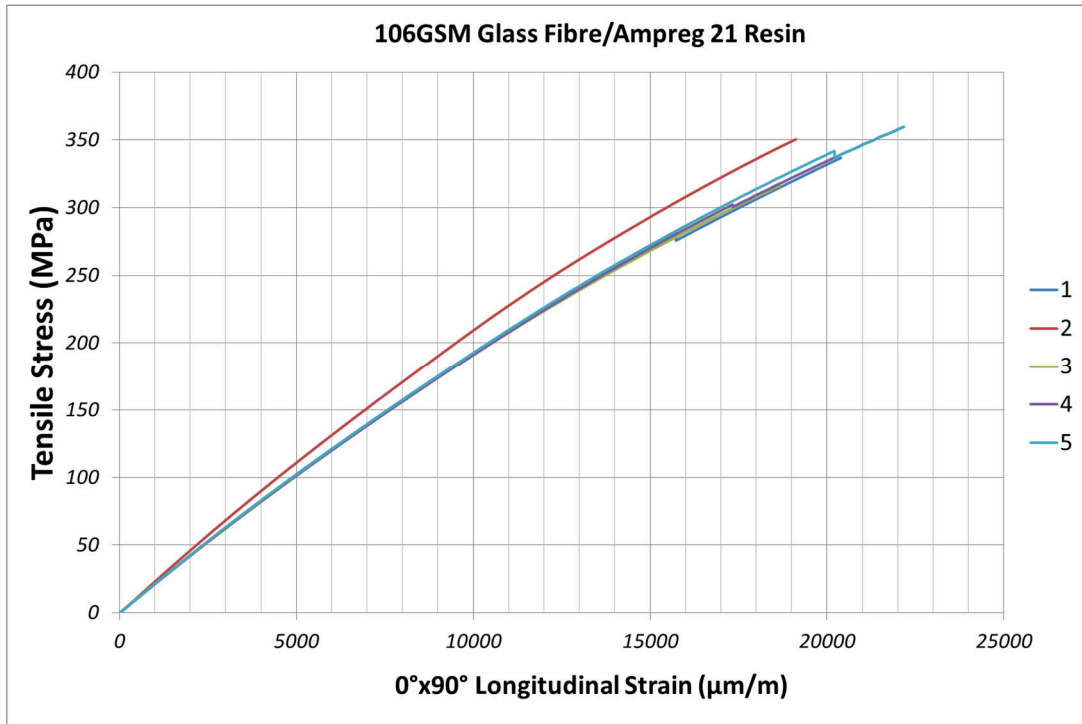


Figure 8 - Plot of laminated 106GSM 0°x90° GFRP tensile stress versus longitudinal strain.

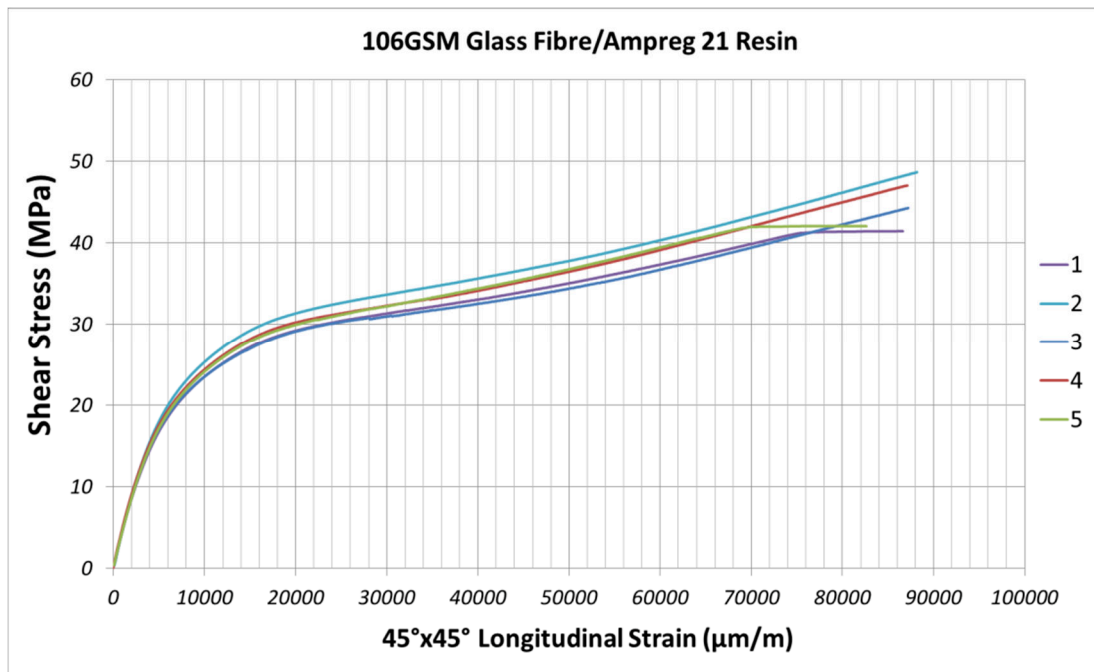


Figure 9 - Plot of laminated 106GSM 45°x45° GFRP shear stress versus longitudinal strain.

### 3.2.4. Limitations of Testing Methodology and Proposed Solutions

The tests conducted on the selected materials are limited in the following ways:

- No compressive tests have been done – knowledge of compressive strengths in both  $x$  and  $y$  directions is vital to the successful implementation of various composite failure theories.
- No out-of-plane tests were done – tensile and compressive strength, stiffness, shear stiffness and Poisson’s ratio in the  $z$  direction are unknown, all of which are required inputs in the SolidWorks Simulation composite material property definition.
- The sample size of the tests was small – a greater number of tests would yield a larger confidence in the results of the tests.

In the light of these limitations, the following solutions are proposed:

- A conservative assumption is made for the compressive strengths of the ply based on standard industry practices of using half of the tensile strength of the ply as the compressive strength. The validity of this assumption is confirmed by Collins (Collins, 1985).
- It is assumed that the out-of-plane properties of the material are resin-dominated properties since the fibre strength in this direction is negligible (Tsai, 2008). The properties in the  $z$  direction are thus taken to be the properties of the resin.
- The number of coupons tested, 5 per material property, is the minimum number of tests recommended by the ASTM standards to obtain a level of confidence in the test results. MSM’s Mr McDuling ruled the testing of an acceptable standard due to the small variation in the results.

## 3.3. Properties of Selected Materials

### 3.3.1. 86GSM Glass Fibre Plain Weave with Ampreg 21 Epoxy Resin

Table 1 - Material properties of 86GSM plain weave glass fibre woven cloth. Source: material testing, see Section 3.2.

Parameter	Symbol	Unit	Value
Tensile Strength $x$ -Direction	$\sigma_{\max, Tx}$	MPa	260
Tensile Strength $y$ -Direction	$\sigma_{\max, Ty}$	MPa	260
Young’s Modulus $x$ -Direction	$E_x$	GPa	21.39
Young’s Modulus $y$ -Direction	$E_y$	GPa	21.39
Poisson’s Ratio	$\nu_{xy}$	-	0.133
Shear Modulus	$G_{xy}$	GPa	1.57
Maximum shear stress	$\tau_{\max}$	MPa	59
Nominal thickness per ply	$t_{86GSM}$	m	0.000083

### 3.3.2. 106GSM Glass Fibre Plain Weave with Ampreg 21 Epoxy Resin

Table 2 - Material properties of 106GSM plain weave glass fibre woven cloth. Source: material testing, see Section 3.2.

Parameter	Symbol	Unit	Value
Tensile Strength <i>x</i> -Direction	$\sigma_{\max, Tx}$	MPa	347
Tensile Strength <i>y</i> -Direction	$\sigma_{\max, Ty}$	MPa	347
Young's Modulus <i>x</i> -Direction	$E_x$	GPa	21.14
Young's Modulus <i>y</i> -Direction	$E_y$	GPa	21.14
Poisson's Ratio	$\nu_{xy}$	-	0.088
Shear Modulus	$G_{xy}$	GPa	1.28
Maximum shear stress	$\tau_{\max}$	MPa	64
Nominal thickness per ply	$t_{810GSM}$	m	0.00009

### 3.3.3. 200GSM Carbon Fibre Twill Weave with Ampreg 21 Epoxy Resin

Table 3 - Material Properties of 200GSM twill weave Carbon fibre woven cloth. Source: (Perini, 2012)

Parameter	Symbol	Unit	Value
Tensile Strength <i>x</i> -Direction	$\sigma_{\max, Tx}$	MPa	464.2
Tensile Strength <i>y</i> -Direction	$\sigma_{\max, Ty}$	MPa	464.2
Young's Modulus <i>x</i> -Direction	$E_x$	GPa	48.9
Young's Modulus <i>y</i> -Direction	$E_y$	GPa	48.9
Poisson's Ratio	$\nu_{xy}$	-	0.16
Shear Modulus	$G_{xy}$	GPa	6.5
Maximum shear stress	$\tau_{\max}$	MPa	125
Nominal thickness per ply	$T_{200GSM}$	m	0.00032

### 3.3.4. 343GSM Carbon UD Tape with Ampreg 21 Epoxy Resin

Since this material is unidirectional the stiffness and strength in the *y*-direction were not determined since they are assumed to be resin-dominated properties and so the properties of the resin will be used for these values.

Table 4 - Material properties of 343GSM Carbon UD tape. Source: (Perini, 2012)

Parameter	Symbol	Unit	Value
Tensile Strength <i>x</i> -Direction	$\sigma_{\max, Tx}$	MPa	1073.4
Young's Modulus <i>x</i> -Direction	$E_x$	GPa	82.1
Poisson's Ratio	$\nu_{xy}$	-	0.28
Shear Modulus	$G_{xy}$	GPa	-
Nominal thickness per ply	$T_{343GSM}$	m	0.0003

### 3.3.5. Ampreg 21 Epoxy Resin

No material directions are given for the properties of the resin since it is assumed that the resin is an isotropic material. The material properties were obtained from AMT (Advanced Materials Technology, 2014) and Bardella (Bardella, 2000). Standard hardener was used for all the layups.

Table 5 - Material Properties of Ampreg 21 Epoxy Resin. Source: (Advanced Materials Technology, 2014), (Bardella, 2000)

Parameter	Symbol	Unit	Value
Tensile/Compressive Strength	$\sigma_{\max, T,C}$	MPa	561
Maximum Inter-Laminate Shear Strength	$\tau_{\max, ILSS}$	MPa	57
Young's Modulus	$E$	GPa	32.2
Poisson's Ratio	$\nu$	-	0.389
Shear Modulus	$G$	GPa	1.31

### 3.3.6. DC Wort NEMA G11 Prepared Glass Fibre Sheet

This material was chosen as it has been used by the CSIR in the past for creating hardpoints for transferring concentrated bearing loads from pins to surrounding material. It is manufactured by a local company called DC Wort and is regarded as being quasi-isotropic: when numerous plies are laminated in 0°, 90°, -45° and +45° angles repeatedly the behaviour of the laminate starts to approach that of an in-plane isotropic material (United States. Department of Defence., 2002). The material properties were obtained from DC Wort (DC Wort, 2016).

**Table 6 - Material Properties of DC Wort 6mm thick prepared glass fibre sheet. Source: (DC Wort, 2016)**

Parameter	Symbol	Unit	Value
Tensile Strength	$\sigma_{\max, C}$	MPa	300
Compressive Strength	$\sigma_{\max, C}$	MPa	300
Young's Modulus	$E_x$	GPa	25
Poisson's Ratio	$\nu_{xy}$	-	-
Shear Modulus	$G_{xy}$	GPa	-
Nominal Thickness	$T_{\text{NEMA G11}}$	m	0.006

### 3.4. Chapter Summary

The materials selected for this research are given and it is explained that these materials are identical to those used in the original Kwadira wing in order to provide a viable comparison of old versus new structural layouts. The process of obtaining the properties of the fibre reinforcements combined with their matrices is detailed and limitations of the testing are considered. Finally, mitigating solutions to these limitations are given and the properties of the selected materials are listed.

## 4. Loads, Structural Layout and Initial Sizing Model

Once the material properties were known, the loads on the wing needed to be assessed in order to conceptualise a new structural layout and find initial layouts that would be capable of resisting these loads.

### 4.1. Loads on the Kwadira Wing

#### 4.1.1. V-n Diagram and Selected Load Cases

The aircraft V-n diagram representing the flight envelope was drawn up according to methods specified by FAR23 (United States. Department of Transport., 1965) and detailed by Perini and Ithurbure for a utility-type aircraft. This diagram is used to read off the maximum load case points that the aircraft structure is to be designed for and is shown in Figure 10.

The first step is to define the positive (dark blue) and negative (purple) stall lines which represent the maximum aerodynamic lift force that the wings can produce without stalling (an aerodynamic phenomenon whereby the airflow over an aerofoil separates from the wing at high angles of attack which sharply reduces the lifting force produced). Next, a VNE (Velocity Never Exceed) line is drawn (light blue) and manoeuvre (dotted brown) and cruise (dotted green) speeds are defined. Finally, the influence of gusts at manoeuvre, cruise and dive speeds is considered (dotted purple, yellow and blue, respectively) and the maximum load points are read from the graph at the intersections of these lines.

The equation for the positive and negative stall lines (dark blue, purple) is given by FAR 23 as:

$$LF = 0.5\rho V^2 c_{L\ Max} S \quad (4.1)$$

Where:

$LF$  = Load Factor (g), equal to the lift produced by the wing at a defined velocity

$\rho$  = Air density ( $\text{kg/m}^3$ )

$V$  = Free stream speed (m/s)

$c_{L\ Max}$  = Aircraft maximum/maximum negative (effectively negative angle of incidence with airflow) coefficient of lift, taken to equal 1.55 and 0.4

$S$  = Total wing area ( $\text{m}^2$ )

To obtain the positive stall line, the  $c_{L\ Max}$  value of 1.55 is substituted into Equation 4.1. Below 1 g the aircraft is not producing enough lift to sustain flight and hence the green stall line is obtained at an airspeed of 18 m/s. Likewise, were the aircraft to attempt to fly inverted, it would need to fly at a velocity greater than 37 m/s in order to avoid stalling.

Similarly, FAR23 gives equations for the gust curves, and recommendations and limitations for cruise speed and VNE.

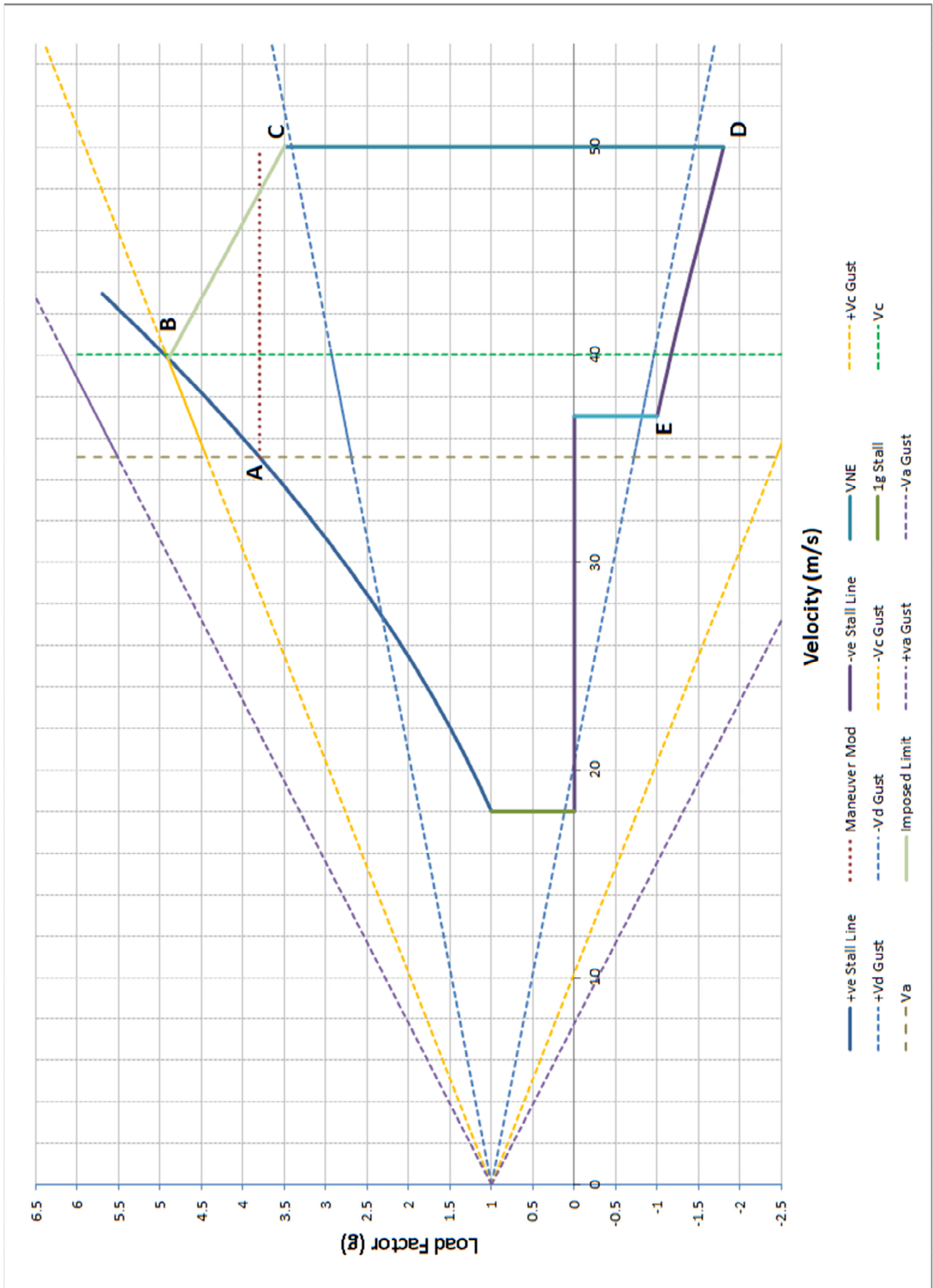


Figure 10 - V-n Diagram for the Kwadira UAV.

Three load cases were selected as being representative of the loading that the Kwadira aircraft experiences during flight. They are:

- **Point A (35 m/s, 3.8 g)**: This is the maximum positive load case that the aircraft will experience at manoeuvring speed  $V_a$ . This is also the highest speed at which the wing control surfaces will be allowed to be fully deflected. The point is found by following the  $V_a$  line (dotted brown) upwards towards the positive  $V_a$  gust line (dotted purple). Since the wing will stall and hence not produce lifting force above the positive stall line (solid blue), point A is taken to be the maximum manoeuvre speed load case.
- **Point B (40 m/s, 4.9 g)**: This is the maximum positive load case that the aircraft will experience at cruise speed  $V_c$ . Typically control surfaces will not be deflected at this speed. The point is found by following the  $V_c$  line (green dotted) upwards towards the positive  $V_c$  gust line (yellow dotted). Since the wing will stall and hence not produce lifting force above the positive stall line (solid blue), point B is taken to be the maximum cruise speed load case.
- **Point D (50 m/s, -1.75 g)**: This is the maximum negative load case that the aircraft will experience at never-exceed-speed (VNE). The point is found by following the VNE line (solid light blue) downwards towards the negative stall line (solid purple). Since the wing will stall and hence not produce lifting force below the negative stall line (solid purple), point D is taken to be the maximum negative load case.

#### 4.1.2. XFLR5 Analyses and Lift Distribution

Once the load cases were determined, the wing was modelled in XFLR5 6.03. Aerofoil polars were created for the SD7062 aerofoil between Reynold's numbers of  $2.5 \times 10^3$  and  $1.5 \times 10^6$  from an angle of  $-10^\circ$  to  $+20^\circ$  using XFLR5. Aerofoil polars are sets of data that detail the aerodynamic performance of an aerofoil such as coefficients of lift, drag and pitching moment at varying Reynold's numbers as defined by the flow velocity. Polars were also created for the aerofoil with a  $15^\circ$  down flap at 75% chord in order to simulate the flap on the outboard section of the wing as is shown in Figure 11.

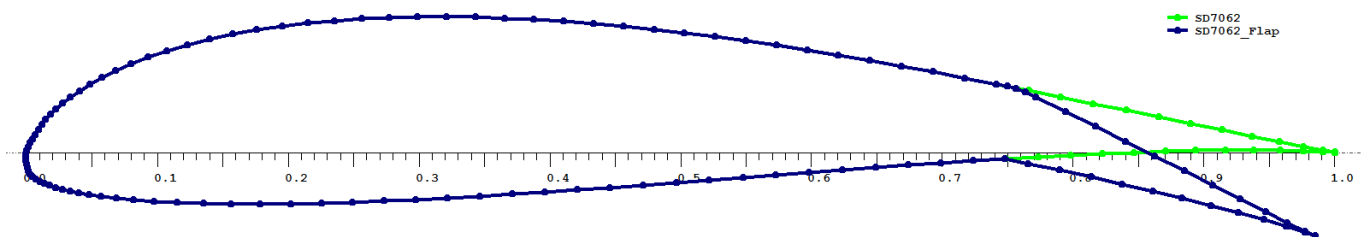


Figure 11 - SD7062 and SD7062\_Flap as plotted by XFLR5.

The wing without flap deflection was then analysed at 40 m/s and 50 m/s and with the flap deflected at 35m/s. The Vortex Lattice Method was used with an air density of  $1.2 \text{ kg/m}^3$  and the maximum number of allowed panels spread evenly over the surface of the wing. The vortex lattice mesh that was used can be seen in Figure 12.

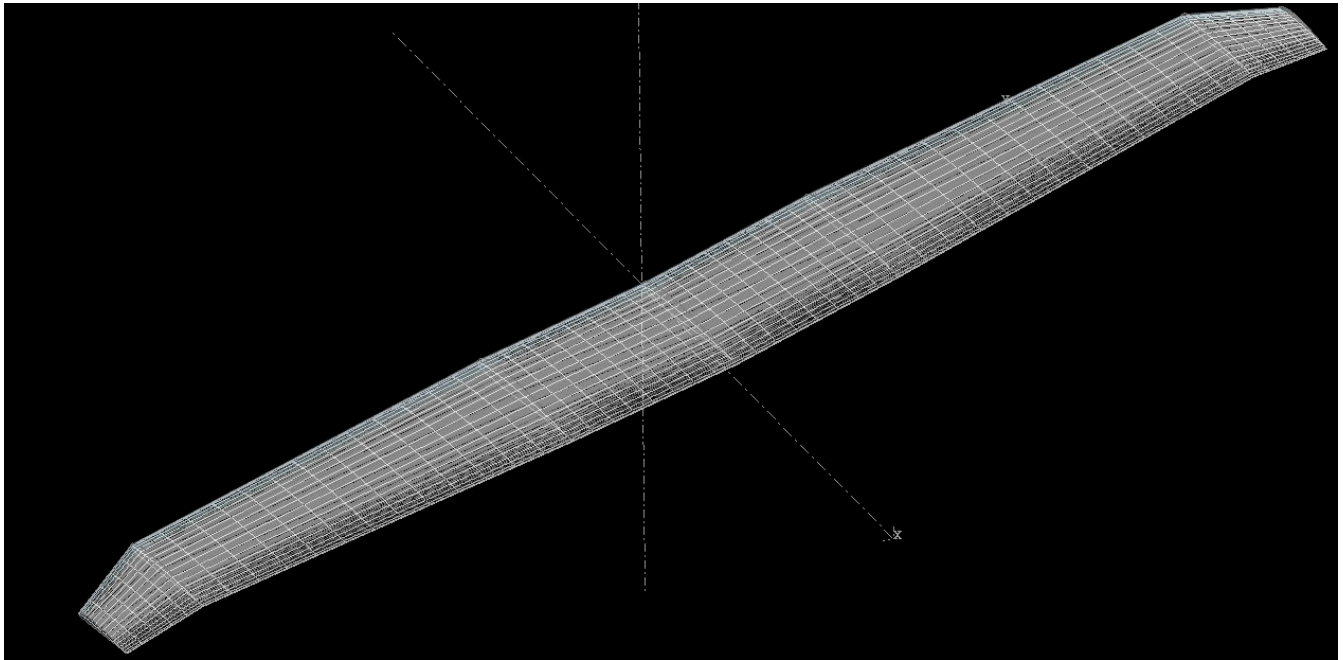


Figure 12 - Vortex-Lattice panels as plotted by XFLR5

The maximum load factors of 3.8 g, 4.9 g and -1.75 g were multiplied by the aircraft MTOW of 75 kg to obtain the lifting force generated by the wings at those load cases. The  $c_L$  (wing total lift coefficient) vs lift force ( $F_z$ ) and the  $c_L$  vs angle of attack (Alpha) graphs generated by XFLR5 (Figure 13) were then used to determine the angle of attack at which the wing produces the lifting force required by the load cases. The angles were found to be 15 °, 9 ° and -8 ° respectively.

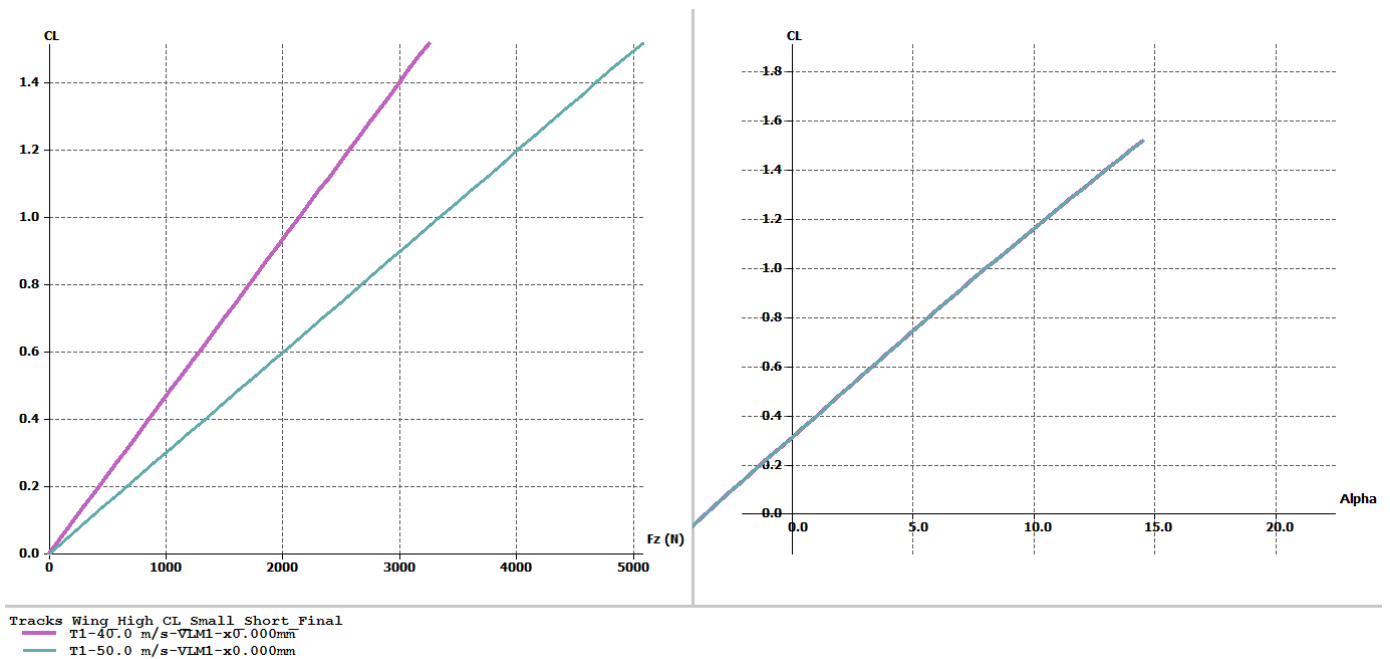


Figure 13 – XFLR5 plots of  $Cl-F_z$  and  $Cl$ -Alpha for the Kwadira wing.

The operating points corresponding to the angles of attack determined above were then exported as .CSV files and opened in Microsoft Excel. The operating points give values for the wing chord, local lift coefficient ( $c_l$ ), local total drag coefficient ( $c_D$ ) and local aerofoil pitching moment ( $c_m$ ) at discrete locations across the wing span. Figure 14 below shows an XFLR5 plot of local aerofoil lift coefficient as a function of wing span. The  $c_l$ ,  $c_D$  and  $c_m$  values were then integrated across the wing span to obtain the actual lift and pitching moment distributions across the wing using equations 4.2 to 4.4:

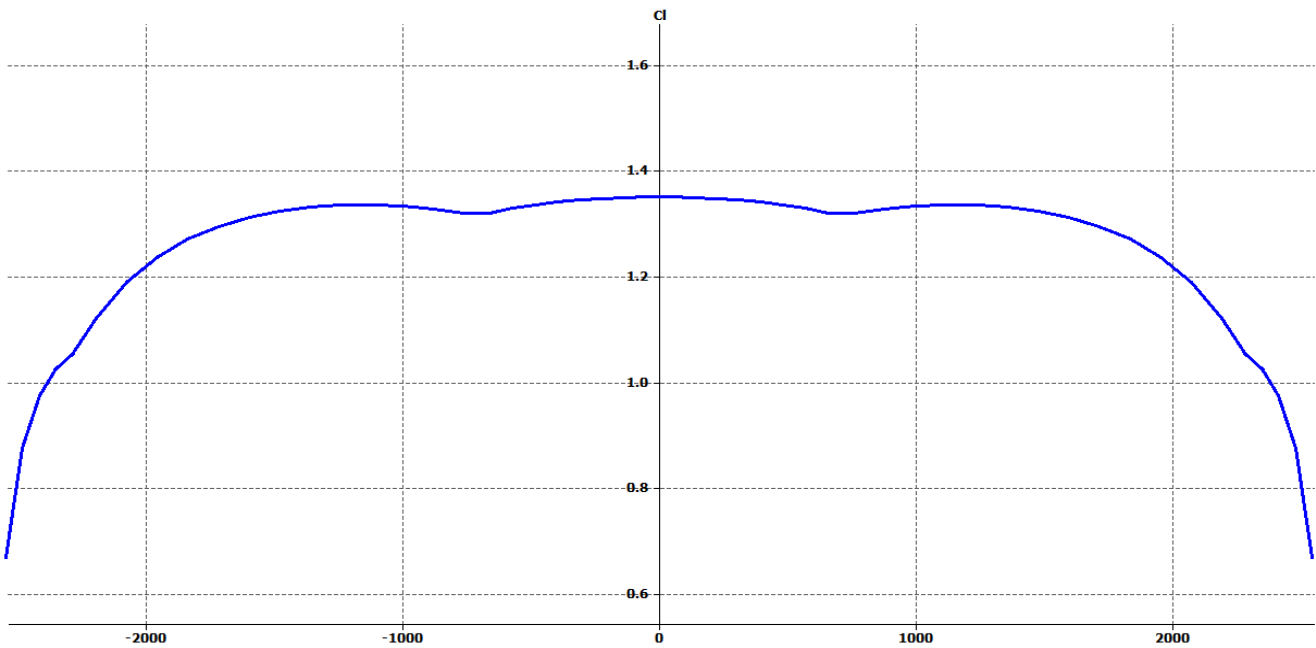


Figure 14 – XFLR5 plot of  $c_l$ -Wingspan for the Kwadira wing at 15 ° angle of attack for the 4.9 g, 40 m/s load case

$$L(x) = 0.5\rho V^2 \int_{x=b/2}^{x=0} c(x)c_l(x) dx \tag{4.2}$$

$$D(x) = 0.5\rho V^2 \int_{x=b/2}^{x=0} c(x)c_D(x) dx \tag{4.3}$$

And

$$T(x) = 0.5\rho V^2 \int_{x=b/2}^{x=0} c(x)^2 c_m(x) dx \tag{4.4}$$

Where:

$L(x)$  = Lift distribution over the wing span (N)

$D(x)$  = Drag distribution over the wing span (N)

$T(x)$  = Pitching moment distribution over the wing span (N.m)

$\rho$  = Air density ( $\text{kg/m}^3$ )

$V$  = Free stream speed (m/s)

$c$  = Local wing chord (m) at a span-wise location along the wing

$c_l$  = Local lift coefficient at a span-wise location along the wing

$c_D$  = Local total drag coefficient at a span-wise location along the wing

$c_m$  = Local pitching moment coefficient at a span-wise location along the wing

$b/2$  = Wing semi-span (m)

### 4.1.3. Tail Boom Loads

A similar process as described above was used to obtain the loads generated by the horizontal and vertical tail surfaces during flight: XFLR5 and Microsoft Excel were used to create aerofoil polars for the SD8020 aerofoil, create a vortex-lattice mesh, analyse the mesh at various airspeeds, obtain the horizontal and vertical tail lift distributions, and calculate the tail loads.

It was decided to take a conservative approach to the tail boom loads and use the maximum lift force (horizontal tail) and maximum sideforce (vertical tail) that the tail surfaces could produce at the selected speeds. This would represent hard manoeuvring or sudden sideways gusts on the aircraft. These maximum loads were taken to be the maximum lift that the tail surfaces could produce before stalling: an aerodynamic phenomenon where an aerofoil surface ceases to produce lift due to flow separation from the surface caused by excessive angles of incidence with the airflow.

The loads applied to the wing through the tail boom socket at the selected load cases are explained below:

- At the Point A load case (refer to Figure 10) at manoeuvre speed  $V_a$  the maximum lift force generated by the horizontal tail at this speed (132 N) and the maximum sideforce generated by the vertical tail (162 N) were added to the loads generated by the wing itself. The application point of these shear loads is at the wing-tail boom junction and the moments generated by these loads were calculated using the distance from this junction to the centres of the horizontal and vertical tail areas.
- At the Point B load case at cruise speed  $V_c$  the maximum lift force generated by the horizontal tail at this speed (190 N) was added to the loads generated by the wing itself. The application point of this shear load is at the wing-tail boom junction and the moment generated by this load was calculated using the distance from this junction to the centre of the horizontal tail area.
- At the Point D load case at dive speed  $V_d$  the maximum negative lift force generated by the horizontal tail at this speed (-122 N) was added to the loads generated by the wing itself. The application point of this shear load is at the wing-tail boom junction and the moment generated by this load was calculated using the distance from this junction to the centre of the horizontal tail area.

### 4.1.4. Safety and Build Factors, Ultimate Loads

FAR 23 (United States. Department of Transport., 1965) specifies that the loads obtained from the V-n diagram are to be seen as the Limit Loads of the aircraft: loads that the aircraft is expected to be capable of withstanding continuously during its service life. FAR 23 further calls for these loads to be scaled up to Ultimate Loads: loads that the aircraft is expected to be able to withstand for a maximum of three seconds and which are expected to cause significant damage to the aircraft structure but still allow the aircraft to land safely.

The CSIR standard policy is to use a:

- Load safety factor of 1.5 to account for uncertainties in the loads applied to the wing as predicted by XFLR5. This is an industry standard factor prescribed by FAR 23 (United States. Department of Transport., 1965)
- Build safety factor of 1.25 to account for variation in materials and wet-layup manufacturing processes.

These safety factors are multiplied together to obtain a final safety factor of 1.875 which is used to scale the limit loads to ultimate loads which are applied to the wing during design and analysis.

The compressive strengths of FRPs are in most cases lower than their tensile strengths due to material irregularities and imperfect fibre orientations which cause buckling. This was accounted for by assuming a conservative uni-directional carbon fibre tape compressive strength ratio of 0.55 of the tensile strength (Corderley, 1994). This resulted in a value of 0.55 of the tensile strength of the 343GSM UD carbon fibre tape being used for designing spar caps in compression.

#### **4.1.5. Shear Force, Bending Moment and Torque Diagrams**

Once the lift distributions and tail boom loads were found, the shear force, bending moment and torsion diagrams were constructed for all three of the load cases. It must be noted that the wing spar carry-over pins, responsible for transferring bending moments from one wing to the other, are located at -0.13 m and +0.13 m from the fuselage centreline and so the shear force and bending moment diagrams (Figures 14 and 15) have discontinuities at these points representing these pins. The wing root rib spigots, responsible for resisting the shear and torsional loads of the wing, are located at 0.18 m from the fuselage centreline and this discontinuity is shown in the torsion diagram. Another point to note is the sharp increase in wing torsion between 0.5 m and 1.0 m as shown in Figure 16 – this is due to the horizontal tail loads entering the wing at the tail boom socket before being transferred to the rest of the aircraft.

Inspection of the shear force, bending moment and torsion diagrams revealed that the loads for Point B (40 m/s, 4.9 g) were significantly higher than those of Point A (35 m/s, 3.8 g) and so Point A was not used during the rest of the analyses. Point B was therefore used as the maximum positive load case and Point D as the maximum negative load case. The shear force, bending moment and torsion diagrams for these points were used in the initial sizing model to determine the stresses in the wing structural components and to design layups capable of resisting these loads and are shown in Figures 15 through 20.

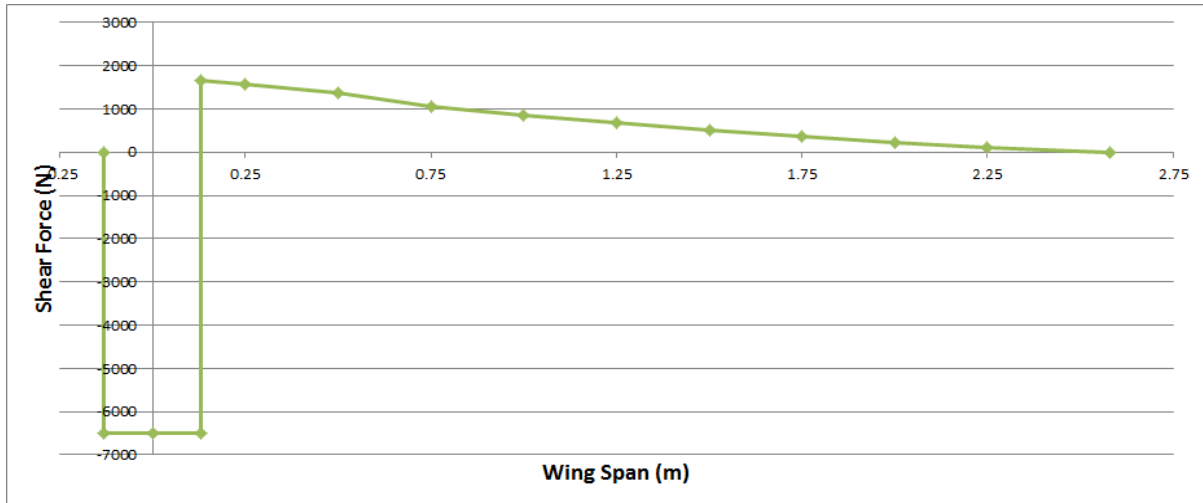


Figure 15- Shear force diagram of the Kwadira UAV for the Point B load case (40 m/s, 4.9 g)

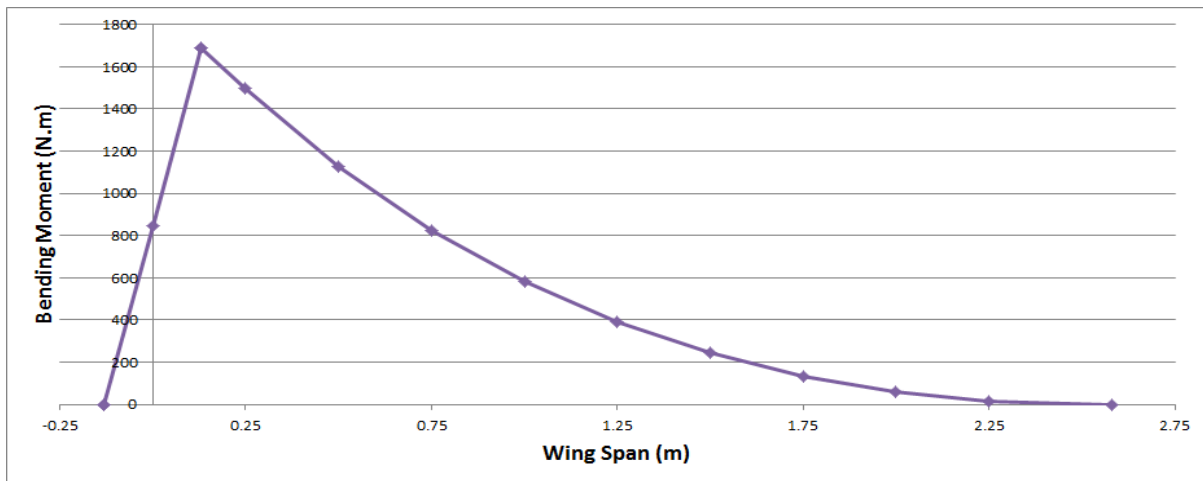


Figure 16- Bending moment diagram of the Kwadira UAV for the Point B load case (40 m/s, 4.9 g)

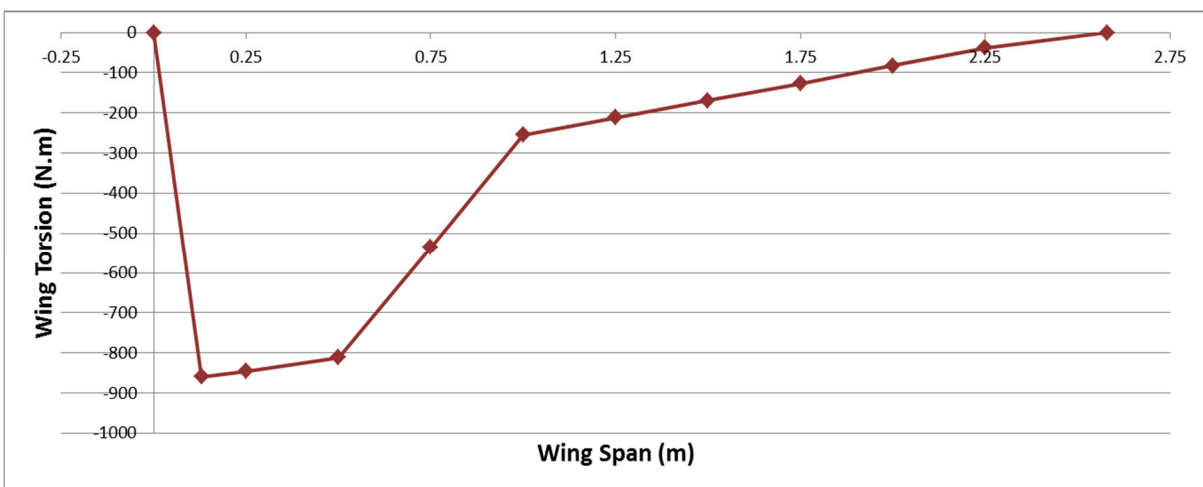


Figure 17- Torque diagram of the Kwadira UAV for the Point B load case (40 m/s, 4.9 g)

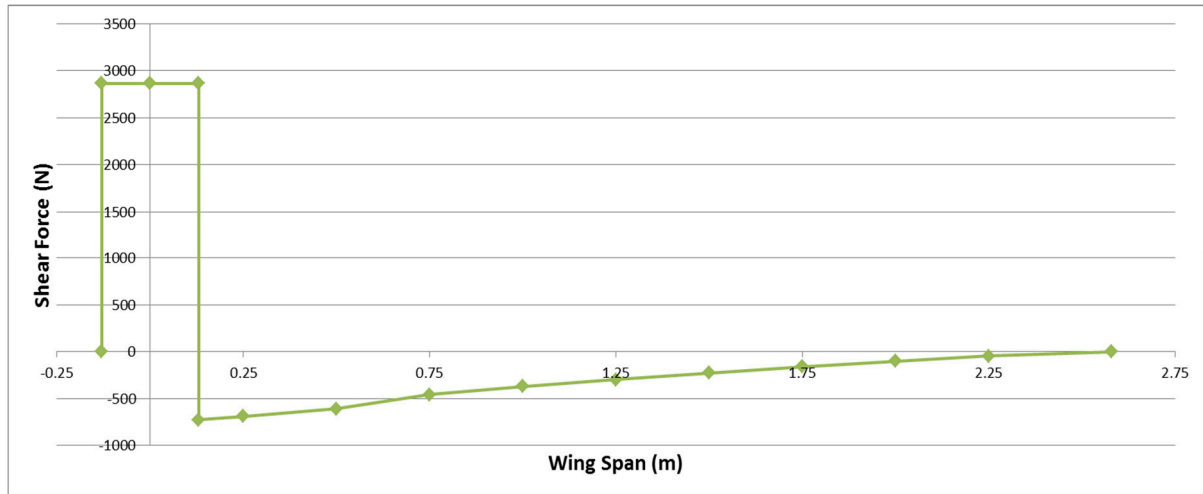


Figure 18- Shear force diagram of the Kwadira UAV for the Point D load case (50 m/s, -1.75 g)

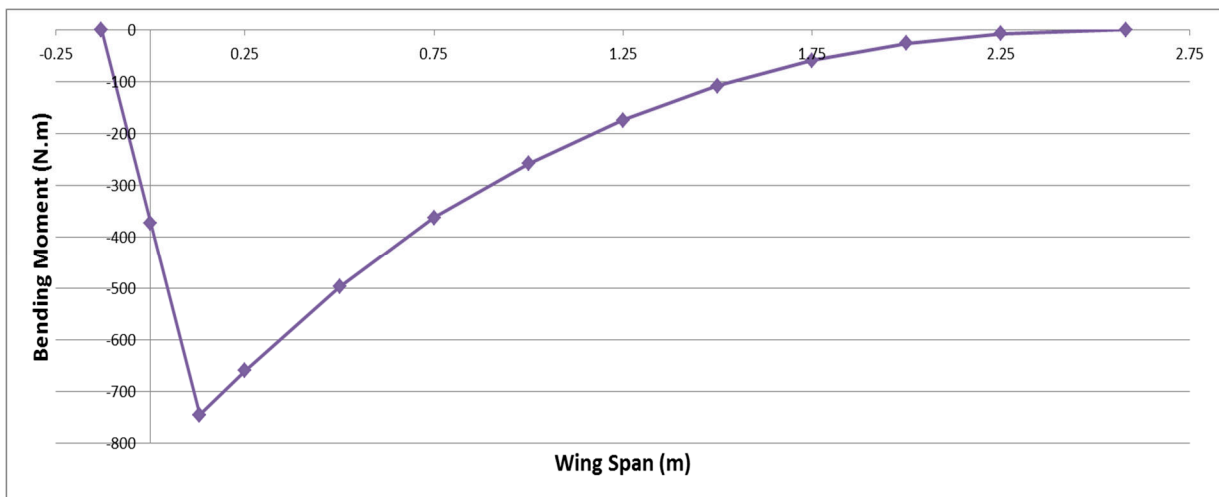


Figure 19- Bending moment diagram of the Kwadira UAV for the Point D load case (50 m/s, -1.75 g)

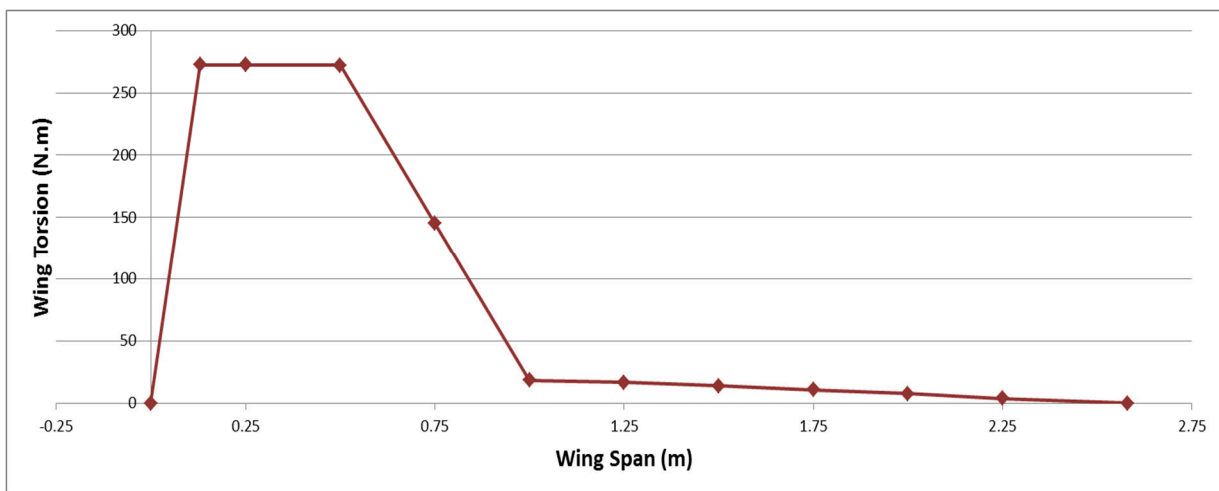


Figure 20- Torque diagram of the Kwadira UAV for the Point D load case (50 m/s, -1.75 g)

## 4.2. Proposed New Structural Layout

### 4.2.1. Description of Structural Components

Modern aircraft wings are constructed from a combination of the following components:

- Spar caps: Forming the flanges of the main beam or spar of the wing, the spar caps' function is to resist the bending loads created by the non-uniform span-wise lift distribution of the wing aerodynamic surfaces.
- Stringers: Running in the span-wise direction, stringers are small webs perpendicular to the wing skin with the primary function of stabilising the wing skins in the span-wise direction. The stringers' secondary function is to resist the bending loads created by the non-uniform span-wise lift distribution of the wing aerodynamic surfaces.
- Spar web: Forming the web of the main spar of the wing, the spar web's primary function is to resist the shear loads created by the non-uniform span-wise lift distribution of the wing aerodynamic surfaces. The spar web's secondary function is to close the torsion box created by the spar web, wing skins and rear web.
- Rear web: Forming the web of the rear spar, the rear web's primary function is to resist the shear loads created by the non-uniform span-wise lift distribution of the wing aerodynamic surfaces along with the main spar web. The rear web's secondary function is to close the torsion box created by the spar web, wing skins and rear web.
- Wing skins: Forming the aerodynamic surface of the wing, the skins' primary function is to provide the aerodynamic lift required for the aircraft to fly. The secondary function is to resist the torsion created by the aerodynamic moment of the wing together with the main and rear shear webs. The usually thin wing skins are stiffened with the aid of stringers, webs and ribs.
- Chord-wise ribs: Running in a chord-wise direction, ribs' primary function is to maintain the shape of the skins and transfer shear and torsion loads to the spar caps and webs. The ribs' secondary function is to stabilise the stringers, spar caps and webs.
- Pins: Aircraft with removable wings use pins to transfer shear and torsional loads from the root rib to the fuselage and bending loads between spars.

### 4.2.2. Proposed New Structural Layouts

As described in Chapter 1, the current Kwadira wing structural layout is of the semi-monocoque with stiffened skin variety. It makes extensive use of GFRP foam sandwich construction in order to stabilise the wing skins and spar webs without using internal ribs. It has also been mentioned that such a construction tends to be heavier than desired due to the inability of excess resin to be removed during a vacuum bagging process, absorption of resin by the core material and the large beads of cotton-resin mixture needed to join parts together. The preparation time and edge finishing of the core material is also a limiting factor in the manufacturing of the wing. The objectives of this research were to decrease the weight of the wing and find a more efficient manufacturing process and these were to be accomplished by eliminating the core material from the wing construction.

In proposing a new structural layout, various combinations of spars, webs, stringers, skin and ribs were considered that would negate the need for sandwich construction to stabilise the skin and webs. This resulted in a semi-monocoque construction with stiffened skin. Two separate yet related layouts were chosen for analysis based on methods described by Megson (Megson, 2013) and Peery (Peery, 1982) and work done by and Vasiliev and Razin (Vasiliev & Razin, 2012). These layouts are:

1. Traditional Metal Wing Layout (TMWL), shown in Figure 21, consisting of:

- a. Unidirectional CFRP spar caps
  - b. GFRP main shear webs
  - c. Thin GFRP wing skins, stiffened by
  - d. GFRP chord-wise ribs and
  - e. A GFRP sub-spar
  - f. Stainless steel pins for transferring loads between spars and to and from the fuselage
2. Tri-Directional Rib Lattice (TDRL), shown in Figure 22, consisting of:
- a. Unidirectional CFRP spar caps
  - b. GFRP main shear webs
  - c. Thin GFRP wing skins, stiffened by
  - d. A tri-directional angle-grid rib lattice
  - e. Stainless steel pins for transferring loads between spars and to and from the fuselage

Chapter 5 describes the iterative process by which these layouts were analysed and optimised using FEA before a final layout was decided upon, while Chapters 6 and 7 detail the manufacturing and testing of the chosen layout.

Two points must be mentioned that are applicable to both layouts:

- Firstly, due to the geometry of the Kwadira fuselage and the placement of components inside it, it was necessary to conform to the originally designed spar layout and wing joining scheme consisting of spar roots angled forward and aft (necessary in order to keep the port and starboard spars inline) which are joined to each other using two high-tensile stainless steel pins.
- Secondly, it was also necessary to conform to the originally designed tail boom fitting geometry which requires two chord-wise ribs to transfer loads from the vertical and horizontal tails to the main spar web and rear shear web.

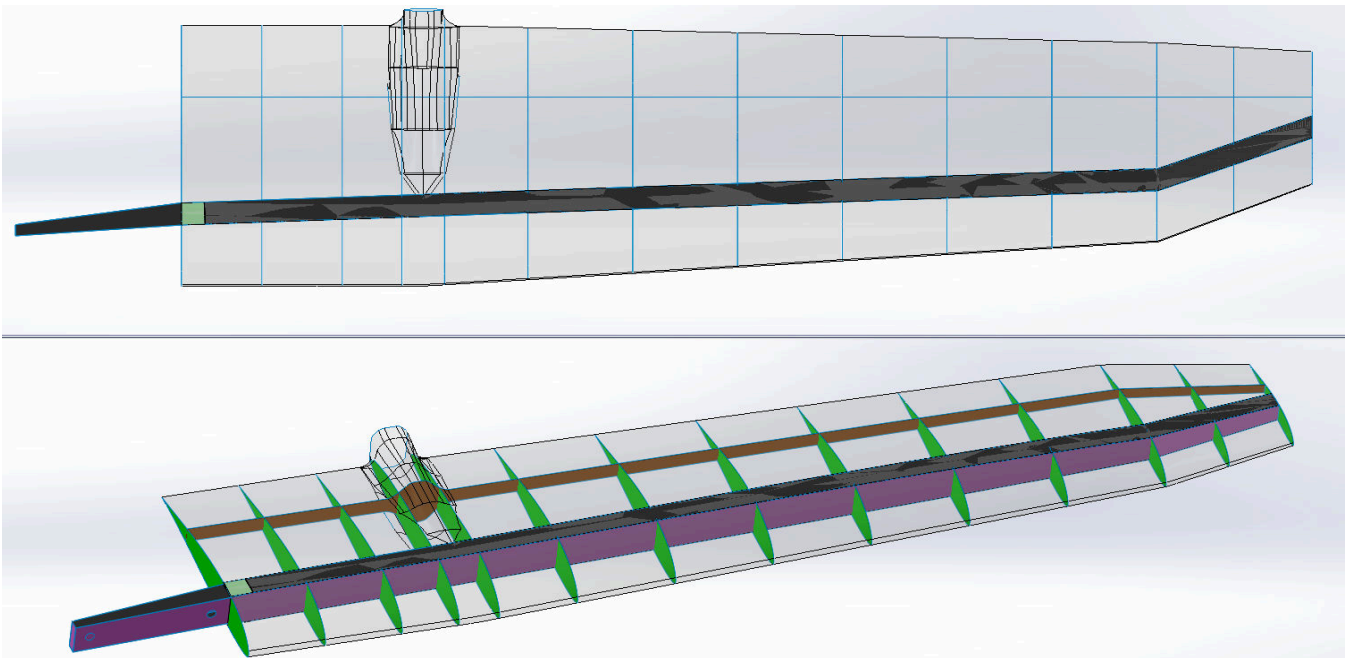


**Figure 21 - The first proposed structural layout consisting of a traditional metal wing layout with a rear web and several chord-wise ribs. Colour key: Spar caps – black, front shear webs – purple, rear shear web – orange, chord-wise ribs – green.**

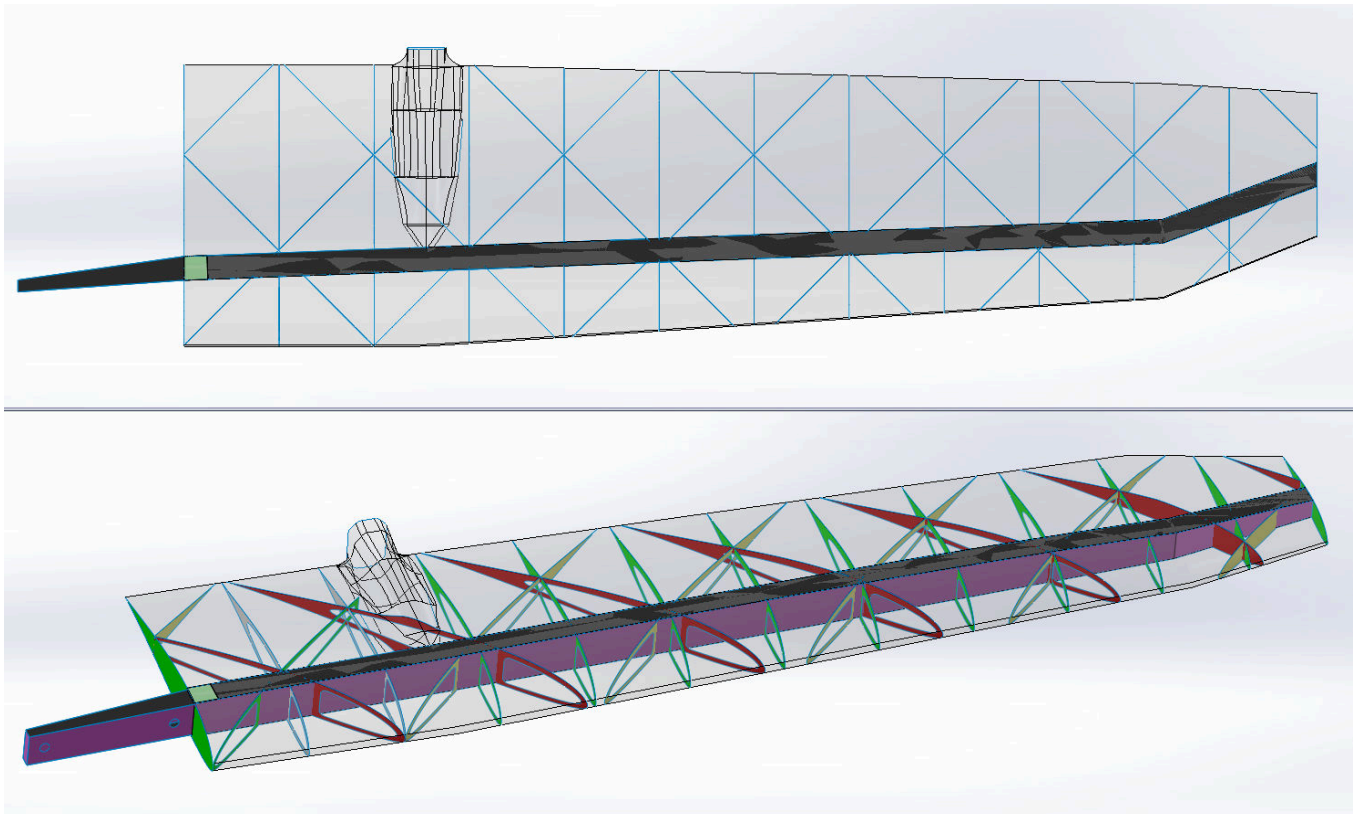


Figure 22 - The second proposed structural layout consisting of an angle-grid rib lattice inside the wing.  
 Colour key: Spar caps – black, front shear webs – purple, rear shear web – orange, chord-wise ribs – green, diagonal ribs – red, yellow

### 4.2.3. Structural Component Interactions

In the design of semi-monocoque wing structural components it is important to understand the secondary interactions between components. Some of the main interactions that should be taken note of include:

- Spar cap and main shear web / chord-wise rib interactions: Since it is assumed that the spar caps and main shear web essentially form a beam structure (either a C-shaped beam or an I-beam) chord-wise ribs play an important role in the buckling of the top section of the beam by effectively shortening the unsupported buckling distance between points along the beam. The span-wise spacing of the ribs therefore not only affects the stability of the skin but also of the spar (Arunkumar & Lohith, 2015).
- Rear shear web / chord-wise ribs: The rear shear web in the first proposed layout not only stabilises the skin in the span-wise direction, but also stabilises the chord-wise ribs in buckling.
- Diagonal ribs / chord-wise ribs: The torsion load generated by the wing pitching moment creates a  $\pm 45^\circ$  shear force in the wing skins and so the diagonal ribs in the second proposed layout are placed at  $\pm 45^\circ$  to most efficiently transfer the shear loading throughout the skins. The chord-wise and diagonal ribs also act to stabilise each other in this layout.

### 4.3. Initial Sizing Model

An initial sizing model was created in Microsoft Excel in order to obtain preliminary layouts for the various components of the new proposed structural layouts. Since manual composite strength and stiffness calculations are not the focus of this research several simplifying assumptions were made in order to obtain the initial layouts to be used as a starting point in the FEA process:

- It is assumed that the spar caps resist most of the bending loads in the wing due to the higher stiffness of the uni-directional Carbon fibre tape compared to the woven glass fibre skin and webs. This idealisation is based on methods given by Megson (Megson, 2013).
- It is assumed that the primary components used to resist torsion loads are the wing skins, main shear web and rear shear web since they form the largest closed ‘torsion box’.
- It is assumed that the primary component used to resist shear loads is the main shear web.
- It is assumed that the root rib pins primarily transfer shear loads to the fuselage, while the spar root pins primarily transfer bending loads between the port and starboard wing spars.

It must be mentioned that the preliminary layouts chosen represent the fibre reinforcement thicknesses that would be capable of resisting the worst-case loads as given by points A, B and D on the V-n diagram. It must also be noted that no literature was found detailing shear flow calculations for wings with diagonal ribs and so the initial layouts calculated for the traditional metal wing layout were used as a starting point for the angle-grid layout as well.

#### 4.3.1. Spar Caps

The spar caps were sized according to the worst case bending moment diagram by using the classical bending stress equation assuming single axis bending with vertical symmetry:

$$\sigma_{Bending}(x) = \frac{M(x)y(x)}{I(x)} \quad (4.5)$$

And the equation for the moment of inertia of an offset rectangular section:

$$I_x(x) = \frac{bh(x)^3}{12} + bh(x)y(x) \quad (4.6)$$

Where:

$\sigma_{Bending}(x)$  = Bending normal stress (MPa) at a span-wise position along the wing, taken to equal the maximum tensile (for the bottom spar cap) and compressive (for the top spar cap) stress of the uni-directional Carbon fibre tape, modified with the safety and build factors mentioned in section 4.1.4.

$M(x)$  = Bending moment (N.m) at a span-wise location along the wing

$y(x)$  = Maximum thickness of the wing (m) at a span-wise location along the wing

$I(x)$  = Area moment of inertia (m<sup>4</sup>) at a span-wise location along the wing

$h(x)$  = Required thickness of spar cap at a span-wise location along the wing

$b$  = Width of the carbon fibre tape, taken to be 50mm.

By combining the above two equations and making use of a Newton-Rhapson routine coded into Excel the required thickness  $h(x)$  of the spar caps was found at discrete points along the wing span. Using the nominal thickness of the carbon fibre tape (0.3mm per layer) a solution was then found for the required number of layers of carbon fibre tape at points along the wing as shown in Table 7.

**Table 7 - Top and bottom spar cap initial layups**

Span-Wise Position (x)	Layers Top	Layers Bottom
0	3	2
0.13	6	3
0.25	5	3
0.5	4	2
0.75	3	2
1	2	1
1.25	2	1
1.5	1	1
1.75	1	1
2	1	1
2.25	1	1
2.58	1	1

### 4.3.2. Shear Flow

The shear flow in the wing skins, webs and ribs was determined using methods detailed by Megson (Megson, 2013) and Peery (Peery, 1982) and by using the shear force and torsion diagrams (Figures 15, 16, 18 and 20). Since it is assumed that the wing skins and webs carry no bending stress, the closed torsion boxes created by points 1, 2, 3 and 4 as shown in Figure 23 below can be analysed using the equations for shear flow due to torsion in thin shell members:

$$T_R = \sum_{R=1}^N 2A_R q_R \tag{4.7}$$

$$\frac{d\theta}{dz} = \frac{1}{2A_R G} (-q_{R-1} \delta_{R-1} + q_R \delta_R - q_{R+1} \delta_{R+1}) \tag{4.8}$$

Where:

$T_R$  = Wing torsion load at section R (N.mm)

$A_R$  = Closed cell area of section R (mm<sup>2</sup>)

$q_R =$  Closed cell shear flow of section R (N/mm)

$\delta_R =$  Closed cell perimeter of section R (m)

$\frac{d\theta}{dz} =$  Closed cell rate of twist

By writing Equation 4.8 for each closed cell (it is assumed that the rear section of the aerofoil behind web 3-4 does not carry any significant load) there are N equations, and with Equation 4.7 there are the necessary N+1 equations to obtain a solution for the shear flows and the rate of twist using matrix methods in Microsoft Excel.

At a selected point along the wing the lengths of the webs 1-2 and 3-4, the lengths of the aerofoil curves 1-2, 1-3 and 2-4 and the areas 1-2 and 1-2-3-4 were obtained from SolidWorks CAD, and the value of the wing torsion was obtained from the torsion diagrams (see Figures 17 and 20).

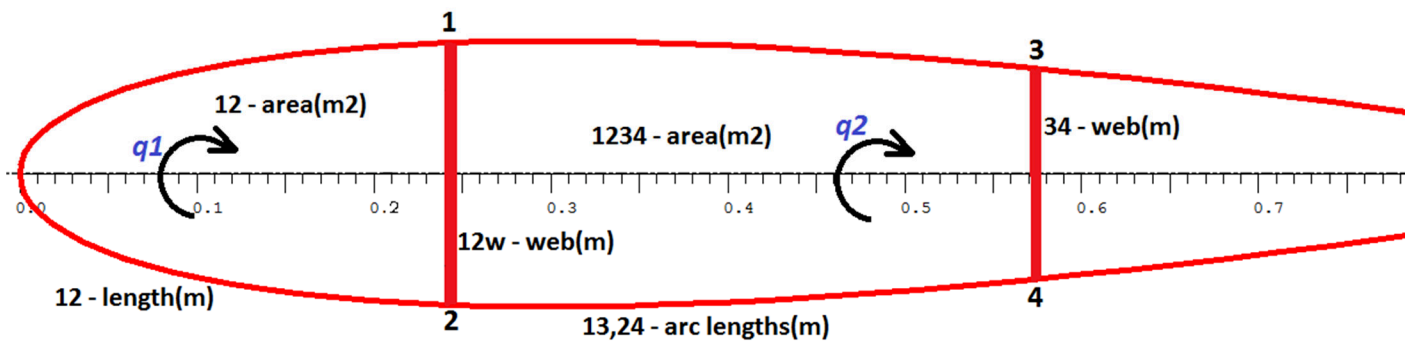


Figure 23 - Diagram showing the closed cells 12 and 1234 and shear flows q1 and q2 that were used to find the shear flow in the wing components

Once the shear flows had been calculated a method detailed by Collins (Collins, 1985) was used to determine the layups needed for the wing skins, webs and ribs (see Table 8) by equating the shear flow to GFRP layup weight using Equation 4.8:

$$W_{GFRP} = q_{component} \frac{\rho_{GFRP}}{\tau_{Max,GFRP}} \tag{4.9}$$

Where:

$W_{GFRP} =$  Estimated weight of glass fibre needed for component (g/m<sup>2</sup>)

$q_{component} =$  Shear flow in component

$\rho_{GFRP} =$  Density of glass fibre (kg/m<sup>3</sup>)

$\tau_{Max,GFRP} =$  Max shear stress of glass fibre

Using a value of 1018 kg/m<sup>3</sup> for GFRP density and 65.6 MPa for GFRP ultimate shear strength (Corderley, 1994) a GFRP weight factor of 15.5 was obtained. This factor was multiplied by the calculated shear flows and the safety and build factors to find a minimum required GFRP weight in g/m<sup>2</sup>.

### 4.3.3. Wing Skins

The wing skins were sized by performing shear flow calculations at 4 span-wise points along the wing: The wing root, the intersection of the wing and tail boom, before the aileron and at the tip as shown in Figure 23. Using SolidWorks, chord-wise sections were made at the points shown in Figure 24 and the lengths and areas required for the shear flow calculations (as shown in Figure 23) were obtained by using the SolidWorks Measure tool (see Figure 25). The required layups are shown in Table 8.

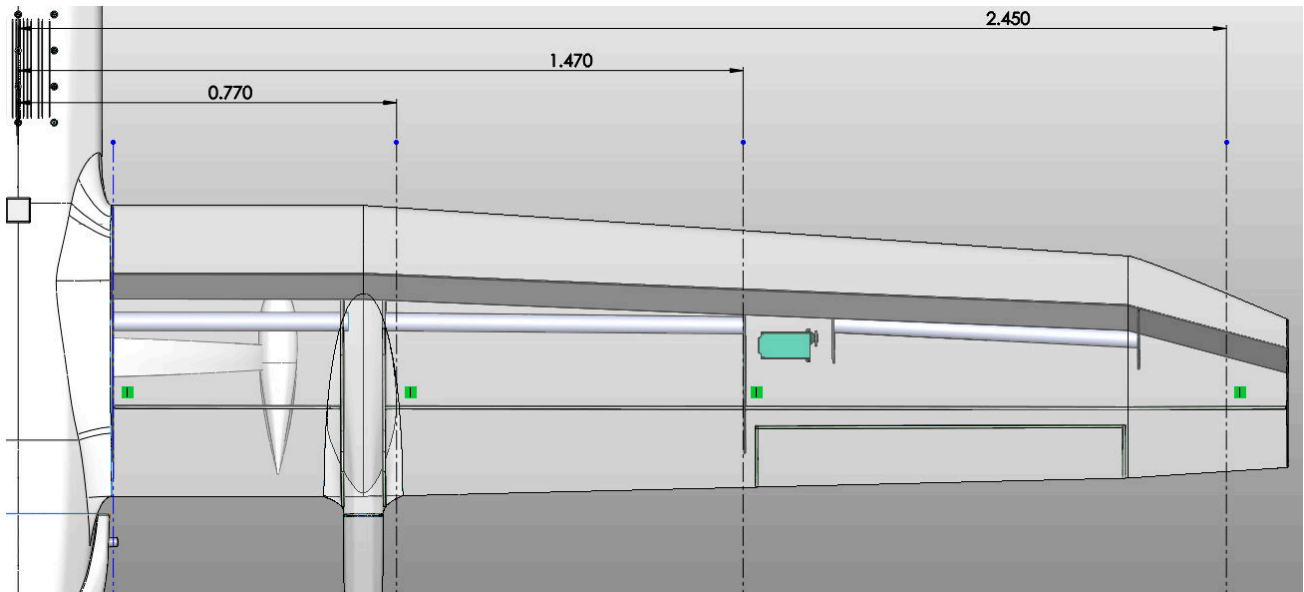


Figure 24 - The locations at which the wing skins' shear flow was calculated

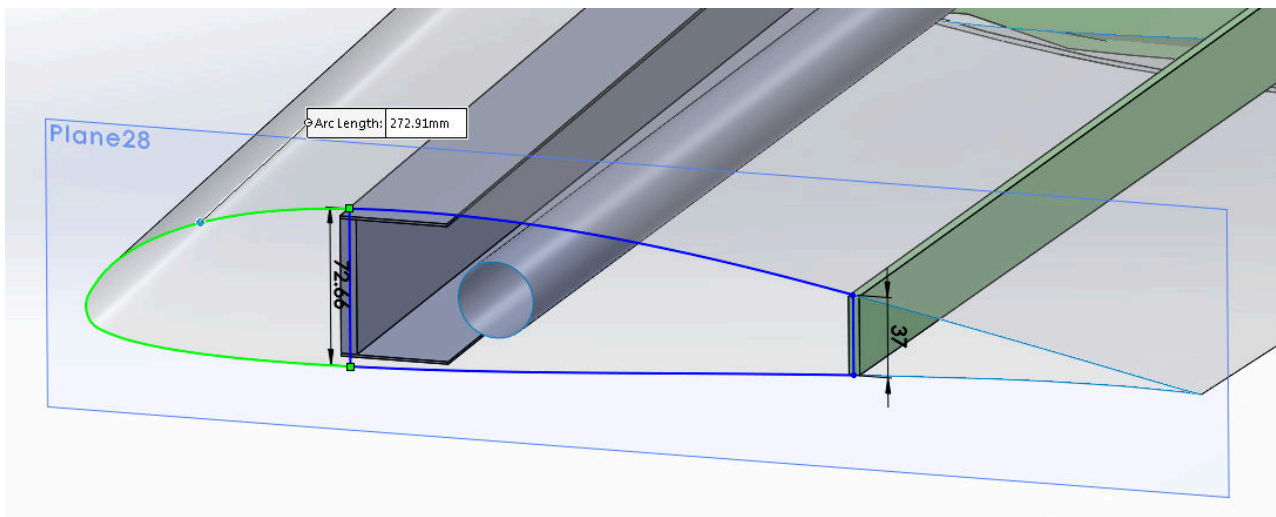


Figure 25 - SolidWorks image showing how the lengths and areas of the shear flow sections were obtained.

**Table 8 - The maximum shear flow, weight of GFRP required and initial layup for the wing skins**

<b>Section</b>	<b>Maximum Shear Flow (N/mm)</b>	<b>W<sub>GFRP</sub> Required (g/m<sup>2</sup>)</b>	<b>Initial Layup</b>
Wing Root	30.5	546	2 x 106GSM 0°/90°, 4 x 106GSM ±45°
After Tail Boom	21.3	331	2 x 86GSM 0°/90°, 3 x 106GSM ±45°
Before Aileron	11.0	171	2 x 86GSM 0°/90°, 2 x 106GSM ±45°
Wing Tip	5.9	92	2 x 86GSM 0°/90°, 2 x 86GSM ±45°

#### 4.3.4. Shear Webs

The same four points along the wing as were chosen for the wing skins were chosen for sizing the shear webs. The shear flow due to lift (obtained using the shear force diagram, see Figure 9) was added to the difference between shear flows  $q_2$  and  $q_1$  (see Figure 23) for each point.

**Table 9 - The maximum shear flow, weight of GFRP required and initial layup for the shear webs**

<b>Section</b>	<b>Maximum Shear Flow (N/mm)</b>	<b>W<sub>GFRP</sub> Required (g/m<sup>2</sup>)</b>	<b>Initial Layup</b>
Wing Root	26.1	405	1 x 106GSM 0°/90°, 3 x 106GSM ±45°
After Tail Boom	11.6	181	1 x 106GSM 0°/90°, 2 x 106GSM ±45°
Before Aileron	12.3	192	1 x 106GSM 0°/90°, 1 x 106GSM ±45°
Wing Tip	1.92	30	1 x 106GSM 0°/90°, 1 x 106GSM ±45°

### **4.3.5. Ribs**

The numerous ribs that are to be incorporated in the new structural layouts will experience the same shear flow as the wing skins that they are attached to, and so their initial layups were assumed to be the same as those of the wing skins.

### **4.3.6. Shear Pins**

The two 12 mm pins that transfer bending loads between the port and starboard spars and the four 10 mm pins that transfer shear loads from the wings to the fuselage were taken from the original Kwadira wing design since these have proven their structural integrity up to ultimate loads of 9 g in the original structural tests.

### **4.3.7. Initial Predicted Mass Reduction vs Current Wing**

A composite mass model that was constructed for the original Kwadira wing was used to estimate the mass of a wing with the new proposed structural layout as given by the initial layups described above. The model uses the basic wing geometry (given in Appendix A) and the layups of individual components to arrive at a final estimated wing mass and takes into account details such as paint mass, joining adhesive lines, web cleating strips, and fibre volume fractions.

The composite mass model predicted a total mass of 5.323 kg for the TMWL as given by the initial layups, which is a 21% improvement in the mass of the original Kwadira wing at 6.778 kg.

## **4.4. Chapter Summary**

The aircraft load cases were determined by using a V-n diagram as prescribed by FAR 23 (United States. Department of Transport., 1965). The chosen load cases were analysed using XFLR5 and the aerodynamic coefficients were processed in Excel to obtain lift, pitching moment and torsional loads across the wing span. These loads were then represented using shear force, bending moment and torsion diagrams. Two different new structural layouts were proposed and their component interactions were discussed. Excel spreadsheets were used to obtain initial layups for the spars, skins, webs and ribs by finding both direct stresses and shear flows in the components. Finally, a composite mass model was used to estimate the weight savings gained from the new structural layout. It was predicted that a weight saving of 21% is possible by using the initial layups.

## 5. FEA Analysis and Optimisation

Once the loads on the wing and the initial layups had been determined the wing structural layouts were modelled using SolidWorks premium 2016 and were subjected to FEA using SolidWorks Simulation Premium 2016. This was done in order to choose the most suitable structural concept, optimise the layups for weight and make predictions of the deflections expected while testing the wing in the CSIR Wing Structural Test Rig's whiffle tree.

An important point to note is the design and analysis methodology employed:

1. The wing was modelled in CAD using surfaces
2. An iterative FEA optimisation on the internal structural layout was performed using simplified fixtures and simulated aerodynamic loads
3. An iterative FEA optimisation on the component layups was performed using simplified fixtures and simulated aerodynamic loads
4. The final optimised layout and optimised layups were analysed using simulated fuselage fixtures and simulated aerodynamic loads as a final design check
5. The final layout and layups were analysed using simulated fuselage fixtures and simulated whiffle tree loads to predict the physical wing's behaviour during testing

### 5.1. SolidWorks CAD Model

#### 5.1.1. Surface Modelling

Since the original Kwadira wing was created as a solid entity in SolidWorks CAD a surface offset was created from this geometry that could be used for thin composite shell modelling. An effort was made to let the surface model be a true representation of the solid model.

The internal structural components were also modelled as surfaces and cut to size using the surface model of the wing skins. In an effort to lighten the internal components, cutouts were made in the centres of the ribs. Attention was paid to correctly model the bonded joining lines between components as they would be constructed and cleated to each other. The surface model is shown in Figure 26.

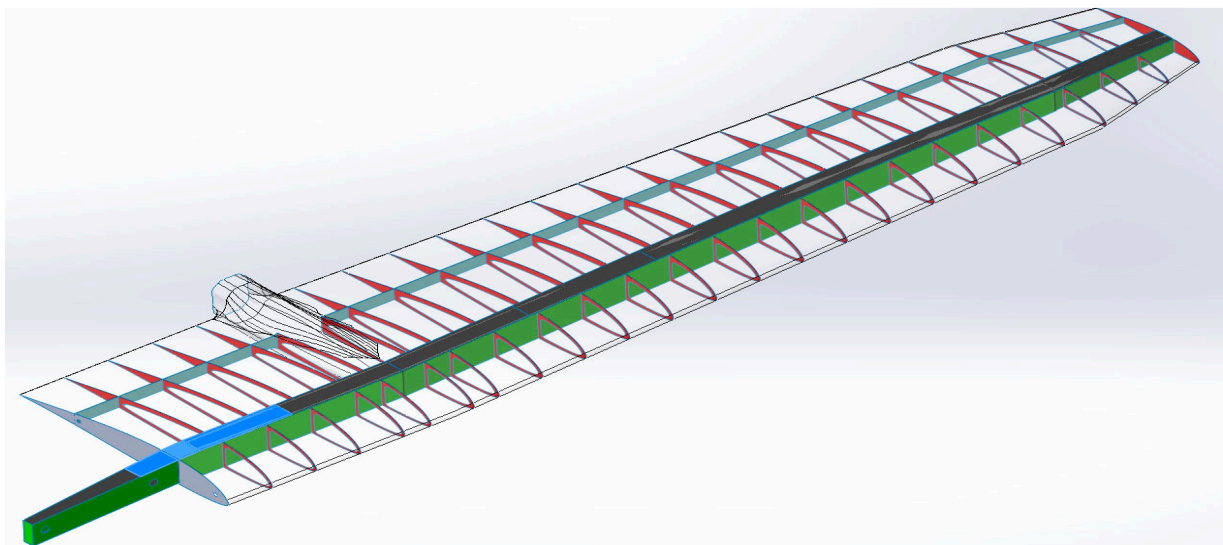


Figure 26 - SolidWorks CAD model showing the surface modelling of the Kwadira wing skins and internal structure. Note the separate spar cap sections (highlighted in blue).

### 5.1.2. Split Lines

Once the surface models had been created split lines were projected onto the surfaces where required in order to facilitate the application of loads to the model and specification of mesh refinement zones.

## 5.2. Material Property Input

The material properties given in Chapter 3 were input into SolidWorks Simulation by specifying material elastic and shear moduli, tensile and compressive strengths, Poisson’s ratios and shear moduli in both the 0° and 90° directions. The 343GSM unidirectional carbon fibre tape was only given properties in the 0° direction, indicating the material as being unidirectional, whereas the CFRP and GFRP woven cloths were given properties in both 0° and 90° directions. SolidWorks Simulation automatically calculates ply and laminate properties in different material directions.

When a ply is assigned an orientation, as is done in Section 5.3, an orientation of 0° indicates only 0° fibres for a unidirectional material and both 0° and 90° fibres (woven cloth) for a multi-directional material.

## 5.3. Laminate Property Assignment

### 5.3.1. Spar Caps

The 343GSM unidirectional Carbon fibre tape orthotropic material model was assigned to the spar caps with the number of layers of tape being specified for each section as defined in Chapter 4. Each spar cap section was checked to ensure the material was oriented in the 0° direction spanwise along the wing as can be seen in Figure 27. Care was also taken to ensure that the top faces of the spar cap sections were aligned with each other so that their offset from the wing surface could be modelled correctly.

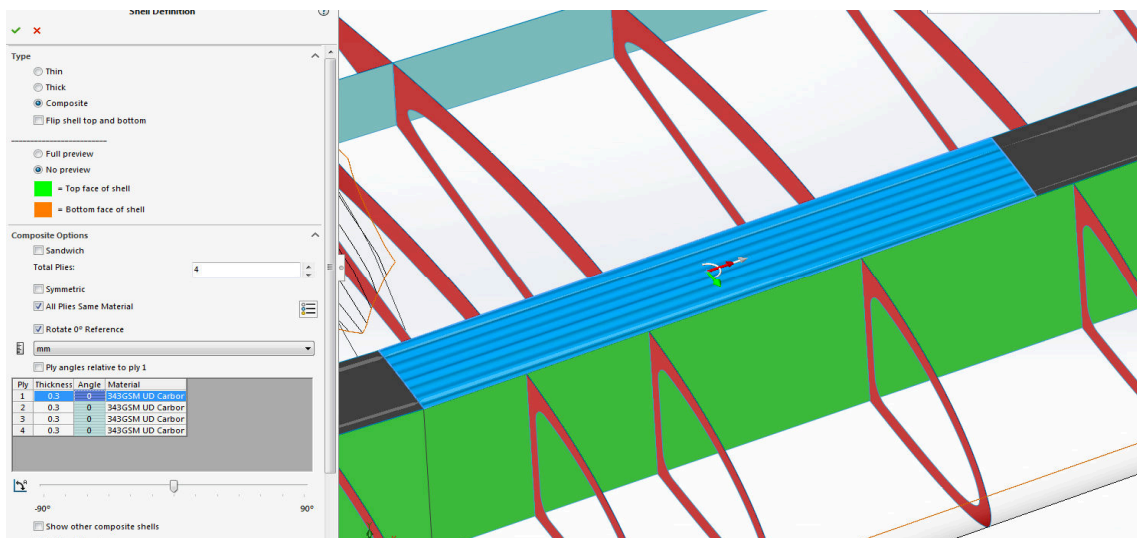


Figure 27 - SolidWorks Simulation image showing the orientation of the Carbon unidirectional tape fibres in the top spar caps.

### 5.3.2. Wing Skins

Since the woven glass fibre cloth used to construct the wing skins has equal properties in the 0° and 90° directions the wing skins were specified with only 0° and 45° angles as is shown in Figure 28. The skin thickness was modelled as being offset inwards of the wing skin surfaces.

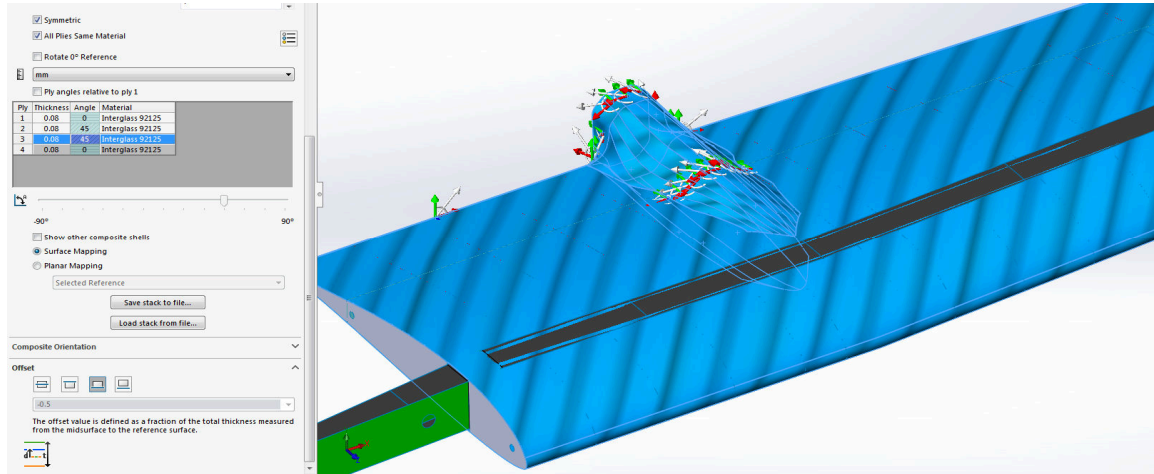


Figure 28 - SolidWorks Simulation image showing the orientation of the 45° ply in the wing skin laminate.

### 5.3.3. Webs and Ribs

The webs and ribs were also modelled using only 0° and 45° angles and are shown in Figure 29. The root rib which transfers the lift shear force and pitching moment torsion to the fuselage via pins was given a thicker laminate than the rest of the ribs. Due to the large shear and torsion loads introduced by the tail surfaces through the tail booms the main spar shear webs were modelled in two sections: one inboard and one outboard the tail boom connection area. The section inboard of the tail boom connection area was modelled using a thicker laminate as it would see larger shear and torsion loads than the outboard section.

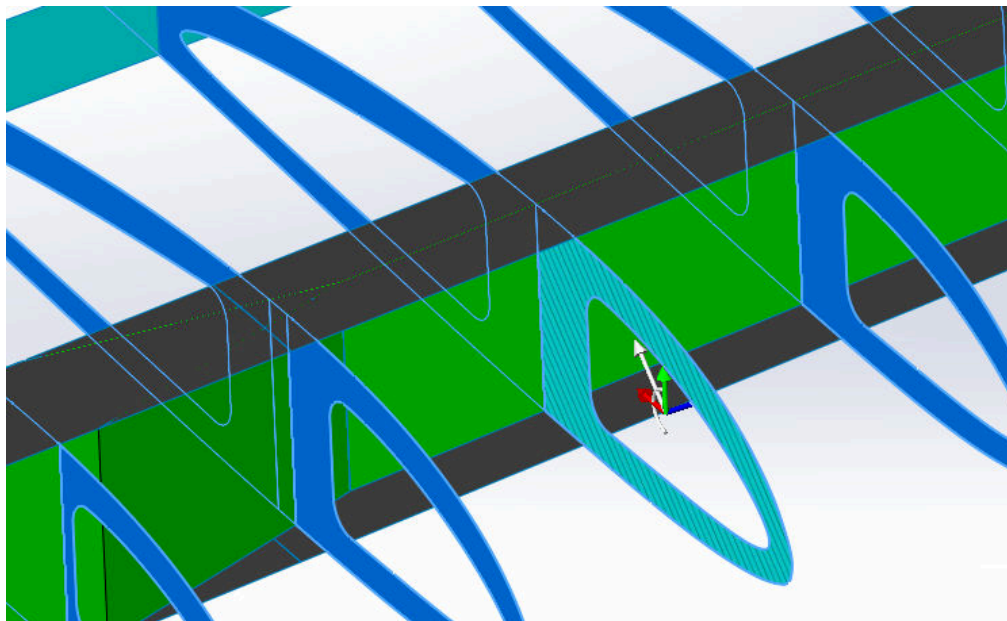


Figure 29 - SolidWorks Simulation image showing the orientation of the 45 plies in the internal rib laminates.

## 5.4. Loads and Boundary Conditions

### 5.4.1. Load Cases

The load cases selected in Chapter 4 were modelled by applying the different loads to the wing in the same analysis file in SolidWorks Simulation. The special case of the whiffle tree loads was modelled in a separate analysis file.

#### 5.4.1.1. Non-Uniform Distributed Lift Load

Since the lift distribution of the wing is known from Chapter 4 a 5<sup>th</sup> degree polynomial equation was derived to model this distribution. The load was applied to the wing using the Non-Uniform Pressure feature in SolidWorks Simulation and by measuring the wing surface area and can be seen in Figure 30. Although it is recognised that the wing top and bottom surfaces work together to create the lift over their surfaces an assumption was made that 75% of the lift of the wing is generated by the top surface and 25% by the bottom surface. This assumption is based on a coefficient of pressure ( $c_p$ ) distribution of the SD7062 aerofoil obtained from XFLR5.

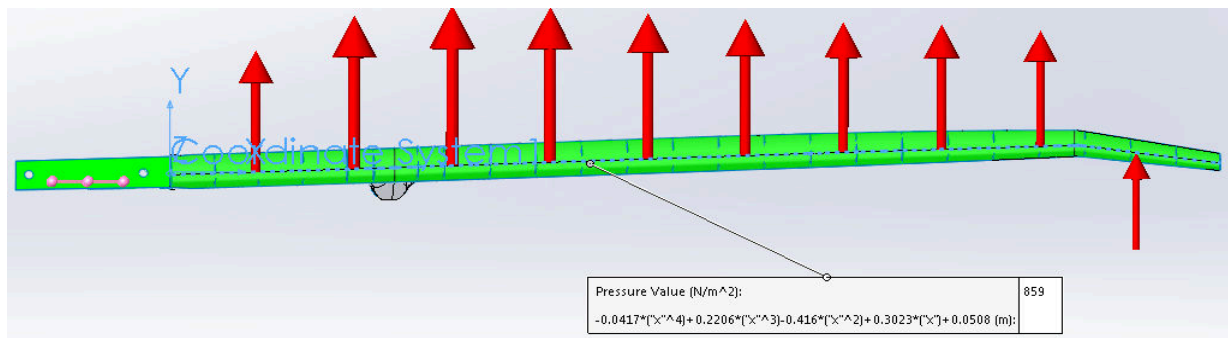


Figure 30 - SolidWorks Simulation image showing the distributed pressure loading applied to the wing surfaces to simulate the lift generated by the wing skins.

#### 5.4.1.2. Torsion Due To Pitching Moment

The torsional loads acting on the wing due to the aerodynamic pitching moment were modelled using the Torque feature around a spanwise centreline aligned with the wing quarter-chord line (a line 25% backwards from the wing leading edge). The torque was applied to the wing ribs using a non-uniform distribution derived from the torsion diagram (see Figures 17 and 20). Figure 31 shows the torsional loads applied to the wing.

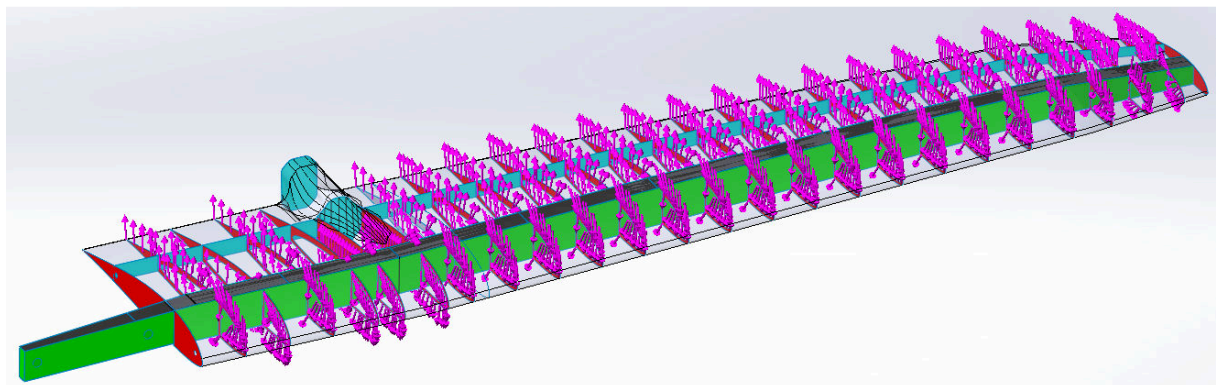


Figure 31 - SolidWorks Simulation image showing the application of the torsional loads to the outboard wing ribs.

### 5.4.1.3. Drag Loads

The combined drag loads obtained from XFLR5 in chapter 4 were modelled simply with the Force feature acting equally on the top and bottom wing skins.

### 5.4.1.4. Whiffle Tree Loads

The process of obtaining the whiffle tree loads is described in Chapter 7. The eight concentrated loads were physically applied to the bottom surface of the wing using polystyrene saddles 100mm wide and were therefore modelled in the FEA as eight separate surfaces to which the loads were applied as can be seen in Figure 32. This was done in order to model the whiffle tree setup as accurately as possible.

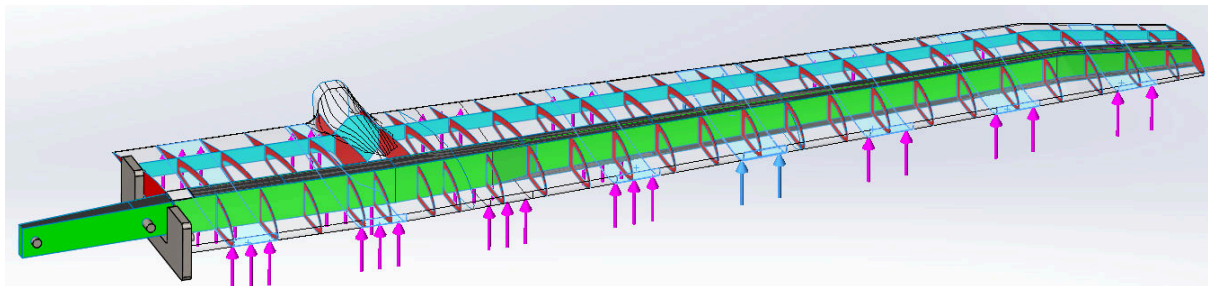


Figure 32 - SolidWorks Simulation image showing the whiffle tree loads distributed over their surfaces.

## 5.4.2. Boundary Conditions

### 5.4.2.1. Simple Fixtures for Optimisation

In order to optimise the structural layouts and laminate layups efficiently a simple set of representative fixtures was used to decrease the computational time needed to solve each iteration and is shown in Figure 33. The fixtures included:

- Constraining the wing pin holes in the  $y$  and  $z$  directions to simulate the effect the pins would have on the root rib of limiting the upwards and rearwards movement of the rib.
- Constraining the spar shear transfer pin holes in the  $y$  and  $x$  directions to simulate the effect the opposite wing spar would have on the spar being analysed of constraining its rotation about the aircraft centreline and constraining the outwards (towards the tip) movement of the spar.

### 5.4.2.2. Simulated Fuselage Fixtures

In order to accurately simulate the whiffle tree fixtures and actual Kwadira fuselage attachment the following fixtures were created as shown in Figure 34:

- A simulated fuselage side was created and placed against the root rib. The root rib's shear pins were also modelled and included in the analysis so as to accurately re-create the interaction between the root rib and the fuselage. The fuselage side was then constrained in the  $x$ ,  $y$  and  $z$  directions.
- A disc was created and positioned next to the wing spar. The spar shear transfer pins were also modelled. Constraining the disc in rotation about the  $z$ -axis was seen as representative of the left and right wings' spar interactions.

The simulated fuselage fixtures were meshed as part of the model and were given no-penetration contact constraints with the wing root rib, root rib shear pins and spar root shear pins.

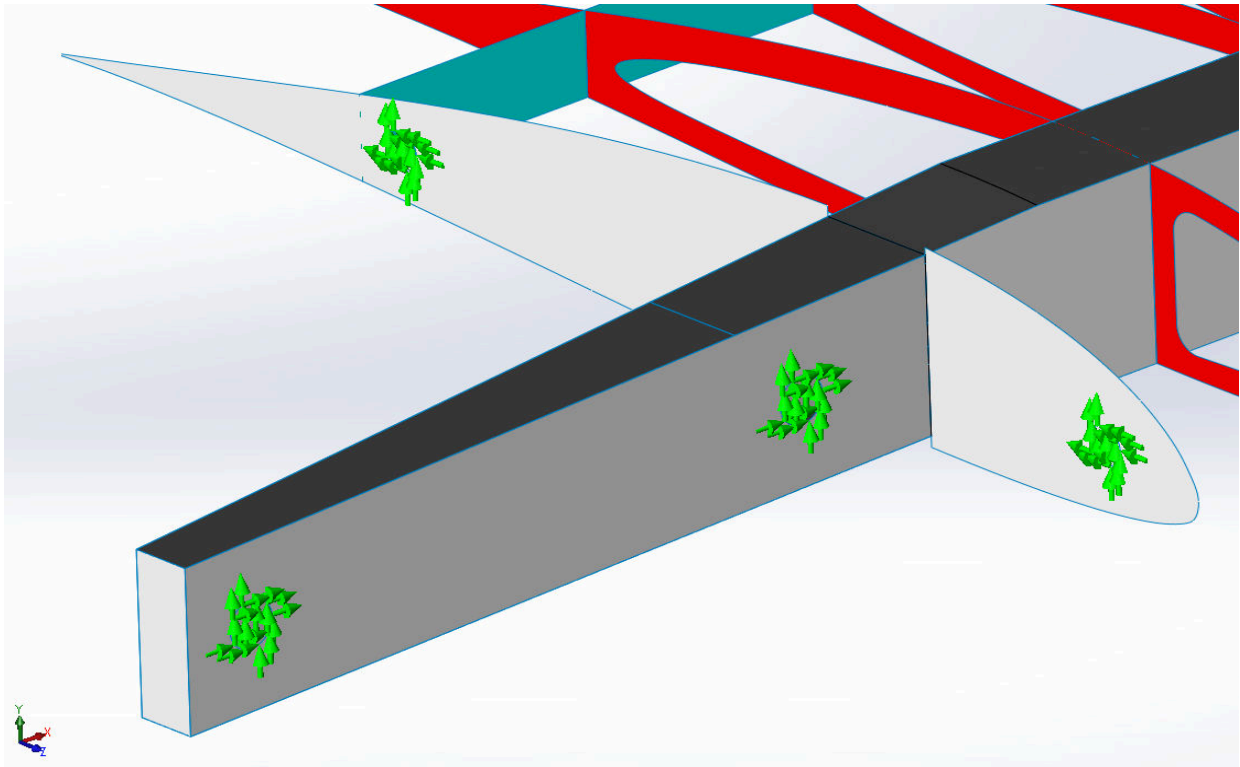


Figure 33- SolidWorks Simulation image showing the simple fuselage fixtures that were used for the optimisation analyses.

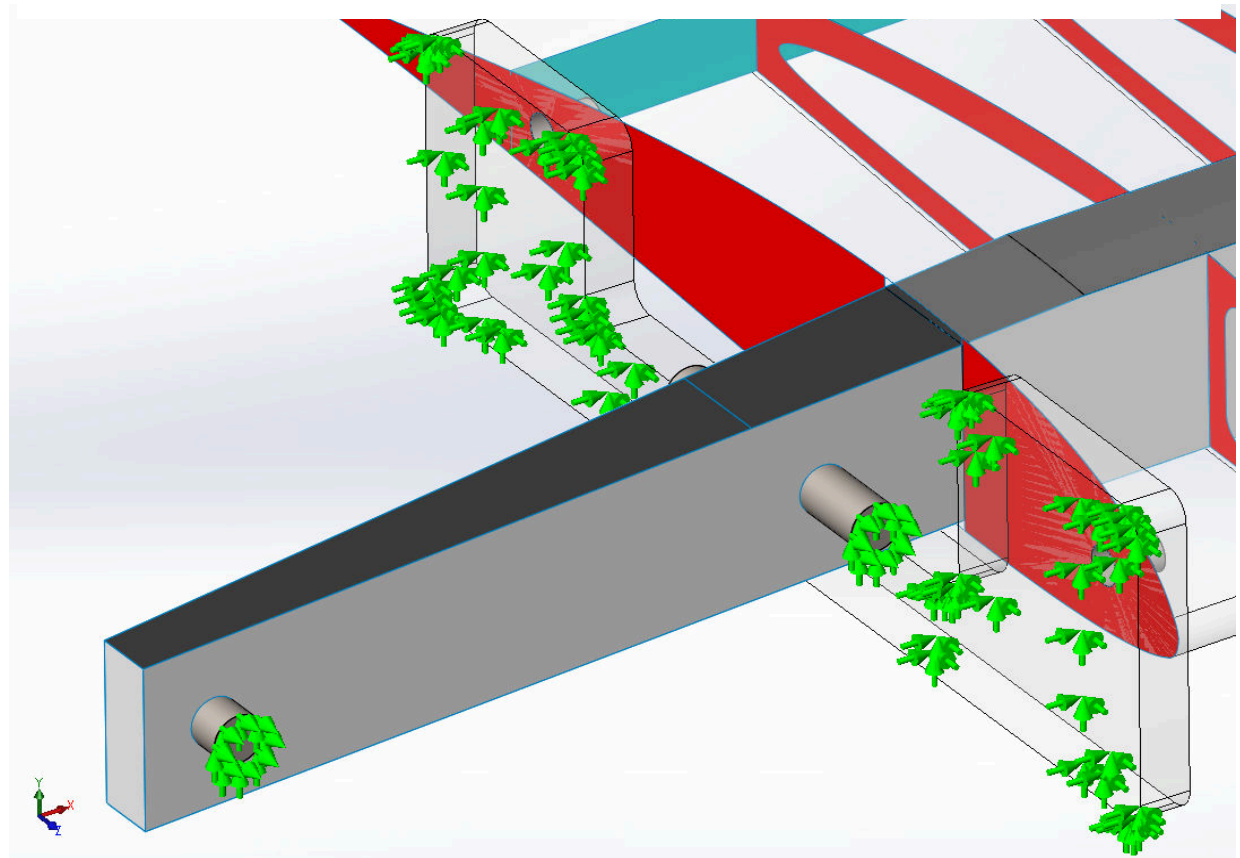


Figure 34 - SolidWorks Simulation image showing the simulated fuselage fixtures that were used for the whiffle tree and final analyses.

## 5.5. Shell Mesh, Component Contact and Solver

### 5.5.1. 2-D Shell Meshing

SolidWorks Simulation's automatic mesher was used to create a two-dimensional shell mesh using the surfaces created in SolidWorks CAD. This mesh is shown in Figure 35. The following mesh parameters were specified:

- Mesh Type: *Curvature Based Mesh*. This was chosen to allow for effective meshing of the aerofoil curvature and complex curves associated with the tail boom socket.
- Elements: *High-Quality Mesh*. This option creates second-order triangular shell elements which are better able to handle curved surfaces.
- Maximum element size: *17.5 mm*. This was chosen to obtain a fine mesh with at least 40 chord-wise elements along the smallest aerofoil found at the wing tip.
- Minimum element size: *1 mm*. This was chosen based on a SolidWorks-calculated minimum radius of curvature of 1.2 mm of the wing skins.

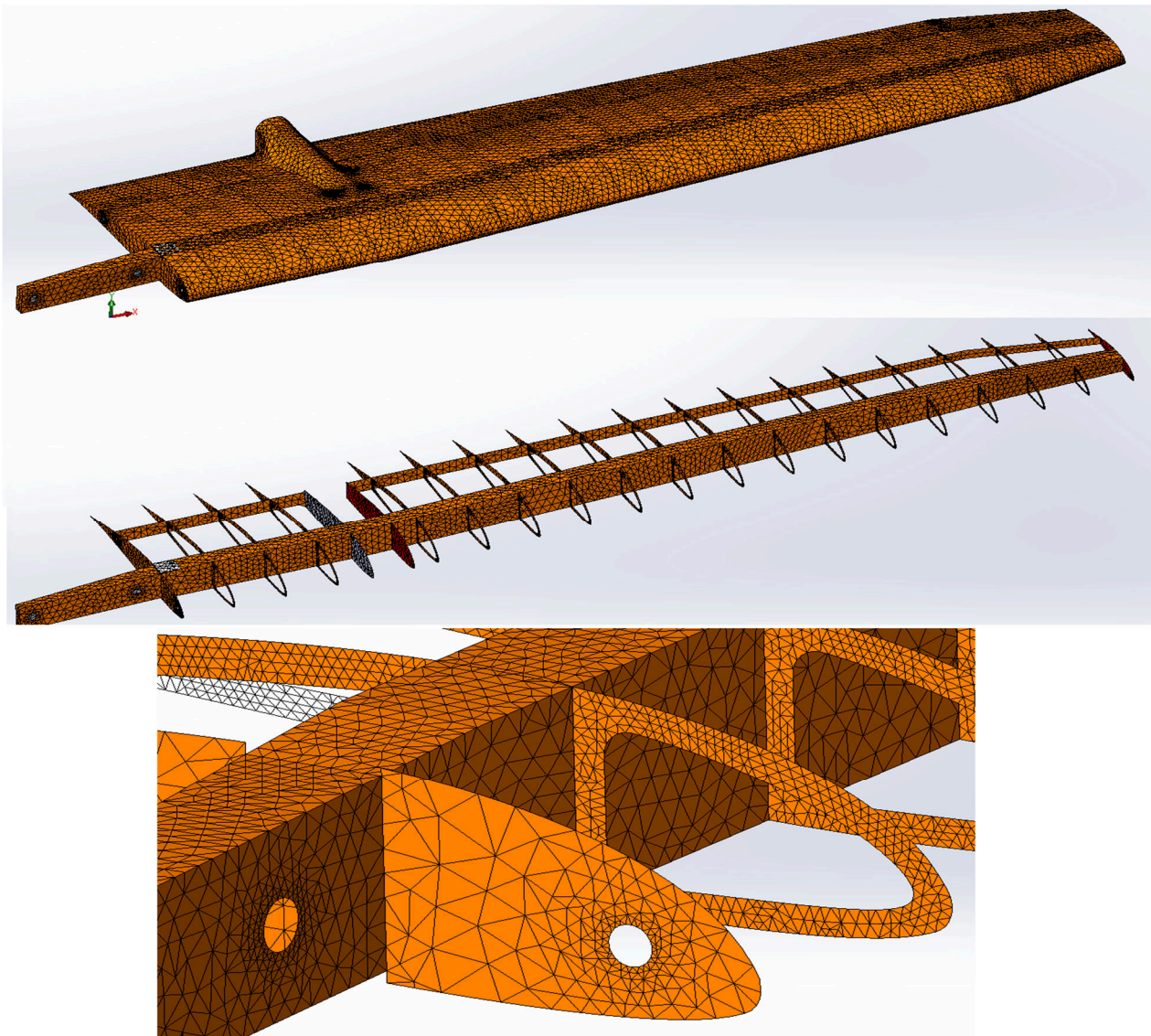


Figure 35- SolidWorks Simulation image showing the mesh generated for the analyses and mesh refinement performed around critical areas of interest.

## 5.5.2. Contact Entities

### 5.5.2.1. Bonded Contacts

A global bonded contact feature was created to specify rigidly bonded contact lines between geometric entities within a specified distance to each other. This models the resin and glass fibre cleating strips that will be used to bond the structural components to each other. A software calculation was done to determine all the lines and areas of bonded contact and the result is shown in Figure 36. The way that SolidWorks Simulation calculates bonded contacts is described in Chapter 2.6.4.

### 5.5.2.2. Non-Penetrating Contacts

Non-penetrating contact features were created to model the interactions of the pins with the root rib and spar, the simulated fuselage and root rib, and the whiffle tree saddles and the bottom wing skin. A SolidWorks Simulation plot of the bonded (red) and non-penetrating (purple) contact entities can be seen in Figure 36. Note the areas indicating the bonding of the spar caps to the top and bottom skins, and all the lines of bonded contact with the ribs and webs.

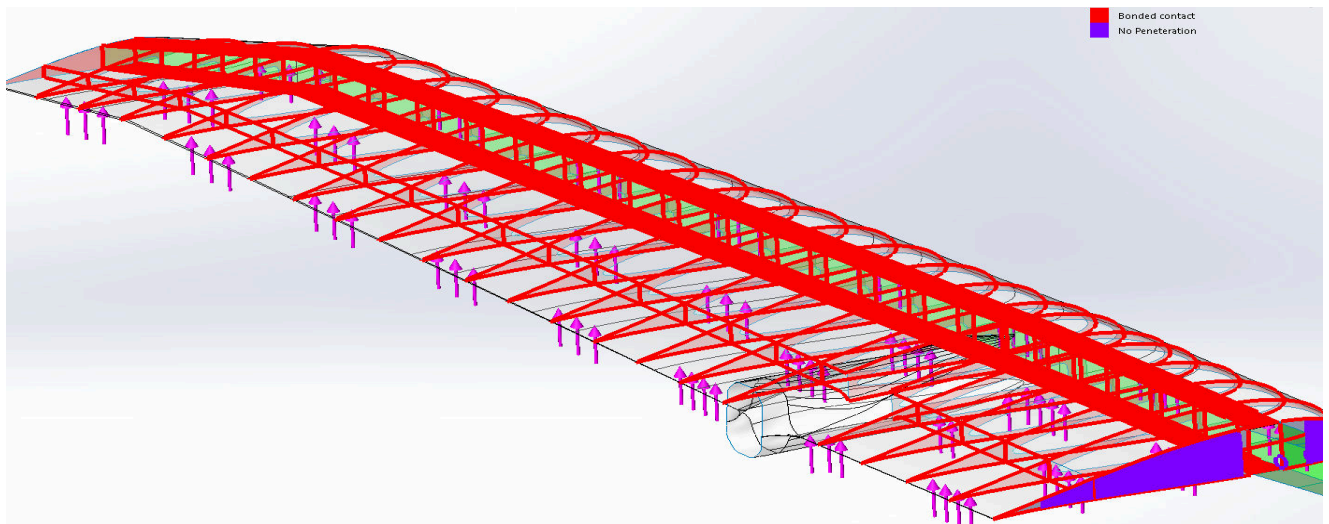


Figure 36 - SolidWorks Simulation image showing the lines/areas of bonded (red) and non-penetrating (purple) contact within the model.

### 5.5.3. Solver Selection

In order to decrease computational time the SolidWorks Simulation Iterative solver was used to perform the structural layout and layup optimisations with the simple fixtures described in section 5.4.2.1. The iterative solver does not make use of computationally expensive matrix inversion methods but instead uses iterative methods to approximate a solution.

The iterative solver is not capable of solving for the non-penetrating contact entities of the simulated fuselage components and so the Large Problem Direct Sparse solver was employed for solving the model with the simulated fuselage fixtures as described in Chapter 5.4.2.2.

### 5.5.4. Mesh Convergence Study

A mesh convergence study was performed as recommended by Comsol (COMSOL, 2016) by decreasing the maximum element size by 2.5 mm and plotting the change in results. It was found that the results for a maximum element size of 17.5 mm differed by around 1% from a maximum element

size of 15 mm. It was therefore decided to update the element sizes used to a maximum of 17.5 mm in order to save on computational time. The minimum element size of 1 mm was kept throughout as a result of the calculated minimum radius of curvature of 1.2 mm of the wing surface geometry in order to effectively capture these radii in the analysis. It must be noted that SolidWorks Simulation automatically refines the mesh around areas of high curvature or around holes using adaptive mesh refinement algorithms.

Once the mesh convergence study had been completed, the mesh was further locally refined by specifying mesh control features for the internal wing ribs, main shear webs and spar caps. This was done in order to have a minimum of 5 elements at the thinnest part of these surfaces in order to capture bending and buckling effects. The bottom of Figure 35 illustrates this additional refinement. Figure 37 shows the Von Mises stress of a point along the top spar cap of the wing as a function of decreasing maximum element size and illustrates the negligible difference between 17.5 mm and 15 mm maximum element sizes. It is acknowledged that Von Mises stress is not commonly used for composite material stress analyses but it was found to be a useful indicator of total stress in an area and was used solely to perform mesh refinement.

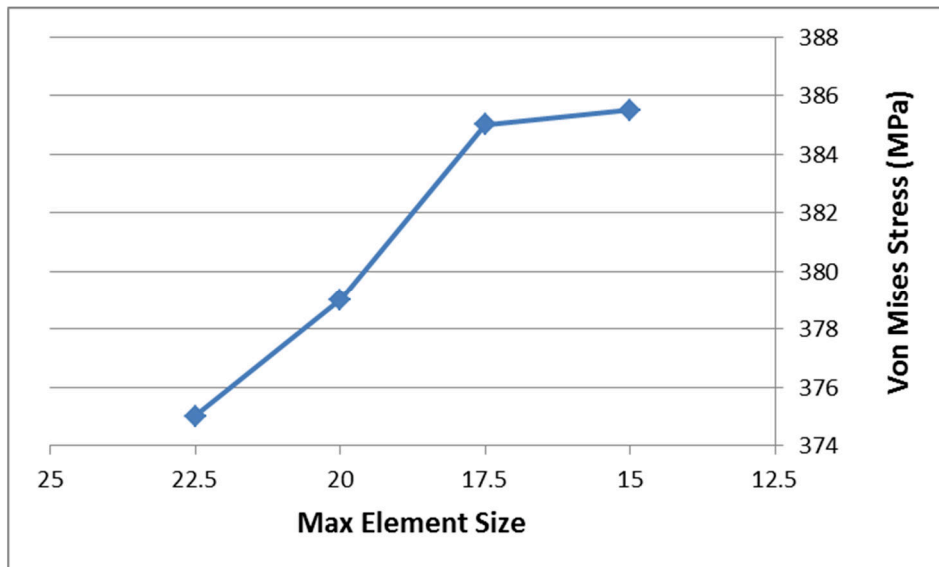


Figure 37 - Von Mises Stress of a point along the top spar versus Max Element Size of the mesh.

## 5.6. FEA Results

### 5.6.1. Tsai-Wu Failure Criterion and Safety Factor

The Tsai-Wu failure criterion was selected to be applied to this study since it caters for differing material strengths in tension and compression (Tsai, 2008). The criterion gives as an output a failure index which is a prediction of first-ply-failure of the composite laminate which is an indication of the commencement of failure for the laminate.

According to the composite failure criterion theory presented in Chapter 2.3.5 a laminate will fail when the Tsai-Wu criterion takes on a value of more than 1. It must be explained that SolidWorks Simulation reports the inverse of the Tsai-Wu criterion and labels it a ‘Factor of Safety’. Therefore, for the purposes of this study, the failure index was seen as a factor of safety against failure with a value of less than 1 being regarded as unsafe. It must be noted again that a general safety factor was applied to the loads as described in Chapter 4.1.4.

The failure index was extracted from SolidWorks simulation by defining a 'Safety Factor' result feature and specifying the Tsai-Wu criterion, an example of which is shown in Figure 38. The option of displaying the worst case across all plies of the lamina was selected, and results below a value of one were displayed in red.

The results of the FEA analyses were all subjected to this criterion and this information was used to iteratively design the internal structural components and final layup of the wing to ensure structural integrity during flight. It must be noted that the images shown are general examples of iteration results and not final results.

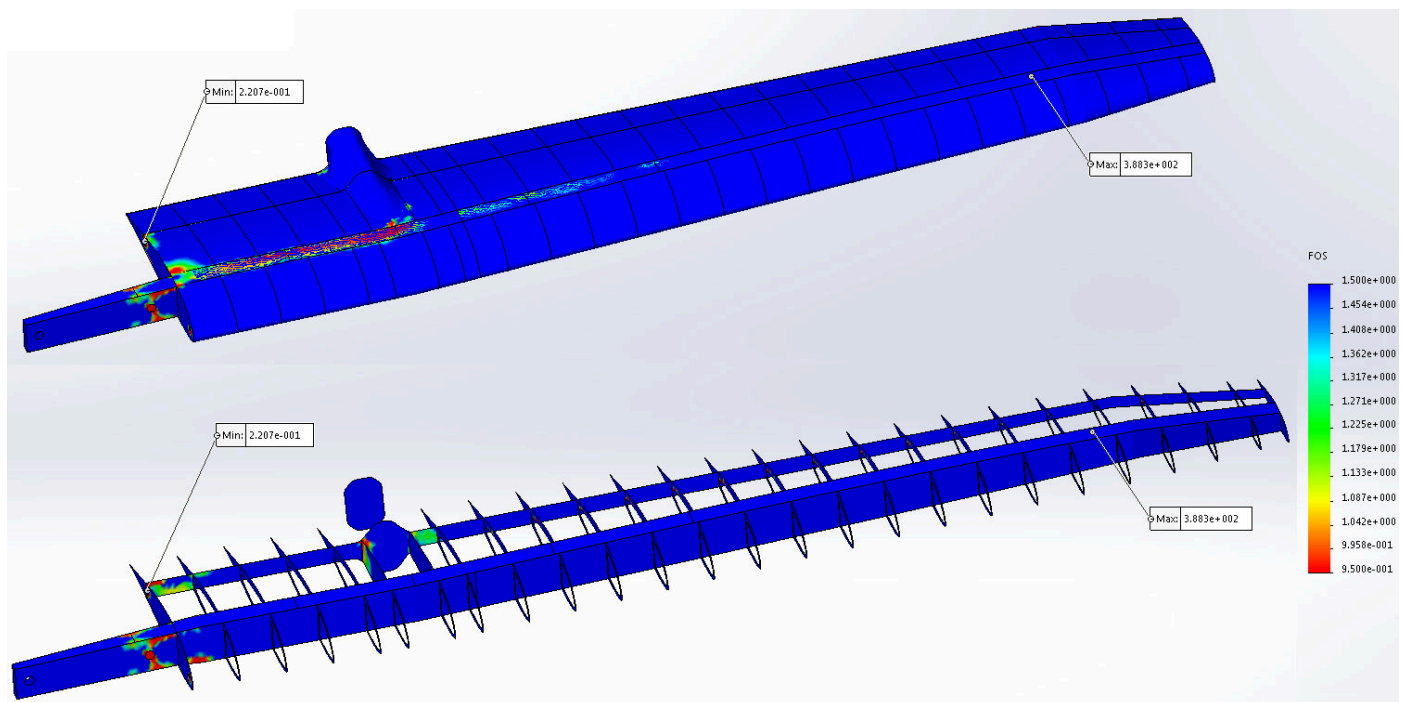


Figure 38 - A SolidWorks Simulation image showing an example of the Tsai-Wu failure index used in the analyses. Note that SolidWorks Simulation reports the inverse of the Tsai-Wu index as a Factor of Safety against failure.

### 5.6.2. Strains and Displacements

Excessive displacements of the wing components can have detrimental effects on the performance of the wing, these are outlined below:

- Excessive bending and chord-wise displacements result in a change in the geometry of the wing planform and would as a result influence the performance of the aircraft.
- Deflection of the wing skins caused by the positive and negative pressures imposed on the wing skins due to lifting effects could cause the aerofoil sections of the wings to deform and influence the performance and stalling characteristics of the wing.
- Excessive axial rotation of the wing relative to the root rib caused by pitching moment effects on the wing skins could cause a change in the lift distribution over the wing and induce unwanted aeroelastic effects such as flutter.

For each iteration in the iterative optimisation process the displacements in the chord-wise, span-wise and primary bending directions were checked by defining a 'Displacement' feature in SolidWorks Simulation and specifying the relevant directions. An example of the deflection results can be seen in Figure 39.

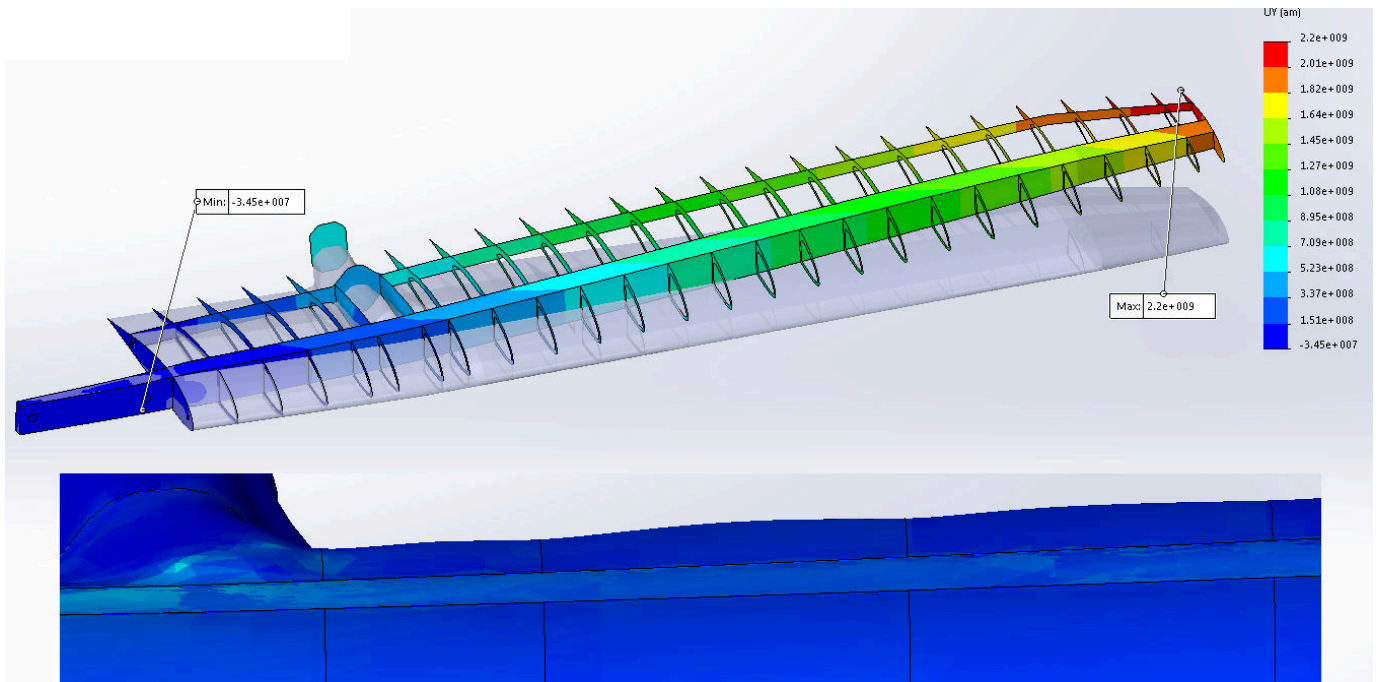


Figure 39 - A SolidWorks Simulation image showing an example of the displacement results used in the analyses. Note the deflection of the wing top surface under aerodynamic loading (blue, bottom) which changes the aerofoil shape.

### 5.6.3. Inter-Laminate Shear Stresses

The Tsai-Wu failure criterion only predicts first-ply-failure and while this is a good indication of the strength of a laminate it does not take into account the inter-laminate shear stresses occurring between the plies of a laminate which are typically limited by the shear strength of the resin matrix. For each iteration in the optimisation process these stresses were evaluated by defining a ‘Stress’ feature in SolidWorks Simulation and specifying inter-laminate shear stresses. An example of this can be seen in Figure 40.

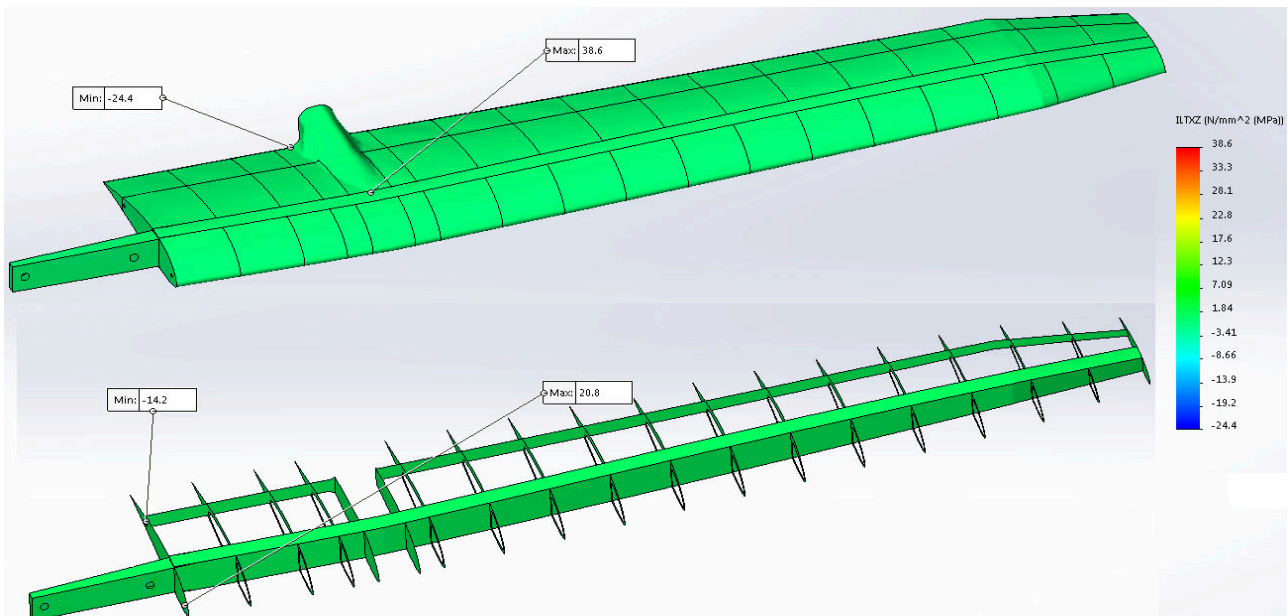


Figure 40 - A SolidWorks Simulation image showing an example of an inter-laminar shear stress plot as was used in the analyses.

## 5.7. Iterative Layout Optimisation

### 5.7.1. Iteration Procedure

An optimisation was performed on both the TMWL and the TDRL layout in order to select the best layout for the Kwadira wing. This was done by iteratively varying the number of internal ribs for each layout while keeping the layups of all the components constant until the next step as discussed in Section 5.8. The point B (40 m/s, 4.9 g) load case was chosen as being the worst load case and was therefore used to perform the layout iterations. Since the aim of this study is to reduce the weight of the wing while still maintaining adequate strength and stiffness the objective of the optimisation was to reach a point where:

- The safety factor of the composite laminates is larger than one (safety factor being the inversion of failure index, see Chapters 4.1.4, 5.6.1),
- The deflections of the wing and sub-components are within acceptable limits and
- The amount of material used is minimised.

This objective was reached by starting with an assumed small rib spacing of 75 mm and iteratively decreasing the number of ribs (and hence increasing the rib spacing) while checking the safety factor, deflections and inter-laminate shear stresses of the components while keeping the spacing between the ribs uniform.

### 5.7.2. Chosen New Structural Layout

The complete set of results of the layout optimisation iterations are given in Appendix C.

It was found that the lightest layout that stays within the limits mentioned above was the TMWL with a rib spacing of 100 mm which results in 22 chord-wise ribs.

The TDRL was not chosen as it was seen that the number of internal diagonal ribs required to keep the wing skin deflections in check was large, resulting in a higher overall wing weight than that of the TMWL.

## 5.8. Iterative Layup Optimisation

### 5.8.1. Iteration Procedure

Once the layout had been finalised, an iterative optimisation was performed on the layups of the individual components. The aim of the optimisation was to minimise the weight of the components while still complying with the limits mentioned in Section 5.6.1 above.

The objective was reached by starting with the initial layups as described in Chapter 4 and decreasing the number of plies in the laminates until deflections became unacceptable, the factor of safety against failure (the inverse of the Tsai-Wu failure index, see Chapter 5.5.1) was less than 1 or inter-laminate shear stresses were found to be higher than the maximum shear stress of the matrix as defined in Chapter 3.3.5. Care was taken to optimise one component or set of components at a time and thereby avoid over or undershooting iterations due to component interactions.

The component layups that were optimised include:

- The wing skins
- The main (spar) shear webs
- The rear shear web

- The root rib
- The internal ribs, inboard and outboard of the tail boom connection

### 5.8.2. Buckling Considerations

Due to the large stresses experienced by the various structural components of the wing and the thin layups given by the iterative layup optimisation procedure it was deemed critical to perform a buckling analysis on several components of the new wing design. Buckling, which can cause component failure at loads lower than what is predicted as safe by other methods, is primarily caused by compressive and shear loads in thin plates (Niu, Airframe Stress Analysis And Sizing, 1997). The following components were checked:

- At the Point B (40 m/s, 4.9 g) load case where the top of the wing sees the largest compressive loading:
  - Several points along the top spar cap
  - Several points along the top wing skin
  - Several points along the main shear web
  - Several points along the rear shear web
- At the Point D (50 m/s, -1.75 g) load case where the bottom of the wing sees the largest compressive loading:
  - Several points along the bottom spar cap
  - Several points along the bottom wing skin
  - Several points along the main shear web

Maximum compressive and shear loads were obtained from the FEA model of the wing and input into a spreadsheet developed to evaluate the compressive and shear buckling of each component based on material stiffness, plate geometry, laminate thickness and edge conditions (see Chapter 2.4.6). Combined compressive and shear buckling failures were also evaluated. The results of these calculations saw the need for an increased thickness in the root areas of both the top and bottom wing skins but showed adequate buckling resistance in the rest of the components.

### 5.8.3. Final Layups

The complete set of results of the layout optimisation iterations are given in Appendix C. The final layups which were to be used for the construction of the wing were obtained from the FEA model of the wing and the buckling calculations and are given in the layup drawings shown in Figures 52 and 53.

The largest change in the layups compared with the initial estimates given in Chapter 4 involve changing the main spar shear web material to carbon fibre. This was done as a result of the high stresses involved in the shear webs and since the increase in electro-magnetic blanking due to using carbon fibre in the shear webs was assumed to be minimal since the main spars already make use of CFRP. The high stresses in the shear webs, especially near the spar root section, were not identified in the initial sizing as a result of the simplified model employed: the initial sizing spreadsheet only considered shear forces to obtain an initial guess but the FEA model considers the complete Tsai-Wu failure criterion as detailed in Equation 2.5 and found the stresses to be much higher than initially predicted.

It was also decided to make use of 3 mm structural foam core for the root rib and the root section of the main shear webs since it was found that the stress concentration in these areas due to the shear pin holes was quite substantial. It was found that the coreless layup required to withstand the high stresses in these areas would be heavier than using a thin sandwich construction. The buckling calculations also pointed to the necessity of a thicker shear web and so the sandwich construction was used.

It is assumed that the use of foam sandwich construction for a reasonably small part of the wing would not invalidate the overall results obtained from this research. The use of sandwich construction in highly localised areas of the wing is employed as a practical design solution. The overall aim of using a coreless design is employed over most of the wing structure. This approach will therefore allow for evaluation of the research hypothesis by determining whether the removal of core over the majority of the wing results in a weight saving and/or reduction in fabrication time. The foam sandwich construction in these areas would also enabled easier use of solid glass fibre hardpoints which spread the large bearing loads.

#### 5.8.4. Final FEA Results

The final results of the layup iterations for the Point B and Point D load cases are presented below in Figures 41 to 51 and were obtained from SolidWorks Simulation. Note that the FOS plots were limited to a maximum of 1.25 to show greater variation in the range. The results are ordered as follows:

- FOS (inverse of Tsai-Wu Failure Index, see sections 4.1.4, 5.6.1) of the composites across all plies, showing the internal structural components
- FOS of the composites across all plies, showing the wing skins
- FOS of the composites across all plies, showing a close-up of the ribs
- Displacement in the aircraft vertical axis (SolidWorks y-axis)
- Resultant displacement of the wing skins, showing a close-up of the top skin
- Inter-laminate shear stress

##### 5.8.4.1. Point B (40 m/s, 4.9 g)

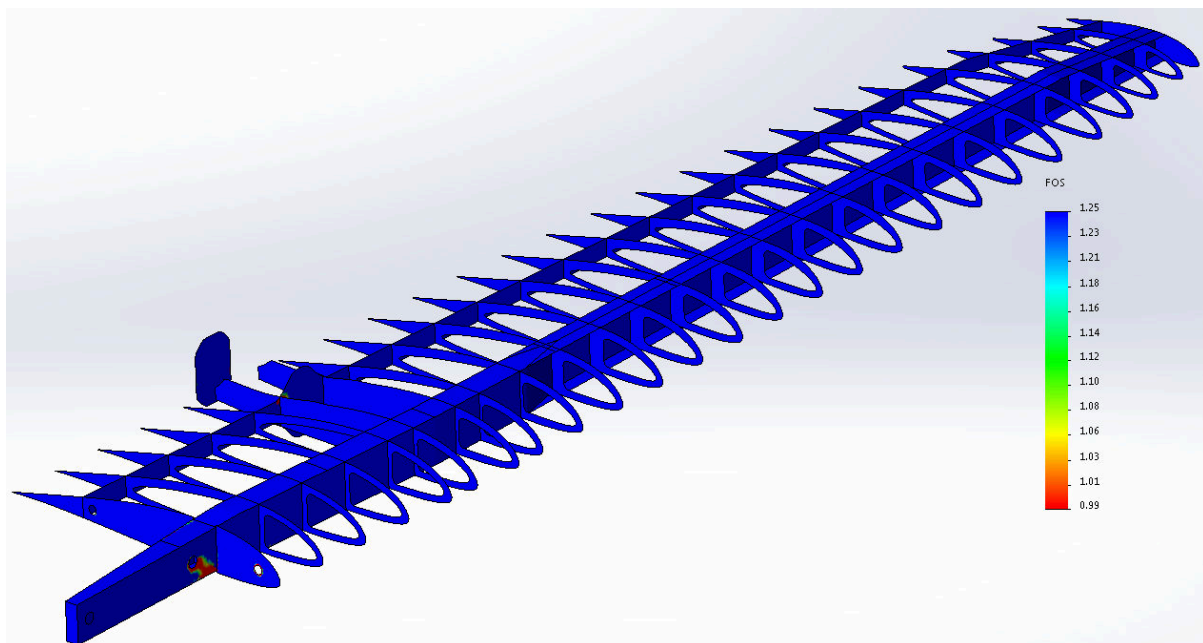


Figure 41 - SolidWorks Simulation image showing the FOS of the wing internal structure at the Point B load case.

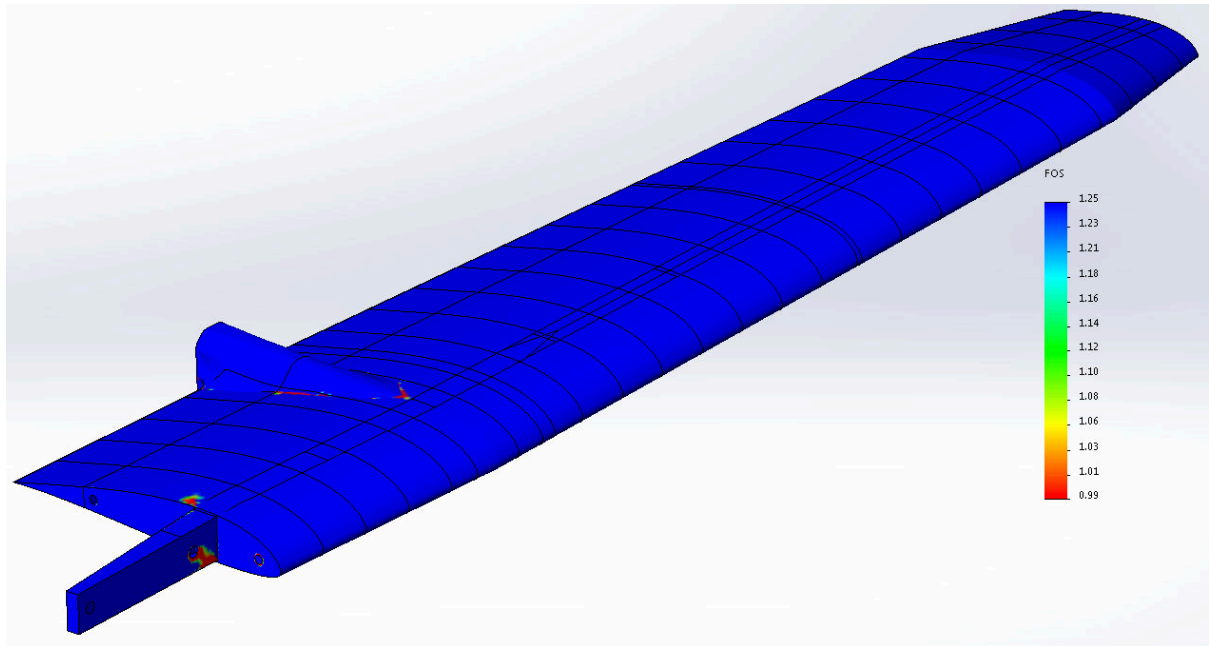


Figure 42 - SolidWorks Simulation image showing the FOS of the wing external structure at the Point B load case.

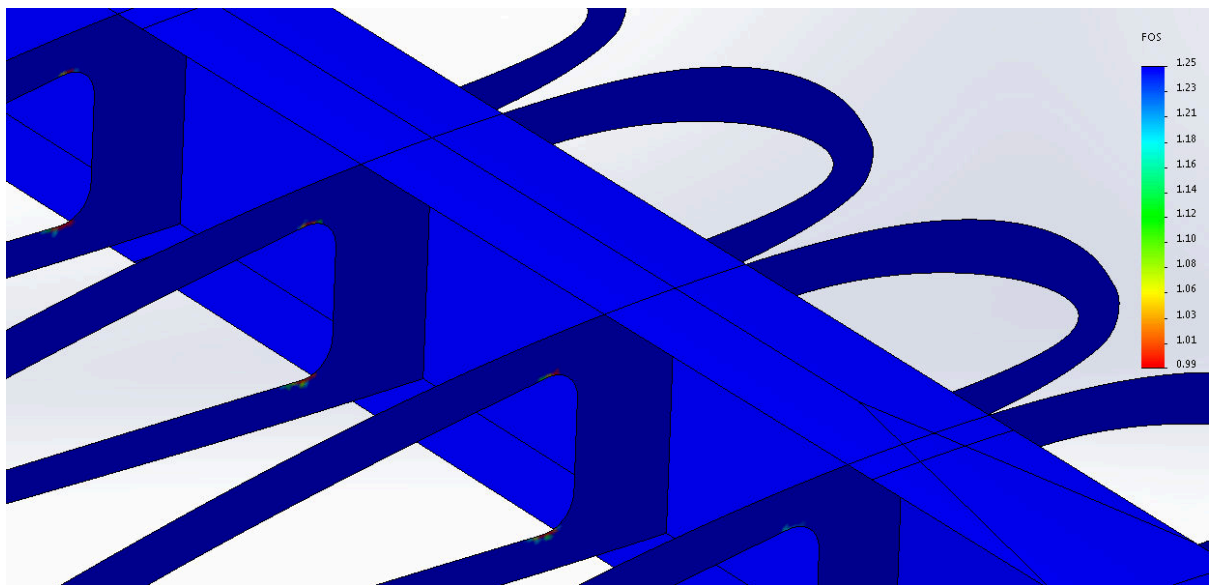


Figure 43 - SolidWorks Simulation image showing a close-up of the FOS of the wing ribs at the Point B load case.

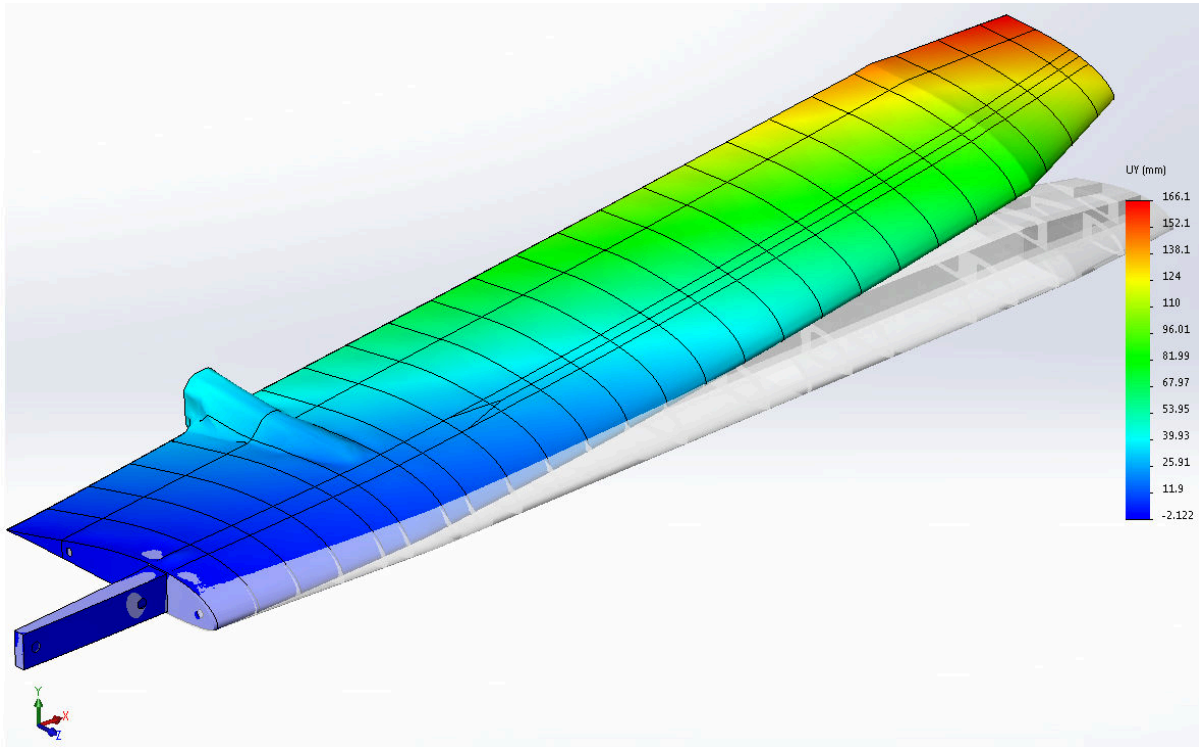


Figure 44 - SolidWorks Simulation image showing the deflection of the wing in the y-direction at the Point B load case.

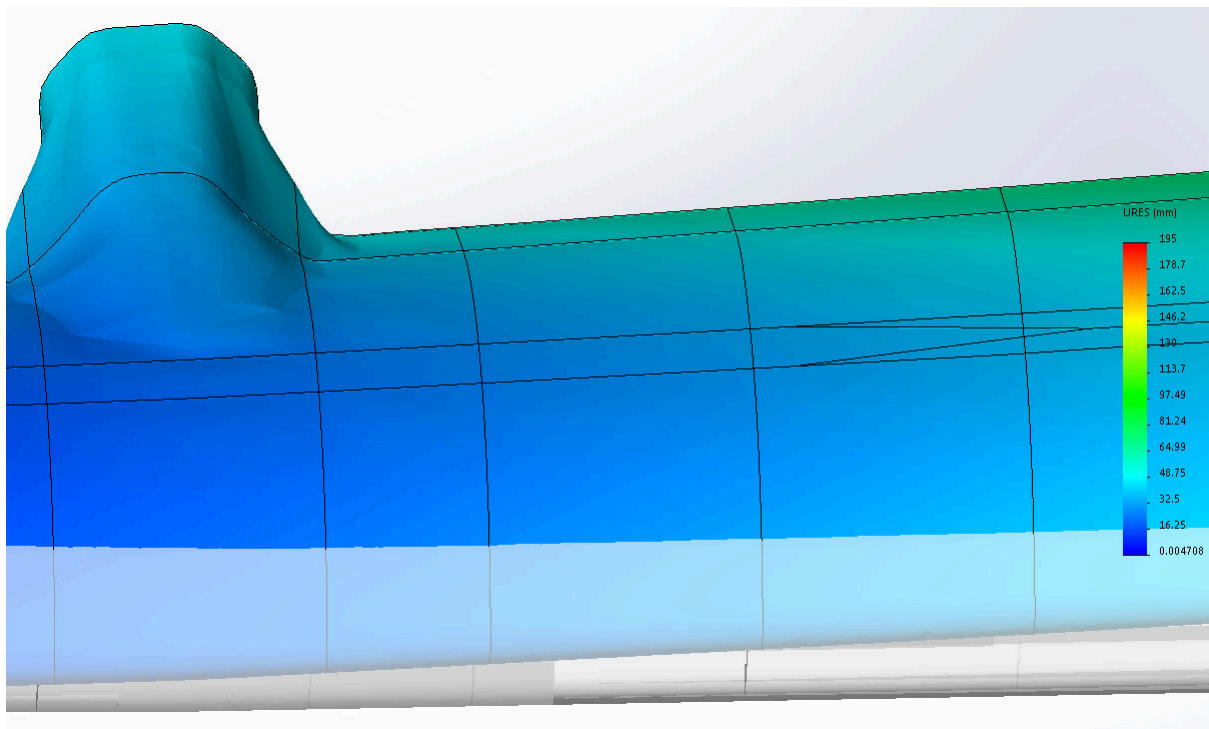


Figure 45 - SolidWorks Simulation image showing a close-up of the top skin resultant deflection at the Point B load case.

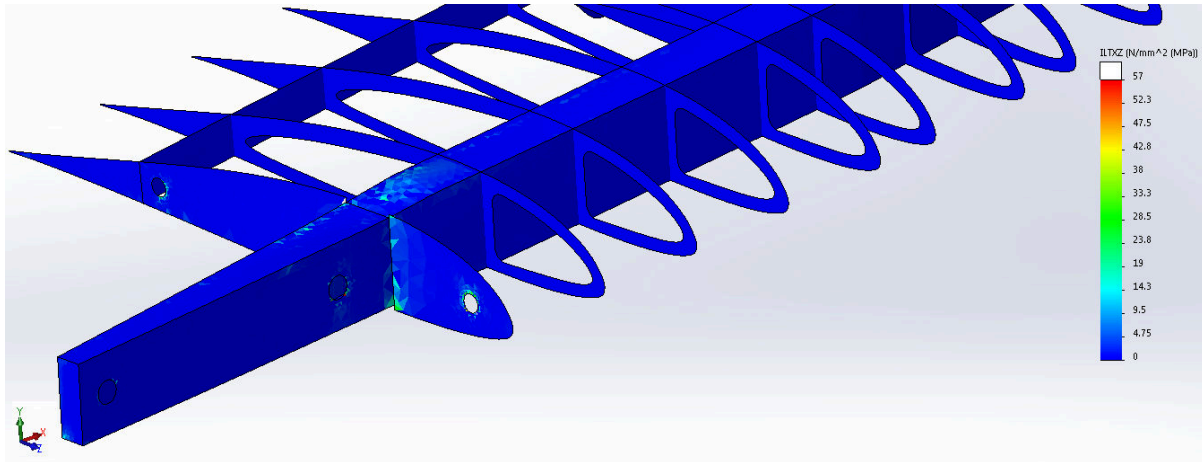


Figure 46 - SolidWorks Simulation image showing the areas of highest inter-laminar shear stress in the model for the Point B load case.

#### 5.8.4.2. Point D (35 m/s, -1.75g)

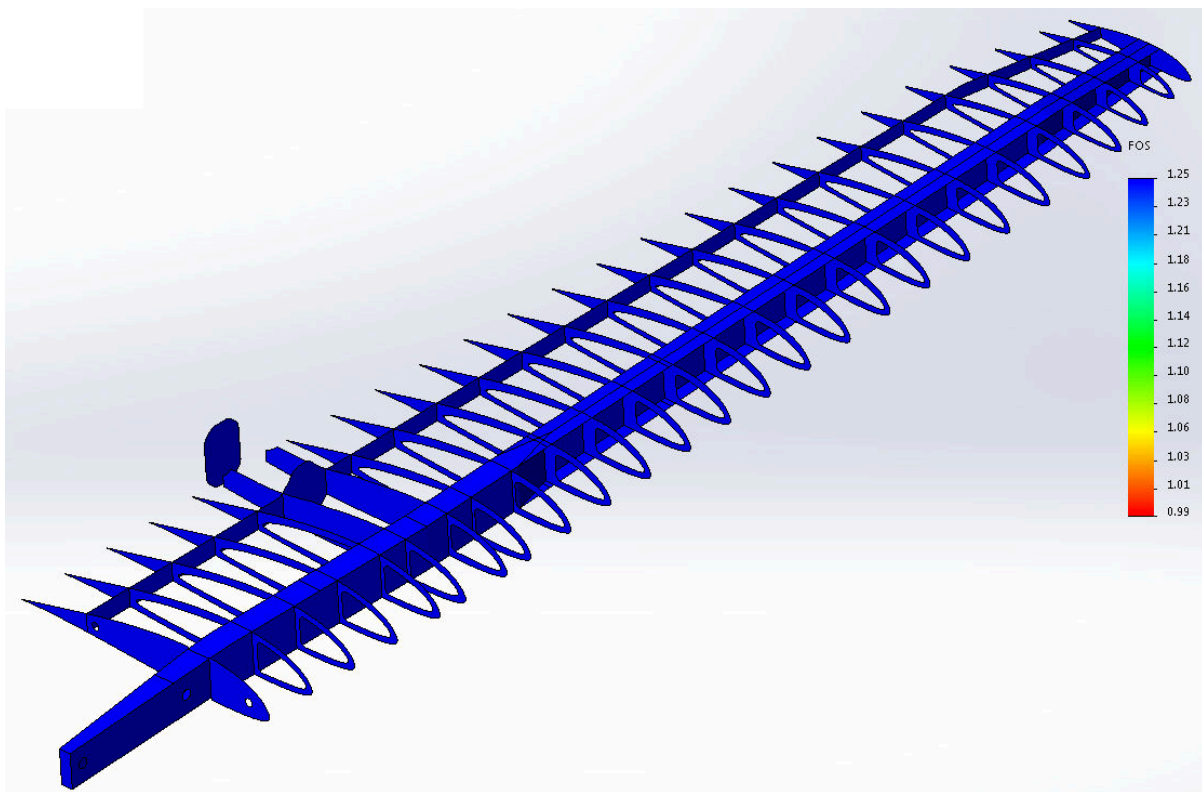


Figure 47 - SolidWorks Simulation image showing the FOS of the wing internal structure at the Point D load case.

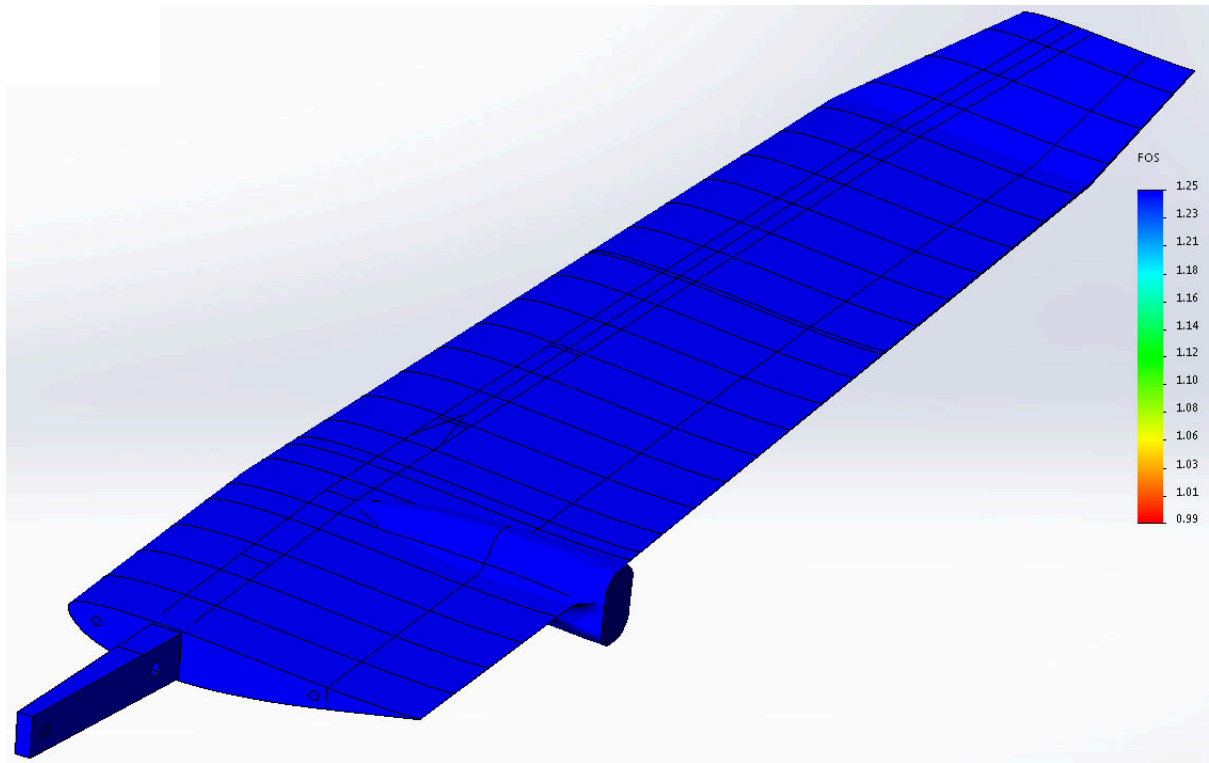


Figure 48 - SolidWorks Simulation image showing the FOS of the wing external structure at the Point D load case.

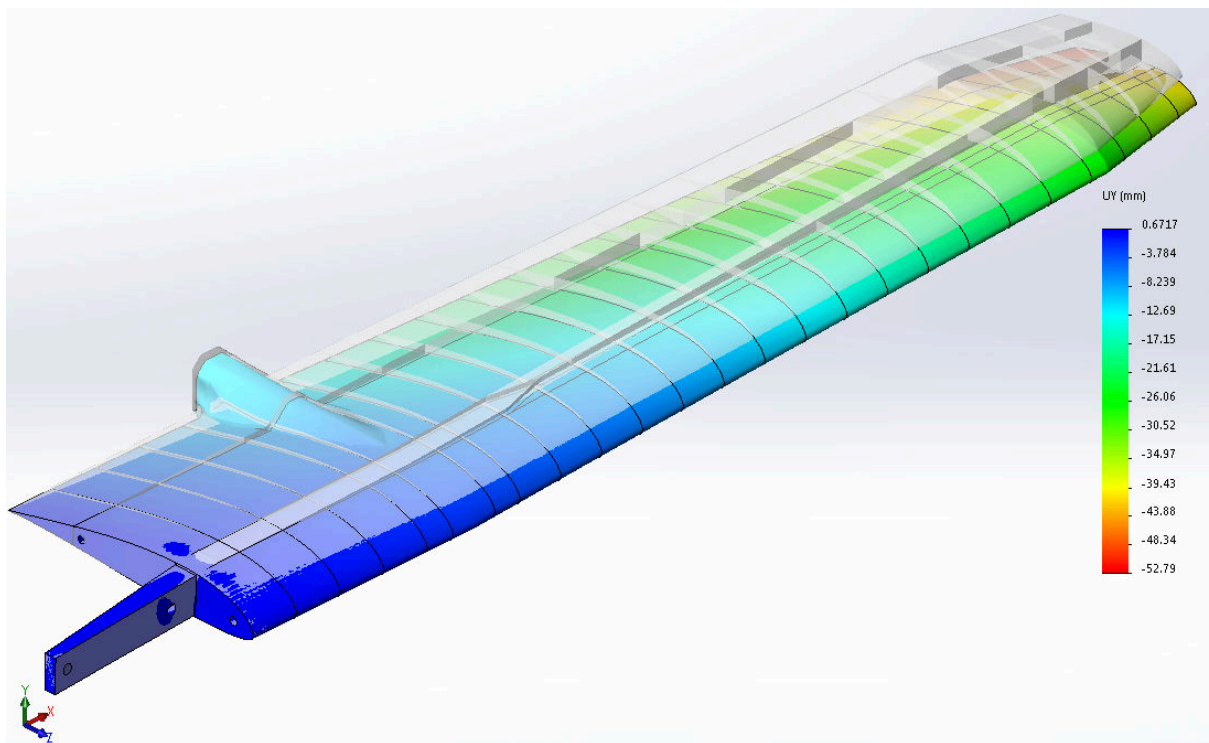


Figure 49 - SolidWorks Simulation image showing the deflection of the wing in the y-direction at the Point D load case.

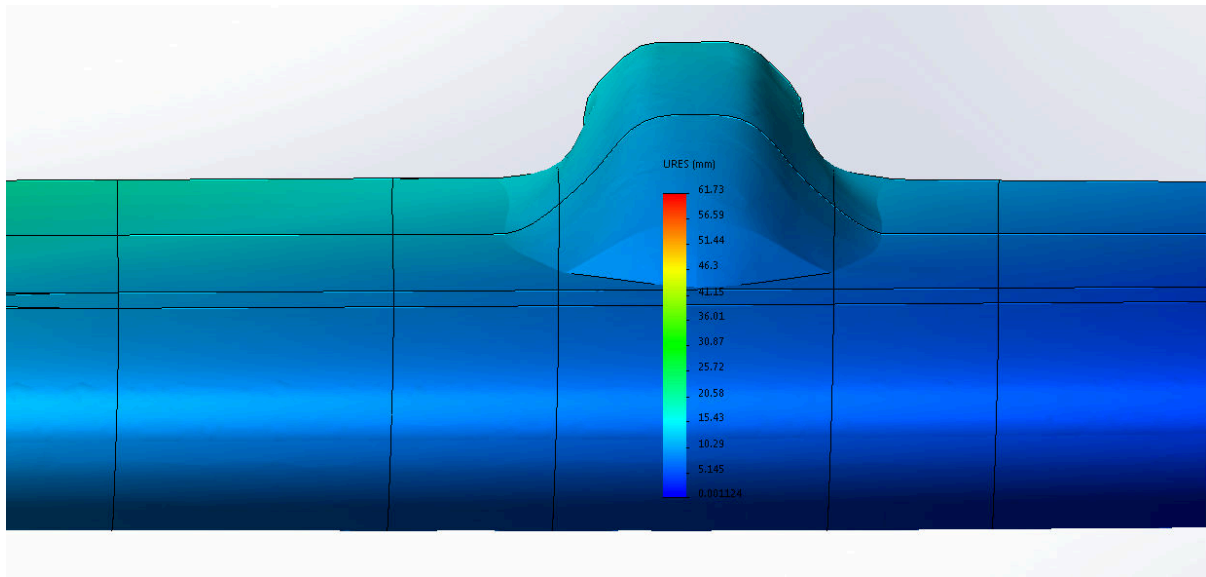


Figure 50 - SolidWorks Simulation image showing a close-up of the bottom skin resultant deflection at the Point D load case.

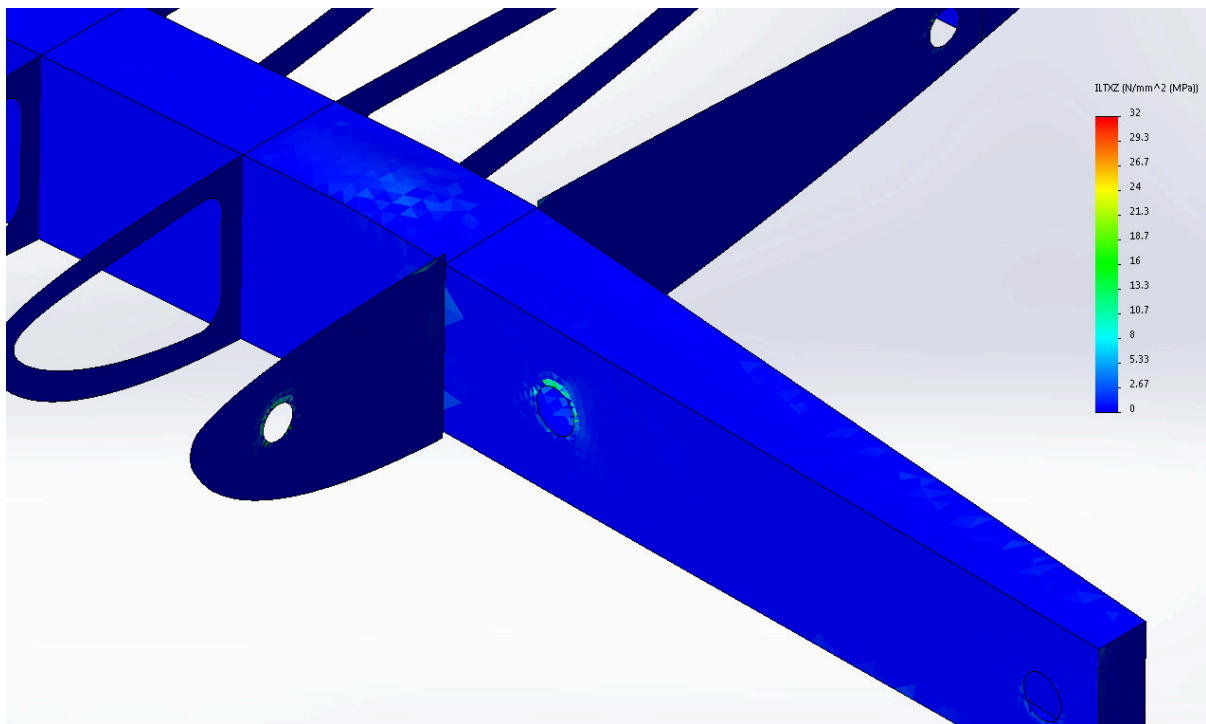


Figure 51 - SolidWorks Simulation image showing the areas of highest inter-laminar shear stress in the model for the Point D load case.

### **5.8.5. Weight Estimation**

The composite mass model developed for Section 4.3.7 was again used to estimate the weight of the final wing with the new, optimised layups. A mass of 5.816 kg was estimated which is an improvement of 0.962 kg or 14.2% over the original wing design.

## **5.9. Chapter Summary**

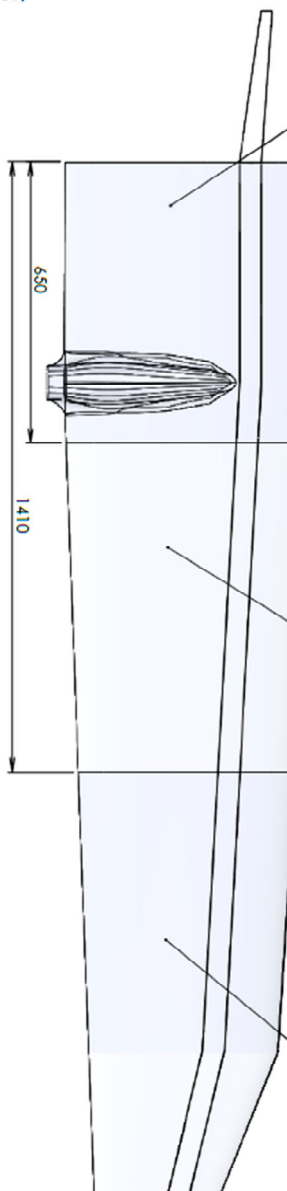
The process by which the new wing structural design was modelled, analysed and optimised is described. Surface models of the wing with the two new structural layouts were created using SolidWorks CAD, and split lines were added to facilitate the application of loads. Using SolidWorks Simulation, material properties were assigned to all the surfaces and care was taken to ensure the correct orientation of the plies in the laminates. Two sets of boundary conditions were defined: a simple set that enabled rapid and efficient optimisation, and a more representative set that simulated the Kwadira fuselage more accurately. The lift, drag and torsion loads were applied to the wing skins and ribs using equations derived from the shear force and torsion diagrams in a manner that was representative of the true aerodynamic loading as well as the whiffle tree test setup. A shell mesh was generated and refined, and examples were given of the FEA results used to evaluate the failure of the models.

An iterative optimisation was carried out to find a well optimised structural layout with the aim of ensuring structural integrity while minimising deflection and total mass, the result of which was the traditional metal wing layout. A second iterative optimisation was performed to determine the lightest component layups that would satisfy the aims of the first optimisation. The result was a wing layup with a predicted weight saving of 14.2% that ensures structural integrity.

**Wing Skins**

- Root Section:
  - 1 x 49GSM Glass
  - 1 x 86GSM Glass
  - 1 x 86GSM Glass, 0x90
  - 1 x 86 GSM Glass
  - 1 x 86GSM Glass
  - 1 x 86GSM Glass, 0x90
  - 1 x 86 GSM Glass
- Mid Section:
  - 1 x 49GSM Glass
  - 1 x 86GSM Glass
  - 1 x 86GSM Glass, 0x90
  - 1 x 86GSM Glass
  - 1 x 86GSM Glass, 0x90
  - 1 x 86 GSM Glass
- Root Section:
  - 1 x 49GSM Glass
  - 1 x 86GSM Glass
  - 1 x 86GSM Glass, 0x90
  - 1 x 86 GSM Glass

**Internal Frames**



- Root Ribs:
  - 3 x 200GSM Carbon
  - 1.5mm Airex C70 Foam
  - 3 x 200GSM Carbon

- Spar Shear Webs: (Before Boom)
  - 2 x 200GSM Carbon
  - 1.5mm Airex C70 Foam
  - 2 x 200GSM Carbon

- Spar Shear Webs: (After Boom)
  - 4 x 200GSM Carbon

- Chord-Wise Ribs:
  - 1 x 106GSM Glass, 0x90
  - 1 x 106GSM Glass
  - 1 x 106GSM Glass
  - 1 x 106GSM Glass, 0x90

- Rear Shear Web (Before Boom)
  - 1 x 106GSM Glass
  - 1 x 106GSM Glass, 0x90
  - 1 x 106GSM Glass, 0x90
  - 1 x 106GSM Glass

- Rear Shear Web (After Boom)
  - 1 x 106GSM Glass
  - 1 x 86GSM Glass, 0x90
  - 1 x 106GSM Glass

**NOTES:**  
 - ALL MATERIAL TO BE ORIENTATED  
 AT 45x45 UNLESS OTHERWISE STATED

NO	DATE	BY	CHKD	APPVD	REV

**CSIR**  
 TITLE: Kwadira Wing Layup MSC

Figure 52 - Layup drawing sheet 1 for the new Kwadira wing structure

**Top Spar Cap**

**Bottom Spar Cap**

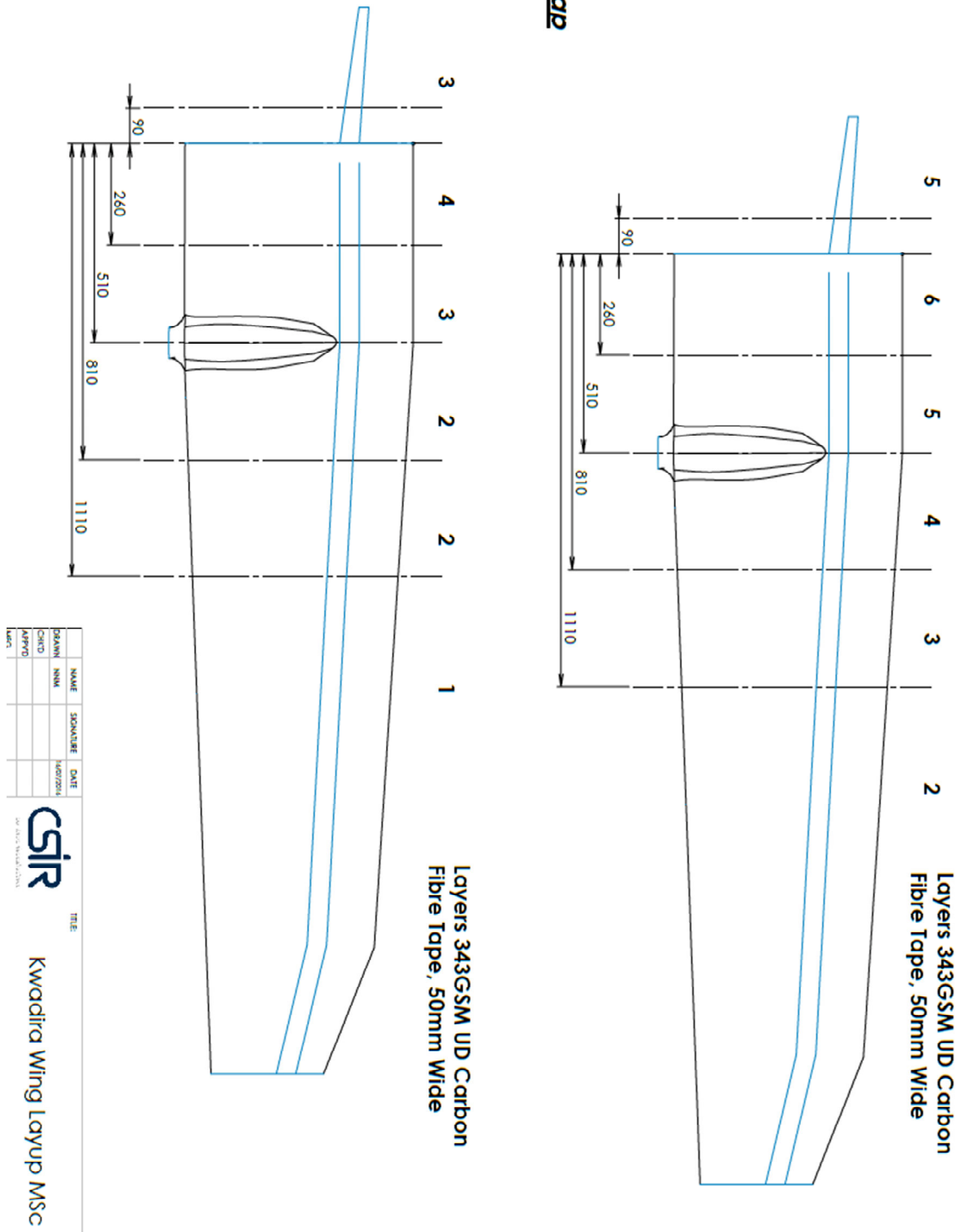


Figure 53- Layup drawing sheet 2 for the new Kwadira wing structure

## 6. Wing Manufacture

The new Kwadira wing was built entirely in the CSIR UAS Laboratory and composites workshop. This chapter describes the process of building the wing structure that was designed in Chapters 4 and 5.

### 6.1. Kwadira Wing Moulds

#### 6.1.1. Mould Preparation

As a result of the wing moulds being placed in storage following the conclusion of the Kwadira project in February 2015 some preparation was necessary in order to render the moulds fit for use. This primarily involved cleaning of fine dust from the moulds using a soft cloth. It was also necessary to remove resin and glass fibre residue that was left on the moulds due to their previous use in constructing structural test sections of the original wing. This residue was removed using a thin mixing stick made of a soft wood so as to avoid damaging the mould surfaces.

#### 6.1.2. Release Agent

Mirrorglaze 87 Carnuba wax was originally applied to the Kwadira wing moulds so it was both necessary and convenient to continue using it for this project since the moulds would have had to be cleaned with a solvent such as Acetone in order to use a different release agent.

Mirrorglaze 87 is a high-temperature release wax that is applied in several layers to a mould surface and creates a thin physical barrier between the mould and applied resin (AMT Composites, 2016). The wax was applied using soft paper towel, allowed to set and then buffed to a smooth finish. This process was repeated until 4 layers of wax were present on the mould surfaces.

### 6.2. Wing Skin and Spar Cap Layup

#### 6.2.1. Material Preparation

The 86GSM, 106GSM and 200GSM woven glass and carbon fibre cloth is supplied in rolls between 1 m and 1.2 m wide with a fibre orientation of  $0^\circ/90^\circ$ . Since the cloth width is limited, several pieces were required to make up the wing skins and these were cut on the UAS Lab cutting table using a steel straight edge and a scalpel. Care was taken to ensure that the  $-45^\circ/+45^\circ$  sections were cut accurately. The 343GSM UD Carbon tape is supplied in a roll and this was cut into lengths to form the spar caps.

In order to vacuum the materials to the moulds to ensure an accurate final shape it was necessary to cut pieces of: (see Figure 54)

- Peelply: A woven Nylon fabric that is applied directly to the material surface and removed after curing. Peelply allows excess resin to seep through it and gives the cured material a coarse surface finish that greatly increases surface area for secondary bonding (AMT Composites, 2016).
- Release film: A thin plastic that has been treated to release from epoxy resin systems and is perforated to allow resin to seep through. This film helps to keep the breather cloth from bonding to the materials (AMT Composites, 2016).

- Breather cloth: A soft polyester material that both absorbs excess resin that seeps through the release film and provides a continuous air path for pulling vacuum on the component (AMT Composites, 2016).
- Vacuum film: A Nylon-based film that is both tough and elastic and is used to pull vacuum on the part. The vacuum film is usually sealed using a special sealant tape that bonds well to non-porous surfaces such as the vacuum film.



**Figure 54 - Picture showing the layers of material used to lay up the GFRP components: Glass fibre (white, outside), nylon peelply (striped), perforated release film (orange), breather cloth (white, inside) and vacuum film (purple).**

### **6.2.2. Layup and Vacuum Bagging**

The glass and carbon fibre layers forming the skins were layed by hand using a wet layup technique. The layers of material were layed in place on the moulds and resin was applied using soft brushes and small foam rollers to spread the resin uniformly across the surfaces of the moulds. The glass fibre layers forming the skins were layed up first, followed by the Carbon fibre tape forming the spar caps. Care was taken to ensure correct material orientation and placement as given by the layup drawings.

Once the material had been layed up the layers of peelply, release film and breather cloth were layed onto the mould surfaces and the entire mould placed in a 3 m x 1.5 m vacuum bag created using vacuum film and sealant tape. The UAS Lab composites workshop vacuum pump was then used to pull a vacuum on the mould and material of near to 1 bar for a period of 5 hours (see Figure 55). The wing skins were left in the moulds to facilitate correct placement of the internal structural components and to ensure accurate joining of the top and bottom skins.



**Figure 55 - Picture showing the bottom wing skin layed up in the mould (blue) and covered with peelply, release film, breather cloth (white) and vacuum film (transparent purple). Note also the vacuum fitting used to pull a vacuum on the materials.**

### **6.2.3. Leading/Trailing Edge Trimming and Lip Layup**

Once the skins had cured, the vacuum bag, breather cloth, release film and peelply was removed from the skins and spar caps and the excess material around the leading and trailing edges of the wing was trimmed away using a scalpel.

In order to facilitate joining of the wing top and bottom skins' leading edges a lip was layed up on the leading edge of the bottom skin using 3 layers of 106GSM glass fibre. An internal lip was layed up using a mould of the top skin leading edge and is therefore profiled to this shape with a 2 mm offset inside the skin. This lip was later trimmed to a height of 30mm from the wing split line and slits were cut to prevent interference with the ribs as shown in Figure 56.



Figure 56 - Picture of the bottom wing skin with leading edge lip.

## 6.3. Web and Rib Construction

### 6.3.1. GFRP/CFRP Sheets

The glass and carbon fibre sheets needed to construct the internal webs and ribs were layed up using the same wet layup technique as for the wing skins. The sheets were formed by laying up the glass and Carbon fibres on a flat granite sheet with a layer of peelply each side of the fibres to create a coarse finish for bonding the webs and ribs to the skins. The material was vacuumed to the granite slab using vacuum film and sealant tape.

### 6.3.2. Laser / CNC Router Cutting

The CAD surface model of the wing created in Chapter 5 was used to create DXF (Drawing Exchange Format) files containing the geometries of all the web and rib pieces need to construct the internal framework of the wing. These files were then used to cut the webs and ribs out of the prepared sheets.

It was originally intended to cut the webs and ribs out using a CNC waterjet cutter but it was found that the waterjet cutter posed a few practical problems and it was therefore decided to pursue alternative cutting methods. The waterjet cutter bed consists of a large tank of water with a number of

metal strakes onto which workpieces are placed for cutting. The system is designed so that the tops of the strakes allow for the workpieces to be placed just above the surface of the water. It was found that the thin, small pieces of the ribs and webs would fall into the water between the metal strakes and be lost in the large body of water. The problem was exaggerated by the large pressures generated by the waterjet cutting nozzle which forced the cut pieces into the water.

Since the prepared sheets of GFRP were relatively thin it was decided to use a laser cutter located in the CSIR National Laser Centre to cut out the ribs and sub-shear webs. The main spar webs, being carbon foam sandwich, were cut out using the ASC UAS Lab CNC router since it was found that the NLC's laser cutter is unable to cut CFRP.

### 6.3.3. Web and Rib Lattice Assembly

The locations of the internal webs and ribs were marked out on the front and rear edges of the top surface mould using strips of masking tape. The webs and ribs were then tacked into place using small amounts of quick-set epoxy adhesive as shown in Figure 57. This allowed for the alignment and spacing of the webs and ribs to be checked before final bonding took place. Due to constraints on the size of the CFRP sheet that could be layed up the main spar web needed to be split into several pieces. These were joined to each other using strips of 200GSM carbon fibre cloth before tacking them in place.

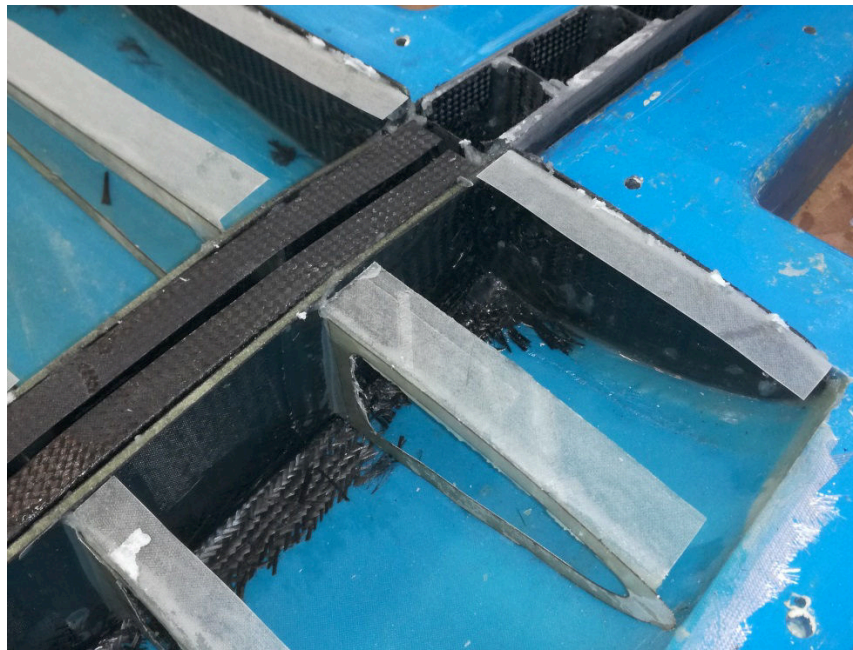


Figure 57 - Picture showing the top wing skin (light blue) in the top skin mould (blue). Note the carbon spar caps and webs (black) and the span-wise ribs (white).

### 6.3.4. Cleating of Lattice to Top Skin

Once all the internal frames had been tacked in place they were cleated to the top skin using thin (30mm) strips of 106GSM glass fibre (for the ribs and sub-shear webs) and 200GSM carbon fibre (for the main webs). This was done in order to ensure proper bonding to the top skin as the webs and ribs were deemed too thin to bond them using any kind of paste adhesive. Care was taken to ensure that resin was used sparingly in this process. The cleating is shown in Figures 58 and 59.

As a further result of the thin webs and ribs a separate process was completed by which thin strips of glass and carbon fibre cloth were layed up and vacuumed around a long rectangular aluminium section which was used as a mould. This produced long strips of right-angled GFRP and CFRP which were bonded to the webs and ribs in order to facilitate bonding with the bottom wing skin as shown in Figures 58 and 59.



**Figure 58 - Picture showing the cleating of the webs and ribs to the top skin. Also note the right-angled strips of GFRP and CFRP bonded to the webs and ribs to create sufficient surface area for bonding the bottom wing skin.**



Figure 59 - Picture showing further detail of the cleating as well as the bonding surfaces bonded to the bottom side of the webs and ribs (the wing is lying inverted).

## 6.4. Wing Closing and De-Moulding

### 6.4.1. Joining Lines

Ampreg 21 laminating epoxy filled with cotton flocks was used to join the bottom skin to the top skin and internal webs and ribs. This adhesive is created by mixing the resin in a roughly one-to-one ratio with the flocculated cotton and results in a mixture that is easy to work with and structurally sound (Technology Innovation Agency, 2008). This adhesive also takes on the mechanical properties of the resin used and approximates an isotropic material due to the random orientation of the fibres. The

adhesive was applied to the leading edge lip, trailing edge and all the edges of the webs and ribs as shown in Figure 60. The top (containing the top wing skin and internal frames) and bottom (containing the bottom wing skin) wing moulds were then closed and bolts were screwed in along the leading and trailing edges of the moulds to ensure proper bonding along the edges.

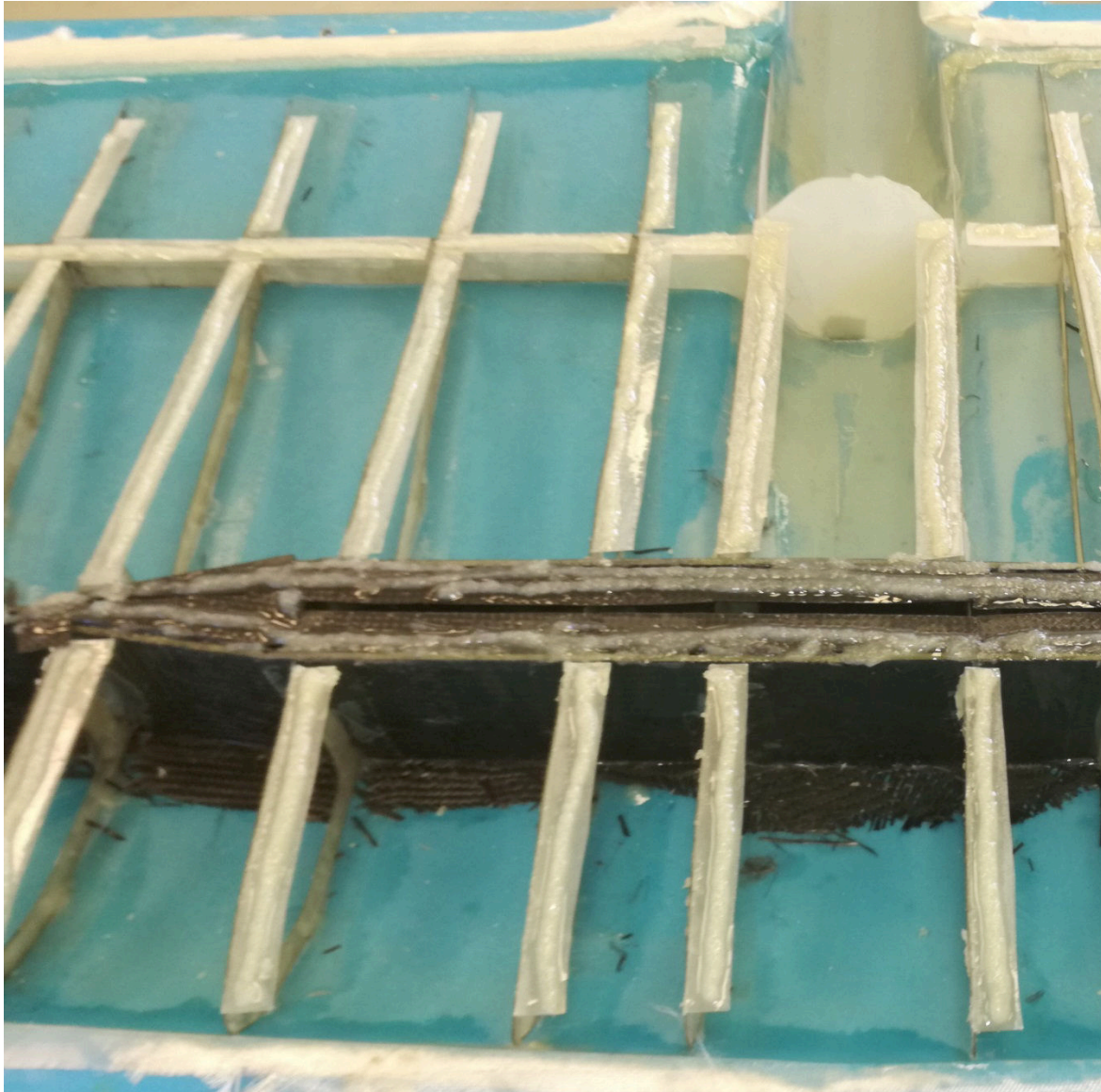


**Figure 60 - Picture showing the lines of filled epoxy resin that was applied to the bonding surfaces of the webs and ribs and the leading and trailing edges of the wing skins.**

#### **6.4.2. De-Moulding**

Demoulding the wing involved removing the clamping bolts from the moulds and applying a firm torque to the moulds. This is done since the moulds are made of glass fibre themselves and are slightly flexible. The wings were demoulded and all the excess fibres were trimmed from the leading and trailing edges of the wing. The final wing is shown in Figure 61.



**Figure 61 - Picture showing the final wing after leading and trailing edge trimming. Note the spar caps (black) as they appear through the semi-transparent GFRP wing skins.**

### 6.4.3. Hardpoints

Due to the poor bearing load carrying capability of thin CFRP faces, such as those that are used in the root rib and main shear webs, it is standard practice at CSIR ASC to make use of relatively thick glass fibre hardpoints to transfer large bearing loads such as those induced by pins into the surrounding material. Circular hardpoints of DC Wort NEMA G11 were cut out of a large sheet using a CNC router and bonded into the root rib and spar root using a mixture of resin and cotton flocks as shown in Figure 62. These were then covered with a layer of 200GSM carbon cloth in order to further enhance load transfer between the hardpoints and the CFRP faces.

It is important to note that the holes in the root ribs and spar roots of the FEA models created in Chapter 5 were sized according to the outer dimensions of their respective hardpoints. The bearing load relief provided by the hardpoints was thus taken into account in the FEA simulations.



Figure 62 - Picture showing the NEMA G11 hardpoint (circled in red) bonded into the wing root rib.

### 6.4.4. Final Weight

The final weight of the wing was measured using a calibrated scale borrowed from the ASC Wind Tunnel Research Group and was found to be 4.66 kg. This weight does not include the mass of the paint that was used in the original wing, a CFRP tail boom socket and a GFRP looming conduit with a total mass of 1.129 kg, all of which are measured weights obtained from previous testing. The final weight of the wing is then 5.814 kg which is 0.02 kg under that which was predicted in Chapter 5 and an improvement of 0.964 kg or 14.2% over the original wing's mass of 6.778 kg.

## 6.5. Chapter Summary

The process by which the new, lighter wing design was constructed is described. Existing Kwadira wing moulds were prepared by cleaning and applying a wax-based release agent and a conventional wet layup method was used to vacuum pieces of glass fibre cloth and unidirectional carbon fibre tape to the moulds thereby forming the wing skins. A lip required to facilitate joining of the top and bottom skin leading edges was layed up on the bottom skin and sheets of glass and carbon fibre were layed up on a flat surface and cut out using a laser cutter and a CNC router due to practical issues encountered with the waterjet cutter. The webs and ribs that were cut out were tacked and cleated to the top wing skin, and right-angled strips were layed up and bonded to the bottom of these to form a surface that would facilitate bonding to the bottom skin. The bottom skin was joined to the top skin and internal frames using a mixture of resin and cotton flocks and the complete wing was demoulded and trimmed. Finally, bearing load-carrying hardpoints were bonded into the root rib and spar root. The final product was weighed and a weight saving of 14.2% over the original design was confirmed.

## 7. Experimental Setup, Testing and Results

It is standard practice in the aircraft industry to perform static structural testing of aircraft wings using a whiffle tree. This chapter describes the procedure by which the wing that was built was tested in order to validate the FEA predictions of Chapter 5.

### 7.1. Experimental Setup

#### 7.1.1. CSIR Wing Structural Test Rig

The ASC Wing Structural Test rig is a frame made out of steel sections that has been designed to test up to 3 m wings with up to 10 000 N of force which is distributed to points along the wing using a custom-setup whiffle tree assembly. The test rig has a hand-operated hydraulic cylinder attached to a hydraulic jack that is used to apply the loads via a simple set of pulleys. Recently the test rig has been upgraded with a variable whiffle tree that can be adjusted on the fly to simulate various wing loadings through the use of movable load points attached to the beams of the whiffle tree.

The test rig has been used to successfully test a number of wings in the recent past, amongst others the original Kwadira wing. The rig with the wing built for this project along with its associated whiffle tree is shown in Figure 63. In normal flight aircraft wings experience an upwards-acting lift force. It must be noted that wings are attached to the wing structural test rig upside-down and that load is applied towards the ground in order to simulate the lift loads on the wing.



Figure 63 - Picture showing the Wing Structural Test Rig (yellow), whiffle tree (silver), new wing (dull green), wing saddles (white), dummy wing (red), hydraulic jack and pump (black, bottom).

### 7.1.2. Whiffle Tree Loads and Set Up

The aim of the whiffle tree was to attempt to accurately simulate complex, non-uniform lift load on the wing using 8 discrete, uniformly spaced points as was provided by the whiffle tree. In order to do this a spreadsheet was created to calculate the forces to be applied to each discrete point.

The spreadsheet receives as inputs the span of the wing and the lift distribution and calculates the magnitude of the force required at each application point along the wing span using an area-weighted centroid method shown in Figure 64: For each point, the total load to be applied to the wing was multiplied by a fraction of the area underneath the lift-wing span diagram. This creates a scenario where the 8 discrete points produce a shear force distribution along the wing that is representative of the actual shear force distribution as was calculated in Chapter 4, as shown in Figure 64. The load case that was chosen to be tested was the Point B (40 m/s, 4.9 g) load case for which a whiffle tree simulation was performed in Chapter 5.4.1.4.

Since the location of the load application points and the force applied at each point was known, the whiffle tree beam lengths could be calculated using simple force and moment equilibriums: The force at each point should be equal to the sum of the two forces above it, and the moments about each point should equal zero leaving the only unknowns being the distances between the load points. This is illustrated in Figure 65. Note that load points 2 and 3 include the loads of the horizontal stabiliser introduced into the wing by the tail boom.

The spreadsheet then takes into account the weight of the whiffle tree components and the weight of the wing itself and subtracts this force from the total force that is to be applied to the whiffle tree to calculate the force to be applied by the hydraulic jack to obtain the desired g-loading. Lastly, the spreadsheet used the beam lengths and loads to check the strength of the whiffle tree beam sections.

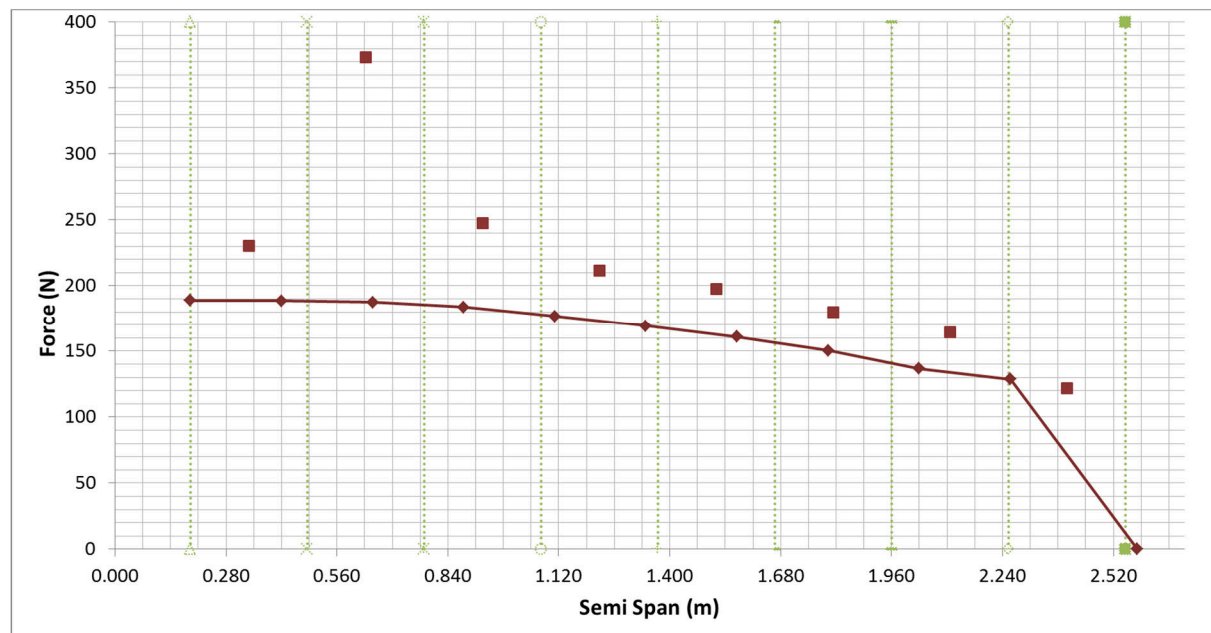


Figure 64 – Diagram showing the magnitudes of the forces applied to each discrete point along the wing span.

Root							Tip
1	2	3	4	5	6	7	8
230	373	248	212	198	180	164	122
x5		x7		x9		x11	
604		459		378		286	
x3			x4		x13		
1063				663			
x1				x2			
1726							

Figure 65 - Image showing the loads to be applied to the wing using the whiffle tree linkages.

### 7.1.3. Test Rig and Wing Setup

#### 7.1.3.1. Whiffle Tree

The whiffle tree consists of standard aluminium sections with custom built clamps that are moveable across the length of the sections and are connected with custom made wire ropes. The whiffle tree was set up according to the spreadsheet mentioned above and is shown laid out on the floor in Figure 66.

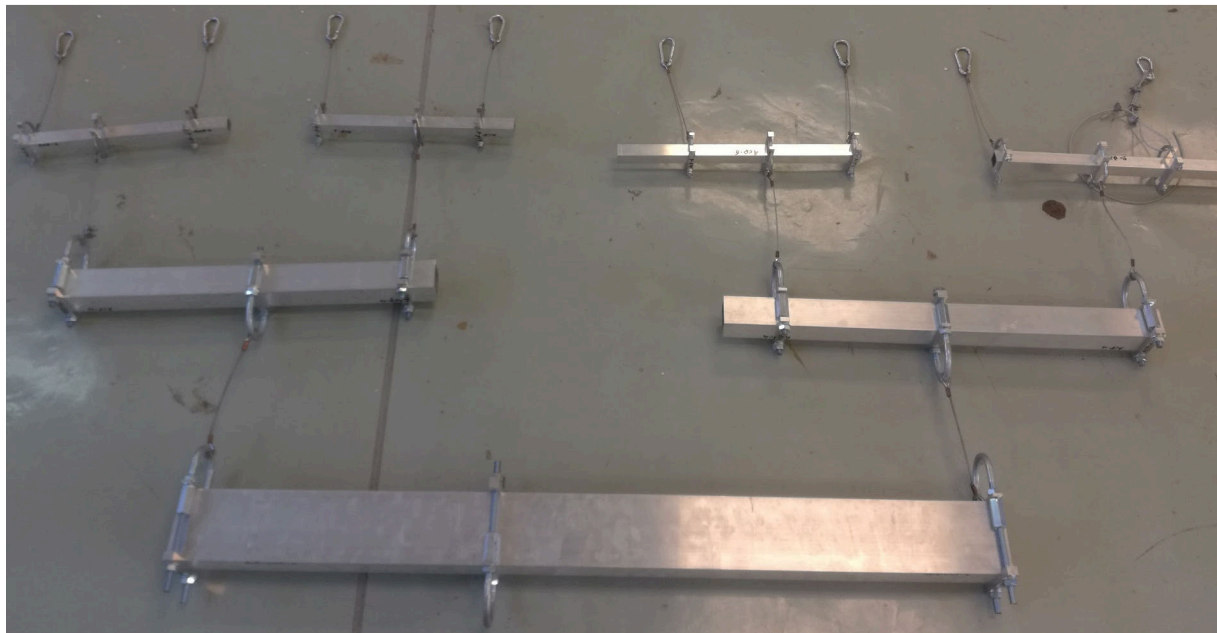


Figure 66 - Picture of the whiffle tree as it was set up for testing of the newly built wing.

#### 7.1.3.2. Wing Saddles

Wing saddles were cut out of expanded polystyrene in the shape of the aerofoil at the chosen eight sections of the wing where loads were to be applied. These polystyrene shapes were then clamped to the wing using square aluminium sections using threaded rod and nuts. The wing saddles, shown in Figure 67, served two purposes:

1. Ensuring that the load application point did not move during the test.
2. Distributing the load through a 100mm wide area onto the bottom wing skin. This mirrors the FEA analysis that was performed in Chapter 5.3.1.4.

The load from the whiffle tree is applied to the wing saddles via a wire rope that passes through the bottom aluminium section.



Figure 67 - Wing saddles constructed out of polystyrene and aluminium beams that were used to transfer the loads from the whiffle tree to the wing.

### 7.1.3.3. Dummy Fuselage and Dummy Wing

As mentioned in Section 4.3.6, the Kwadira aircraft wing attachment mechanism uses two 12 mm pins per wing to transfer wing shear and torsion loads from the wing root ribs to the fuselage and two 16 mm pins to transfer wing bending loads between the main spars. In order to replicate these mechanisms a dummy fuselage and a dummy wing was constructed. The dummy fuselage replicates the Kwadira fuselage shear pin hardpoints and locations and is constructed from cored GFRP. The dummy fuselage was fastened to the top of the Wing Structural Test Rig and provided a strong attachment point for the wing and dummy wing. The dummy wing was constructed from standard steel sections that were welded together and provided hardpoints for the wing spar pins to attach to. The dummy wing also attaches to the dummy fuselage using two pins. This is shown in Figures 68 through 70.

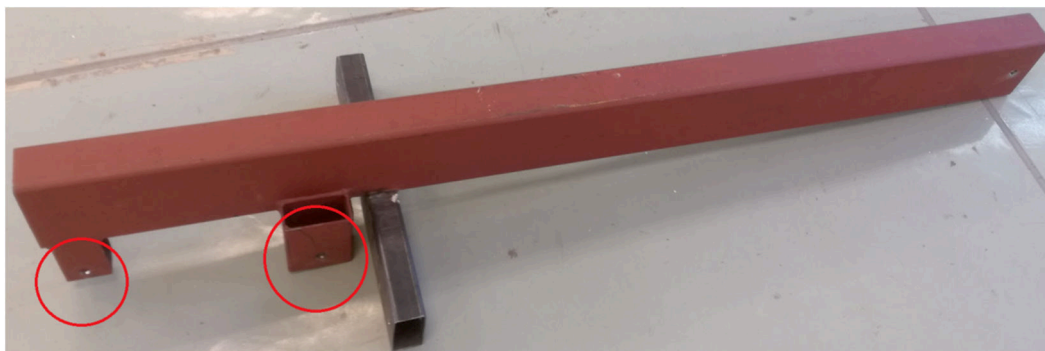


Figure 68 - Picture of the dummy wing that provides hardpoints (circled in red) to transfer the wing bending loads from the new wing.



Figure 69 - Picture of the dummy fuselage that was constructed which provided hardpoints (circled in red) for the wing shear/torsion pins to attach to.

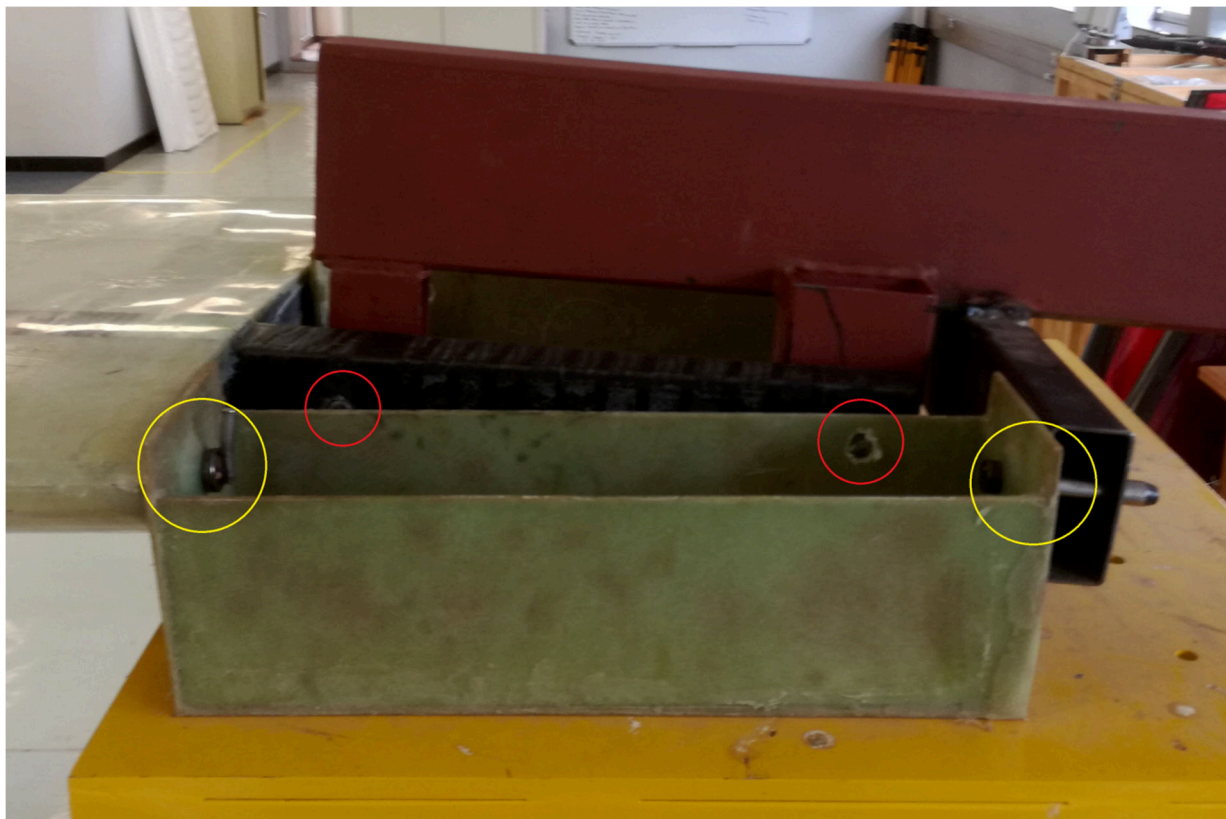


Figure 70 - Picture showing the attachment of the wing and dummy wing to the dummy fuselage. Note the wing shear/torsion pins (circled in yellow) and the spar pins (circled in red).

#### 7.1.3.4. Hydraulic Jack and Wire Rope

A strong steel wire rope was used to connect the whiffle tree via a pulley to the one side of a hydraulic jack that is operated using a simple hand pump. The opposite end of the hydraulic jack was connected to the dummy wing also via a pulley. This setup is shown in Figure 71. This results in the same overall load being applied to each wing and creates the correct bending moment reaction in the dummy wing to counteract the bending moment created in the new wing's spar root.

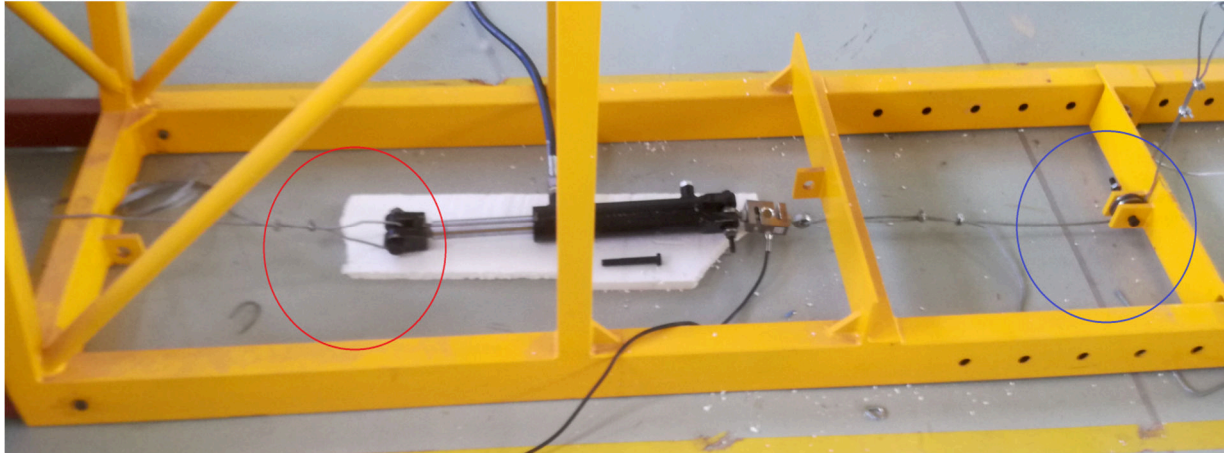


Figure 71 - Picture showing the hydraulic jack in the Wing Structural Test Rig. Note the hydraulic line exiting the top of the picture. Also note the pulley around which the wire rope is passed to the whiffle tree (circled in blue) and the attachment of the wire rope (circled in red) that is attached to the dummy wing. Also shown is the load cell attached to the right side of the jack.

#### 7.1.3.5. Load Cell

A load cell was connected between the hydraulic jack and the whiffle tree to measure the load applied to the whiffle tree. The load cell was given a 24V input from a dedicated power supply and the output was read using an Arduino UNO electronics prototyping board (serving as an ADC) via a dedicated load cell amplifier and signal conditioner developed for a previous project. The load cell has been calibrated in increments of 0.5 kg in a previous project conducted by the author. The output from the electronics prototyping board was translated using a simple Arduino program that displayed the tension applied to the whiffle tree in real-time on a laptop. The Arduino program also included a function to convert from tension applied to the whiffle tree in N to g-load experienced by the wing.

#### 7.1.3.6. Deflection Measurement

The deflection of the wingtip was measured using a measuring tape attached to the wing tip. The wingtip was chosen since it was predicted to have the largest offset from its resting position as the wing deflected and would provide for the least error in measurement. At each set increment of g-loading as measured with the load cell the deflection was measured and several test runs were performed in order to obtain an average of results. This was done in order to account for any initial stretching of the wire rope and settling of the wing saddles and to reduce any measurement errors.

## 7.2. Test Procedure and Results

As discussed in Chapter 5.4.1.4, the wing was modelled in FEA with the whiffle tree loads applied to it and the tip deflection recorded. This was done for a loading of 1 g up to 4.9 g in increments of 0.5 g.

The wing was tested by applying load to the hydraulic jack and hence the whiffle tree and wing by using the hydraulic hand pump. This was continued until the load cell readout displayed the desired g-loading. After the load cell readout had stabilised the deflection of the wing tip was measured and recorded. This sequence was done several times in order to obtain an average of results and to reduce any errors in measurement.

The results of the FEA analyses and the physical testing are presented in Table 10 and Figure 72 below, and show a good correlation between the FEA model and the physical test piece, with an average error in prediction of 3.9%.

Table 10 - Results of the FEA whiffle tree analyses and the physical testing compared side by side.

g-Load	Measured Tip Deflection Values (mm)	Relative Measured Tip Deflection (mm)	FEA Predicted Tip Deflection (mm)	Relative FEA Tip Deflection (mm)	Percentage Difference
1	874	0	38	0	-
1.5	856	18	56.5	18.5	2.8%
2	838	36	73	35	2.8%
2.5	820	54	94	56	3.7%
3	796	78	111	73	6.4%
3.5	781	93	129	91	2.2%
4	769	105	145	107	1.9%
4.5	755	119	163	125	5.0%
4.9	749	125	171	133	6.4%

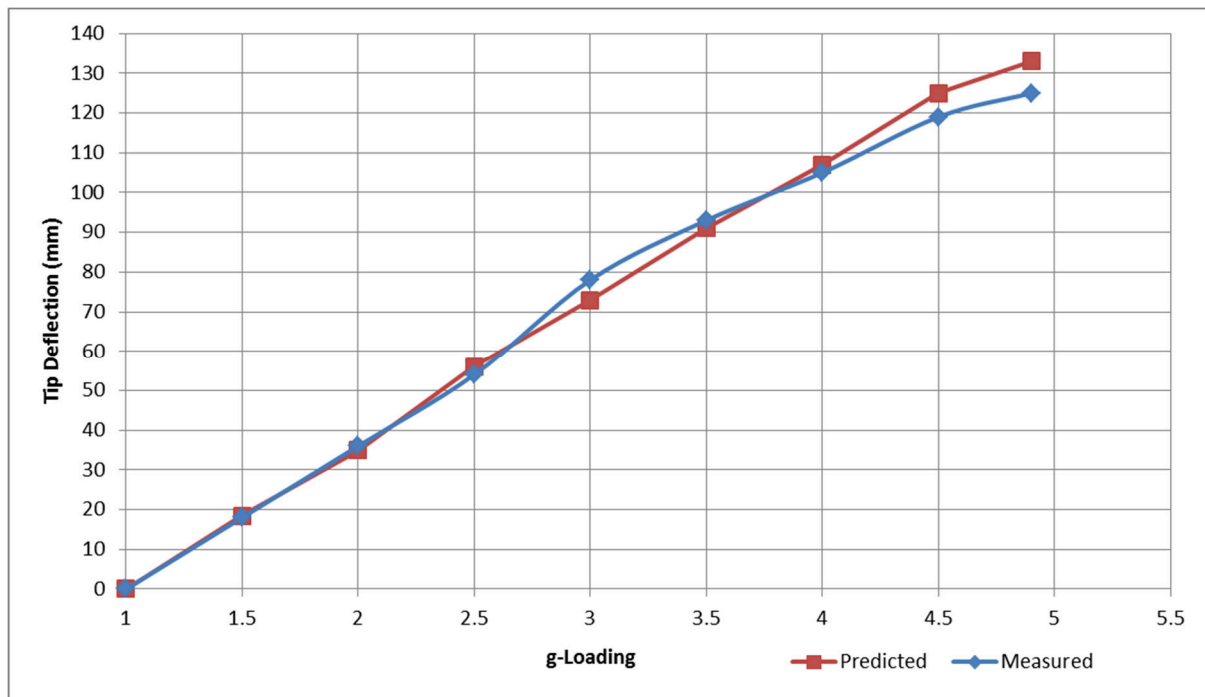


Figure 72 - Plot of the measured tip deflection versus the predicted tip deflection.

### 7.3. Chapter Summary

The process by which the new wing design was tested in order to verify the FEA model of the wing is described. A spreadsheet was developed to translate the distributed lift loads experienced by the wing at the point B load case (40 m/s, 4.9 g) into 8 concentrated point loads using an area-weighted method to closely approximate the same shear force distribution as compared to that created by the distributed lift loads. Wing saddles were constructed to distribute the point loads across a 100 mm wide area (mirroring the FEA model) and an aluminium whiffle tree was adapted to create the required point loads from tension applied to it using a hydraulic jack. A dummy fuselage and dummy wing were built to produce the required reaction loads at the wing root. A small electronics prototyping board displayed the output from a load cell on a laptop and measurements of wing tip deflection were taken at set increments of g-loading. The test was completed multiple times and the deflection results averaged. The measured deflection results show a good correlation between the physical wing and the FEA model with an average error in prediction of 3.9%.

## 8. Discussion

### 8.1. Discussion of Literature Review

A wide array of literature was reviewed for this research and indeed the author found it necessary to search for more information along the way as challenges were encountered during the course of the project. An example is the initial sizing spreadsheet model created for Chapter 4 where it was necessary to reference a number of sources on aircraft structures before a model could be created that was simple yet accurate enough to yield a good starting point.

The creation of the aircraft flight envelope and the determination of the flight loads was guided by the FAR-23 regulations and interpreted by several authors.

The literature guided the author through the composite material design and testing process by which progressively more complex elements of a system are built and tested. This was evidenced by the construction of composite test coupons which yielded material properties and the later testing of the complete wing.

It was deemed critical to review multiple internal structural layouts and to weigh the advantages and disadvantages of each in order to make an informed decision on a more optimal layout. Several sources presented methods for designing traditional metal wing layouts while others detailed methods of designing for composite materials. Different design philosophies were also considered such as the different views on numbers of spars and ribs of Western and Eastern designers. This led to the decision to attempt to optimise several internal layouts to find the lightest one.

The review of composite materials and their unique properties and failure theories led to the choosing of the Tsai-Wu failure theory which allows for differing material yield strengths in tension and compression.

It was also important to model the wing in FEA as accurately as possible and again the work of several authors and organisations was considered in this. Important aspects such as modelling contact and fibre direction correctly were highlighted and were executed correctly as a result of this literature investigation. Accuracy was of utmost importance when designing at close to the limit of what composite materials allow.

Different methods for testing the static strength of wings were reviewed and the outcome of this was the selection of the whiffle tree method of wing testing by which a single load point is distributed to several points along the wing thereby replicating the primary shear loading on the wing.

### 8.2. Discussion of Material Properties and Testing

The author was fortunate enough to be in possession of material properties of various forms of laminated carbon fibre as a result of assisting with the project of Perini several years prior to the commencement of this project. Since accurate material properties for one half of the materials used was available it was deemed non-sensical to assume properties for the other half and so funding was applied for to perform material tests on the 86GSM and 106GSM laminated glass fibre materials.

The material tests that were performed proved to be a valuable learning experience and highlighted the importance of checking for inter-laminar shear stress failure. The relatively large difference in properties between the two weights of glass fibre proved to be a surprise and this highlighted the importance of material testing and accurate composite property assignment in the FEA model. The aim of designing a wing to be as light as possible would not have been possible without a complete picture of the limits of all the materials involved.

### 8.3. Discussion of Analytical Wing Loadings, Structural Layouts and Initial Sizing Model

Creation of the aircraft flight envelope in the form of a V-n diagram resulted in three points chosen as maximum load cases: Point A (35 m/s, 3.8 g), Point B (41 m/s, 4.9 g) and Point D (50 m/s, -1.75 g). Shear force, bending moment and torsion diagrams were constructed for each load case by using spreadsheet methods combined with lift and moment distributions obtained from XFLR5's VLM analysis tools. It was seen that, even with full aileron deflection, the loads imposed on the wing at Point A were less than those imposed by Point B and so Point B was used as the maximum positive load case.

The two structural layouts that were chosen for FEA analysis and optimisation were the traditional metal wing layout and the tri-directional rib lattice layout which were chosen based on the literature reviewed and work done by previous authors. The interactions between the wing skins, internal ribs, webs, spar caps, and shear pins were explored and a spreadsheet-based initial sizing model was developed to obtain a starting point for the FEA analyses and optimisation. This model saw the use of basic bending and shear flow equations to find FRP layups for each of these structural components.

A weight saving of 21% over the original Kwadira wing's weight was predicted based on this initial sizing which was obtained using a composite mass model which takes into account all individual structural components as well as the necessary adhesive joining lines and cleating strips.

### 8.4. Discussion of the FEA Models

Creating the CAD surface model for the FEA analysis proved to be a challenging task as a result of the large number of surfaces involved and the several layout optimisation iterations performed which each required a new geometry to be created. Some time was also spent on ensuring that the composite ply directions assigned to each surface were modelled correctly. Much thought was put into the two different sets of fixtures since it was found to be important to simulate the fuselage attachments correctly in order to be able to compare the FEA model with the subsequent whiffle tree testing, but still have a set of fixtures that enabled optimisation iterations within a reasonable timeframe.

The mesh convergence study found that the model was more sensitive to changes in the maximum element size and that the decision to make the minimum element size smaller than the smallest radius of curvature proved to be correct. As mentioned in Chapter 5 additional subsequent mesh refinement was performed on several surfaces to capture stress concentration effects especially on thin parts.

Application of the loads to the models proved to be simple once the correct coordinate systems had been set up but the application of the torsional loads proved to be a challenge. When these loads were applied to the wing skins an unrealistic situation was created where an aerodynamic twisting moment was being represented by couple forces and so it was decided that these loads would be applied to the wing ribs which would effectively transfer the loads to the skin and shear webs.

Some time was spent completing the layout and layup iterations, all the while keeping track of the new estimated weight of the wing using the composite mass model spreadsheet which estimated the mass of each spar cap, web, skin section, rib, lip, cleating strip and joining line with lengths and areas obtained directly from the CAD model. The predicted (and subsequently measured) decrease in weight of the final wing of 14.2% equates to a saving of nearly 1 kg per wing and a total weight saving of 2 kg on the complete aircraft. This equates to 2 kg more fuel that can be carried which will significantly extend the range of the aircraft.

## 8.5. Discussion of the Construction and Testing

It was originally anticipated that the construction time of the new wing would be less than compared to that of the original wing which made extensive use of foam core which needed to be cut, sanded to various angles and curved to specific shapes using a heat gun. It was however found that the construction time of the new wing design was longer than that of the original wing. Several factors are thought to have played a role:

- The number of parts in the wing internal structures (considering individual rib pieces fore and aft of the main shear web and sub shear web, the main shear web being split into several pieces, etc.) needing to be tacked in place by hand and then subsequently cleated increased construction time.
- Several jigs needed to be constructed in order to hold the pieces in place and the time required to construct them was not taken into account when performing the new design.
- Construction time was further increased due to the multiple over-night curing cycles being required during the construction process, i.e. the requirement for all the pieces to be bonded in a specific order.

It is thought that with the design of dedicated jigs and a well thought-out construction sequence the time needed to manufacture the new wing design could be substantially reduced.

The testing of the wing was completed without any significant complications. The whiffle tree was setup according to the spreadsheet described in Chapter 7 and was attached to the wing using custom-made polystyrene saddles. These saddles served the dual purpose of distributing the individual point loads to 100 mm wide areas along the wing span and also fix the load application point on the wing by providing a clamping force. A load cell and data acquisition system developed for a previous project was used to record the load applied to the wing which was displayed as a real-time readout of the equivalent g-loading applied to the wing.

The decision to use the deflection of the wing tip as a means to validate the FEA model was reached based on the desire to minimise errors in measurement by measuring a parameter that was likely to give a large, quantifiable output as opposed to measuring deflection at the wing mid-span which was predicted to deflect to a lesser degree.

## 8.6. Validation of FEA with Test Results

The wing testing, which was performed several times in order to obtain average results, showed a good average error of 3.9% between the physical wing and the FEA whiffle tree model. It was seen in Chapter 7 that the largest errors in prediction were found closer to the more extreme loadings where the FEA model predicted larger deflections than what was found during the physical testing. Generally, wings are required to be as stiff as possible to avoid rapidly fluctuating aerodynamic phenomena such as flutter and so a conservative FEA prediction as was found is seen in a better light than the opposite as it will cause the designer to err on the side of caution.

Several causes exist for the 3.9% difference between predicted and measured deflections:

- As the wing deflects the directions of the individual load application points change slightly. This slight change in load application direction was not modelled in the FEA model and could possibly contribute to the measurement error.
- The whiffle tree's wing saddles were positioned on the wing with an accuracy of roughly  $\pm 2$  mm and this combined with any slight misalignment in the aluminium beam load spreaders

could point to the possibility of different load application point positioning which could produce results different to that of the FEA model.

- Although it was taken into account in determining the final loads to be applied to the whiffle tree, the mass distribution of the whiffle tree (and wing saddles) and the mass distribution of the wing itself could have been different to what was originally predicted.
- The varying amount of bonding agent (due to the prototype nature of the wing) used to bond the internal webs and ribs to the skins and spar caps could have influenced the measured results due to under- or over-stiffening of the bonded joints.

The good correlation between the FEA model and the physical wing conveys confidence in the FEA model and significantly validates the FEA predictions obtained from using the distributed lift, torsion and drag loads which predict survival of the wing at its ultimate loads (see Section 4.1.4). This ultimately suggests that a lighter, more optimised wing making use of stiffened skins instead of cored sandwich construction is indeed a possibility.

## 9. Conclusions and Recommendations

### 9.1. Summary of Objectives

At the beginning of this research the objectives were defined as being:

1. To determine if an existing UAV constructed using cored composite materials could be lightened through the use of a coreless composite construction while maintaining adequate strength and stiffness.
2. To determine if coreless composite construction mentioned in Objective 1 would enable a decreased construction time by foregoing the preparation and placement of core material and instead relying on waterjet cut components.

### 9.2. Synopsis of Research Conducted and Findings

An array of literature was reviewed and it was found that multiple wing internal structural layouts have been considered throughout the history of aircraft design with the common theme of achieving lower mass while maintaining or increasing strength and stiffness. The theory behind the analysis of composite materials, aircraft wing loading and FEA of composite materials was discussed. Materials similar to those used for the original Kwadira wing were selected and material testing was combined with material properties obtained from literature to form a complete picture of the chosen materials' properties. The maximum loads acting on the wing during flight were found by a combination of panel codes and spreadsheet calculations following the creation of a flight envelope according to FAR23 methods.

Two new structural layouts were proposed that could offer weight savings over the original design. It was initially predicted that a weight saving of 21% could be achieved. The new layouts were modelled in an FEA package and an iterative optimisation process was carried out on the traditional metal wing layout to obtain a more optimal internal layout and composite layup, since it was found that the tri-directional rib lattice layout did not provide adequate strength. The Tsai-Wu criterion for composite failure was used due to its greater accuracy as compared to other failure criterion, and buckling of the skin, spar and web panels was considered. The final layups predicted a weight saving of 14.2%.

The wing was constructed in the CSIR UAS Laboratory and it was found that the large number of parts and several curing cycles resulted in construction time being increased rather than decreased as was initially predicted. The final weight saving achieved was measured to be 14.2% which was on par with the final prediction. The wing was finally tested using a custom-designed whiffle tree setup that simulated the lift loads on the wing. It was found that the tip deflection of the wing deviated from the FEA-predicted deflection by an average of 3.9% which served to validate the FEA model.

The findings thus speak to the objectives as follows:

1. It was found that the new wing design making use of a coreless composite construction was noticeably lighter than the original wing constructed using a cored layup. It was also found that the new wing design maintained adequate strength which was proven by a combination of physical testing and validated FEA models.
2. It was found that the construction time of the new wing design was significantly longer than the construction time of the original wing design due to the large number of components involved and the multiple curing cycles required.

### **9.3. Hypothesis**

This work shows that the wing structure of a UAV can indeed be significantly lightened through the use of a coreless structural design employing stiffened skins instead of a sandwich construction, while maintaining adequate strength.

It was also found that such a structural design will not decrease the construction time as was originally thought but rather increases construction time due to an increase in complexity and part count. This was partly due to the new design being at a prototype level and it is thought that purpose-built jigs could decrease this construction time.

### **9.4. Recommendations for Future Work**

Based on the research conducted for this project it is recommended that the following topics are investigated in more detail:

- The original Kwadira wing skins were required to be constructed out of glass fibre as a result of EMI interference and blanking that would be caused by using carbon fibre for the wing skins. The use of carbon fibre skins could potentially yield an even lighter construction than the one obtained from this research but would require externally mounted antennae which would increase the drag of the airframe and could hence offset the gains obtained from a lighter construction. An interesting exercise could be the comparison of the gain in endurance obtained from the use of carbon fibre wing skins versus the increase in drag (and subsequent decrease in endurance) caused by the necessity of externally mounted antennae.
- Many of the disadvantages of using sandwich construction arise from the use of PVC foam as a core material that is difficult to shape and absorbs excess resin. An interesting exercise could be the quantification of the reduction or increase in effort and cost resulting from switching to a more expensive core material such as Nomex honeycomb.
- Lastly it is recommended that the methods used in this research project be applied to the rest of the components of the Kwadira airframe: the fuselage, the tail booms, the vertical fins and the horizontal stabiliser. This could result in further increases in weight savings and subsequent increases in aircraft endurance.

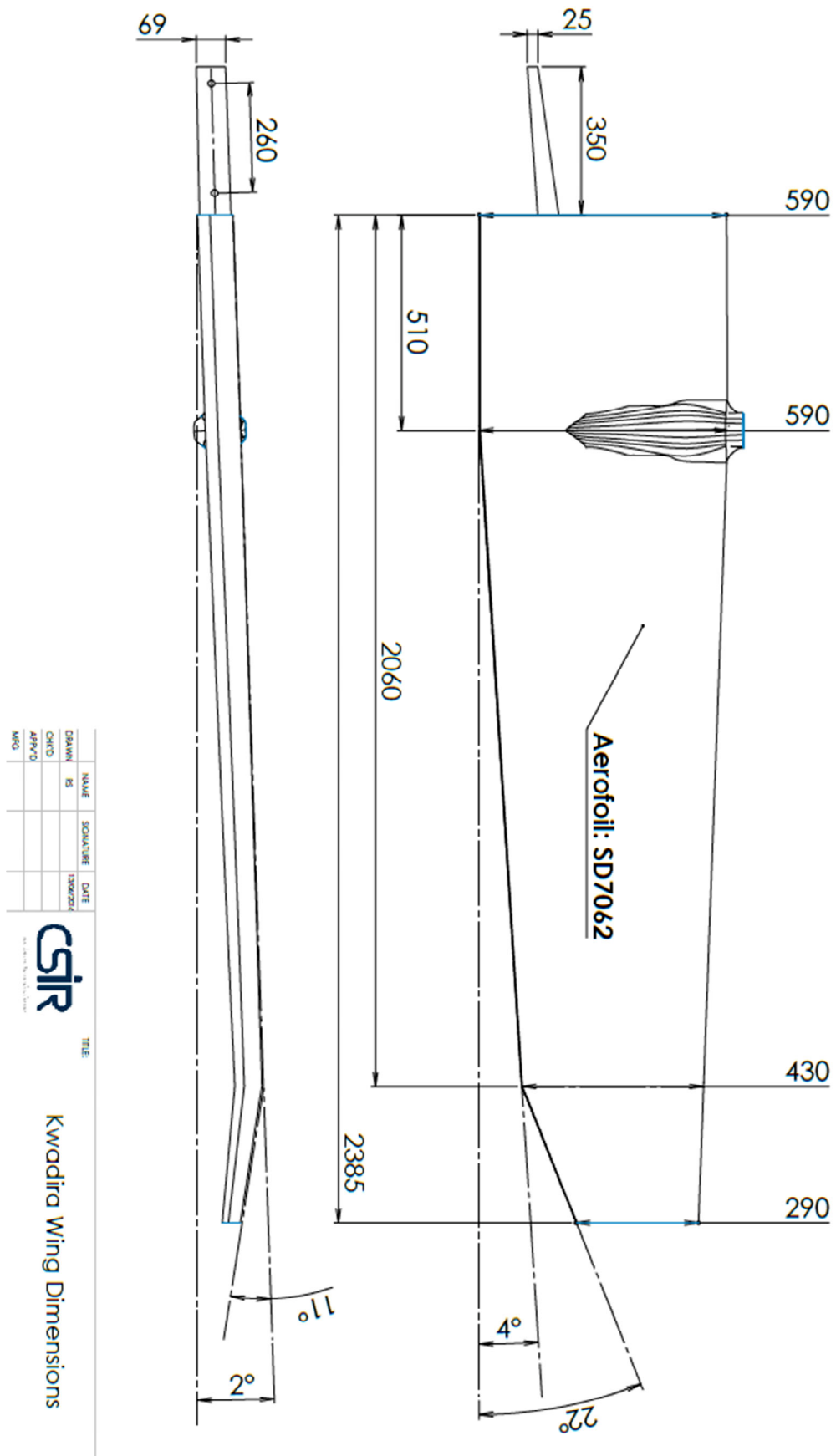
## References

- Advanced Materials Technology. (2014). *Ampreg 21 Tech Data*. Retrieved 02 13, 2016, from [http://www.amtcomposites.co.za/sites/default/files/media/data-sheets/Ampreg%2021\\_v8.pdf](http://www.amtcomposites.co.za/sites/default/files/media/data-sheets/Ampreg%2021_v8.pdf)
- AMT Composites. (2016). Retrieved September 22, 2016, from Vacuum Bag & Infusion Consumables: <http://www.amtcomposites.co.za/products/vacuum-bag-infusion-consumables>
- Anderson, J. D. (2007). *Fundamentals of Aerodynamics* (5th ed.). New York: McGraw-Hill.
- Anderson, J. D. (2008). *Introduction to Flight* (6th ed.). New York: McGraw-Hill.
- Arunkumar, K. N., & Lohith, N. (2015). Effect of Ribs and Stringer Spacings on the Weight of Aircraft Composite Structures. *ARPN Journal of Engineering and Applied Sciences*.
- ASTM International. (2001). ASTM D3518. *Standard Test Method for In-Plane Shear Response of Polymer Matrix Composite Materials by Tensile Test of a  $\pm 45^\circ$  Laminate*. West Conshohocken, United States of America.
- ASTM International. (2002). ASTM D3039. *Standard Test Method for Tensile Properties of Polymer Matrix Composite Materials*. West Conshohocken, United States of America.
- Bardella, L. (2000). *Mechanical Behaviour of Glass-Filled Epoxy Resins: Experiments, Homogenization Methods for Syntactic Foams, and Applications*. PhD Thesis, University of Brescia, Owensboro.
- Bart Boon Research and Consultancy et al. (2006). *Best Practice Guide for Sandwich Structures in Marine Applications*. Newcastle: European Commission FP6.
- Body, J. (2007). *Airbus Future Composite Wing*. Nantes: Airbus UK R&T.
- Collins, V. E. (1985). *Leghorn Structural Design Report*. National Institute for Aeronautics and Systems Technology. Pretoria: CSIR.
- COMSOL. (2016). *Finite Element Mesh Refinement*. Retrieved from Multiphysics Cyclopedia: <https://www.comsol.com/multiphysics/mesh-refinement>
- Corderley, G. (1994). *ACE Aircraft Material Properties*. Pretoria: CSIR Material Sciences and Manufacturing.
- Dassault Systemes. (2014). SolidWorks Simulation Premium Help File.
- Dassault Systemes. (2015). *SolidWorks NAFEMS Benchmarks*.
- DC Wort. (2016). *Epoxy Glass (LEO)*. Retrieved 04 03, 2016, from DC Wort Glass Composites: [http://www.dcwort.co.za/files/content/docs/epoxy\\_-\\_leo.pdf](http://www.dcwort.co.za/files/content/docs/epoxy_-_leo.pdf)
- Deo, R. B., Starnes, J. H., & Holzwarth, R. C. (2001). Low-cost composite materials and structures for aircraft applications. *Low Cost Composite Structures*. Loen: RTO AVT.
- Gagauz, P. (2013). *Composite Sandwich Panels Design and Structural-Technological Solutions*. Kharkov: National Aerospace University.
- Guo, S. J. (2007). Stress Concentration and Buckling Behaviour of Shear Loaded Composite Panels with Reinforced Cutouts. *Composite Structures* 80, 1-9.
- Hassan, P. H. (2012). Modern Design Trends of Metal Aircraft Fuselage Structures. *International Science Postgraduate Conference*. Selangor: University Teknologi Malaysia.

- Hicks, M. T. (2001). *Design of a Carbon Fibre Composite Grid Structure for the GLAST Spacecraft Using a Novel Manufacturing Technique*. PhD Thesis, Stanford University, Stanford.
- Howe, D. (2004). *Aircraft Loading and Structural Layout*. London, United Kingdom: Professional Engineering Publishing Limited.
- Huybrechts, S., & Tsai, S. W. (1996). Analysis and Behaviour of Grid Structures. *Composites Science and Technology* 56.
- Ithurbure, R. P. (1999). *Design of the Wing of a Regional Airliner in Composite Material*. Memorandum, Delft University of Technology, Delft.
- Juracka, J., Jebacek, I., & Pistek, A. (2000). *Strength testing of the UFM-10 Samba composite wing structure*. Brno: Institute of Aerospace Engineering, BRNO University of Technology.
- Kanou, H. e. (2013). Numerical Modeling of Stresses and Buckling Loads of Isogrid Lattice Composite Structure Cylinders. *International Journal of Engineering, Science and Technology*, 42-54.
- Ladzinski, M., & Abbey, T. (2009). *An Introduction to Composite FEA Analysis*. NAFEMS.
- Leissa, A. W. (1985). *Buckling of Laminated Composite Plates and Shell Panels*. Ohio: AF Wright Aeronautical Laboratories.
- Marsden, W., & Irving, D. (2002). *How to Analyse Composites* (1st ed.). Surrey: NAFEMS Press.
- Megson, T. H. (2013). *Aircraft Structures for Engineering Students* (5th ed.). Oxford: Elsevier Press.
- Morishima, R. (2011). *Analysis of composite wing structures with a morphing leading edge*. Cranfield: Cranfield University.
- Mukhopadhyah, V. (2005). Blended-Wing-Body (BWB) Fuselage Structural Design for Weight Reduction. *46th AIAA Structures, Dynamics and Materials Conference*. Austin: AIAA.
- NAFEMS. (2016). *The Importance of Mesh Convergence*. Retrieved from NAFEMS Knowledge Base: <https://www.nafems.org/join/resources/knowledgebase/001/>
- Niu, M. C. (1988). *Airframe Structural Design*. Hong Kong: Conmilit Press Ltd.
- Niu, M. C. (1997). *Airframe Stress Analysis And Sizing*. Grenada Hills, California: Conmilit Press.
- Nurhaniza, M. e. (2010). Finite Element Analysis of Composite Materials for Aerospace Applications. *9th National Symposium on Polymeric Materials*. Selangor: Universiti Putra Malaysia.
- Peery, D. J. (1982). *Aircraft Structures* (2nd ed.). New York: McGraw-Hill.
- Perini, F. (2012). *Structural design, manufacturing and testing of a new wing for the CSIR's Modular UAS in composite materials*. MSc Thesis, University of Bologna, Bologna.
- Prinsloo, T. (2011). *Damage Detection Methodology for Composite UAV Wings using Modal Analysis and Probabalistic Concepts*. MSc Thesis, University of Pretoria, Pretoria.
- Robinson, J. (2004). *Structural Testing and Analysis of a Joined Wing Technology Demonstrator*. Dayton: Air Vehicles Directorate, USAF.
- Scott Bader Company. (2005). *Crystic Composites Handbook*.
- Sedaghati, R., & Elsayed, M. (2006). *Wing Rib Stress Analysis and Design Optimisation*. MOSAIC Project Report, Concordia University, Montreal.
- Sensmeier, M. D., & Samareh, J. A. (2004). *A Study of Vehicle Structural Layouts in Post WW2 Aircraft*. Prescott: American Institute of Aeronautics and Astronautics.

- Shanygin, A., Zichenkov, M., & Kondakov, I. (2014). Main Benefits of Pro-Composite layouts for Wing and Fuselage Primary Structure Units. *29th Congress of the International Conference of the Aeronautic Sciences*. St Petersburg: ICAS.
- Stavrev, V., & Stavrev, M. (2014). *SkyFall - Aerobatic at the edge of space*. Retrieved November 28, 2015, from Designboom.com: <http://www.designboom.com/project/skyfall-aerobatic-at-the-edge-of-space/>
- Technology Innovation Agency. (2008). Bonding and filling using laminating epoxy resin. *AMTS Standard Workshop Practice*.
- Tsai, S. W. (2008). *Theory of Composites Design* (3rd ed.). Stanford: Stanford University Press.
- Unal, M. (2013). *Lockheed 1049 Super Constellation Aircraft Wing Structural Investigation*. Istanbul: Istanbul Technical University.
- United States. Department of Defence. (2002). *Composite Materials Handbook* (MIL-HDBK-17-3F ed.). Maryland.
- United States. Department of Transport. (1965). *Part 23 - Airworthiness standards: Normal, utility, acrobatic and commuter category airplanes*. FAA.
- United States. Department of Transport. (2008). *Pilot's Handbook of Aeronautical Knowledge*. FAA.
- United States. Department of Transport. (2012). *Advanced Composite Materials*. FAA.
- Vasiliev, V. V., & Razin, A. F. (2012). Development of Geodesic Composite Aircraft Structures. *28th International Congress of the Aeronautical Sciences*. Brisbane: ICAS.
- Wright, S. A. (1970). *A Study of the Design and Construction of a Full Scale Aircraft Component Demonstration Fatigue Test*. MSc Thesis, University of Missouri, Rolla.
- Xu, R. (2012). *Optimal Design of a Composite Wing Structure for a Flying-Wing Aircraft Subject to Multi-Constraint*. Cranfield University. Cranfield: Cranfield University.

# Appendix A – Kwadira Wing Dimensions



NAME	SIGNATURE	DATE
DRAWN RS		
CHECKED		
APPROVED		
MRD		



TITLE

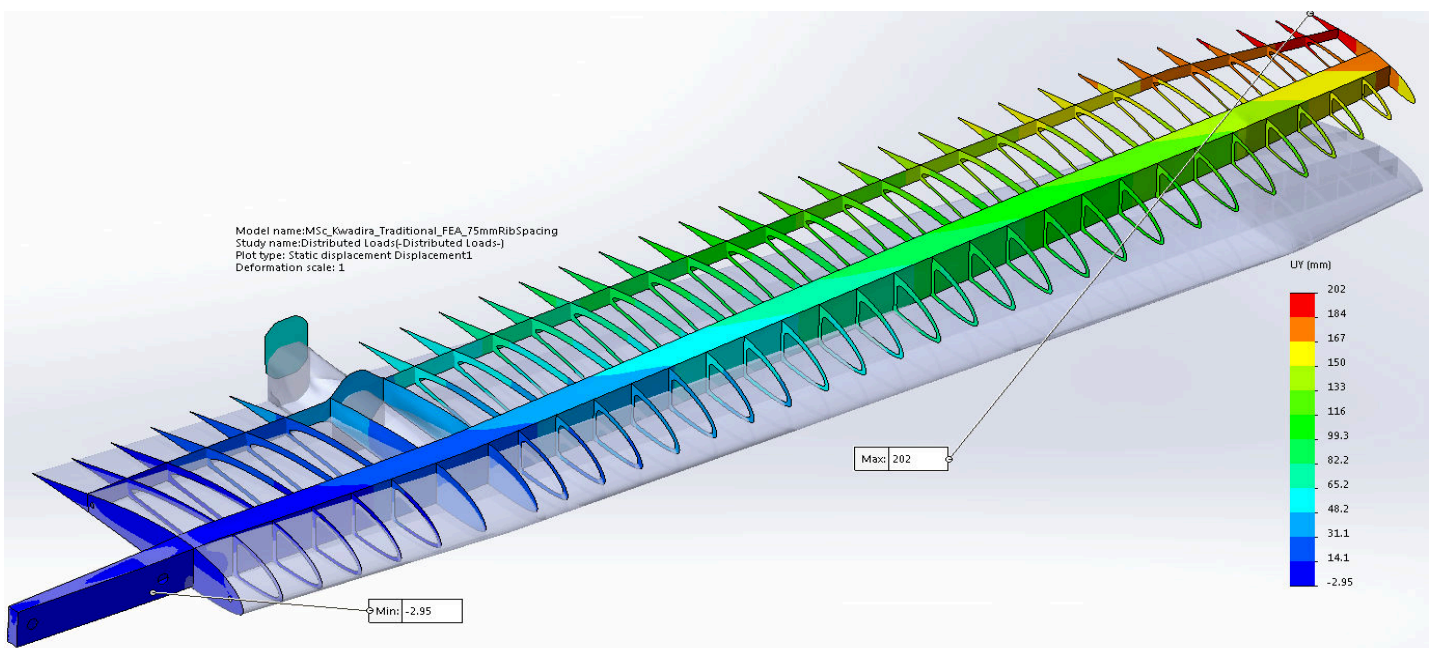
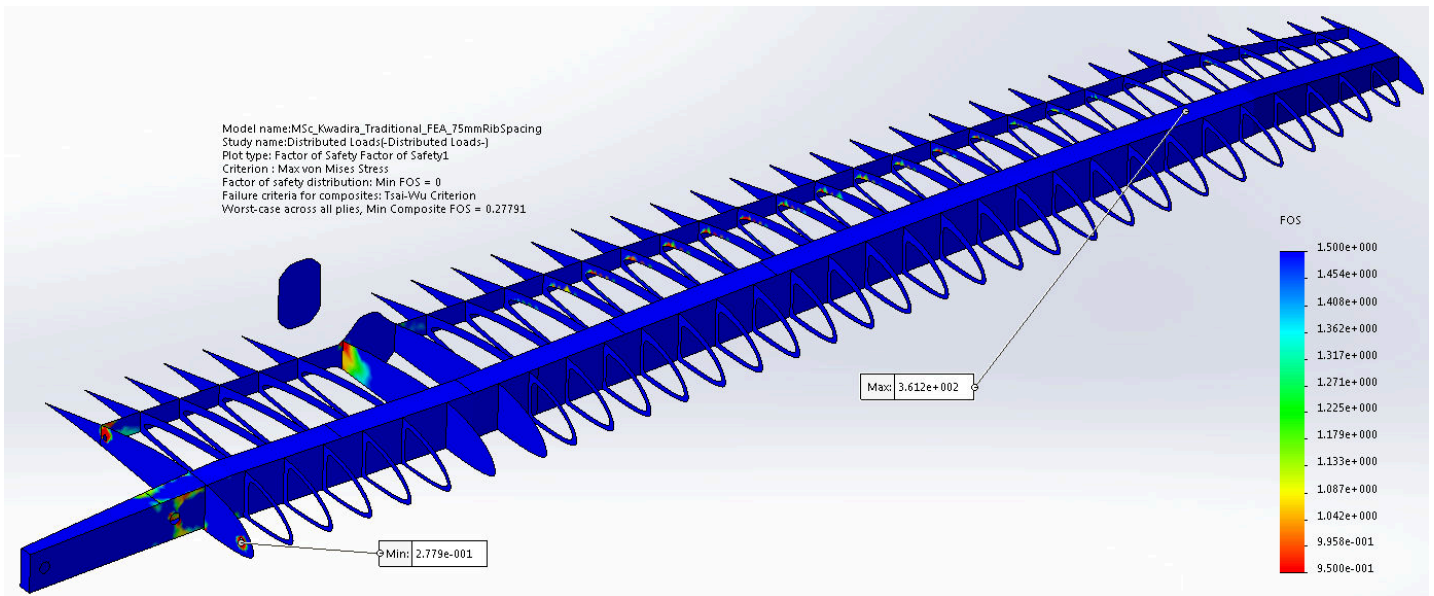
Kwadira Wing Dimensions

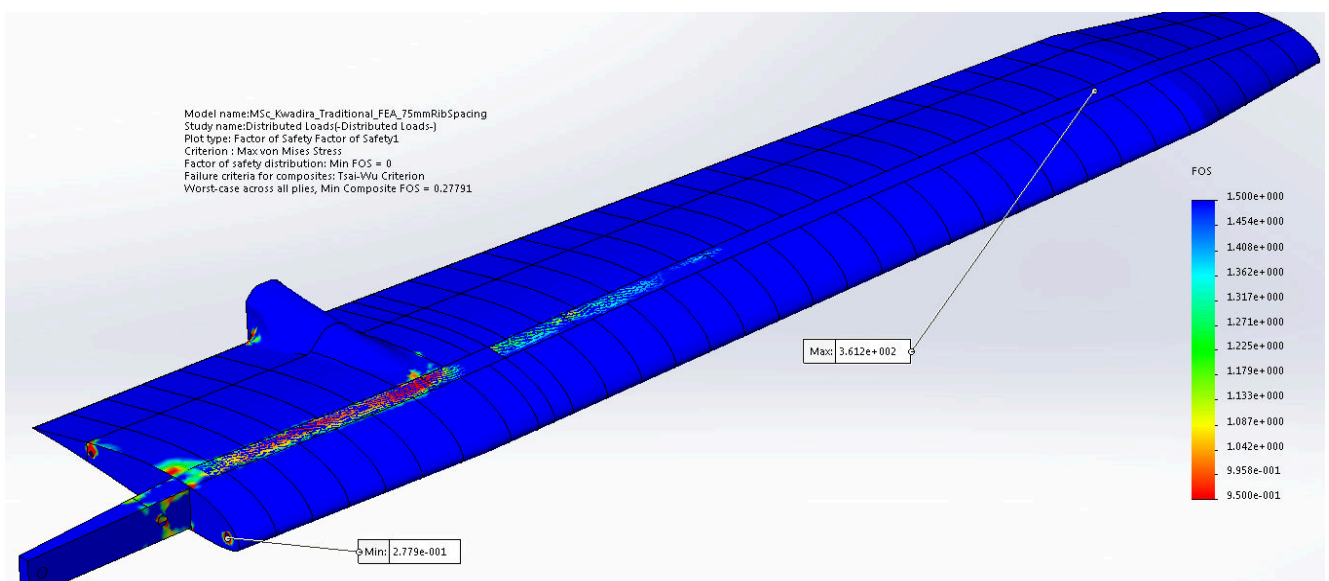
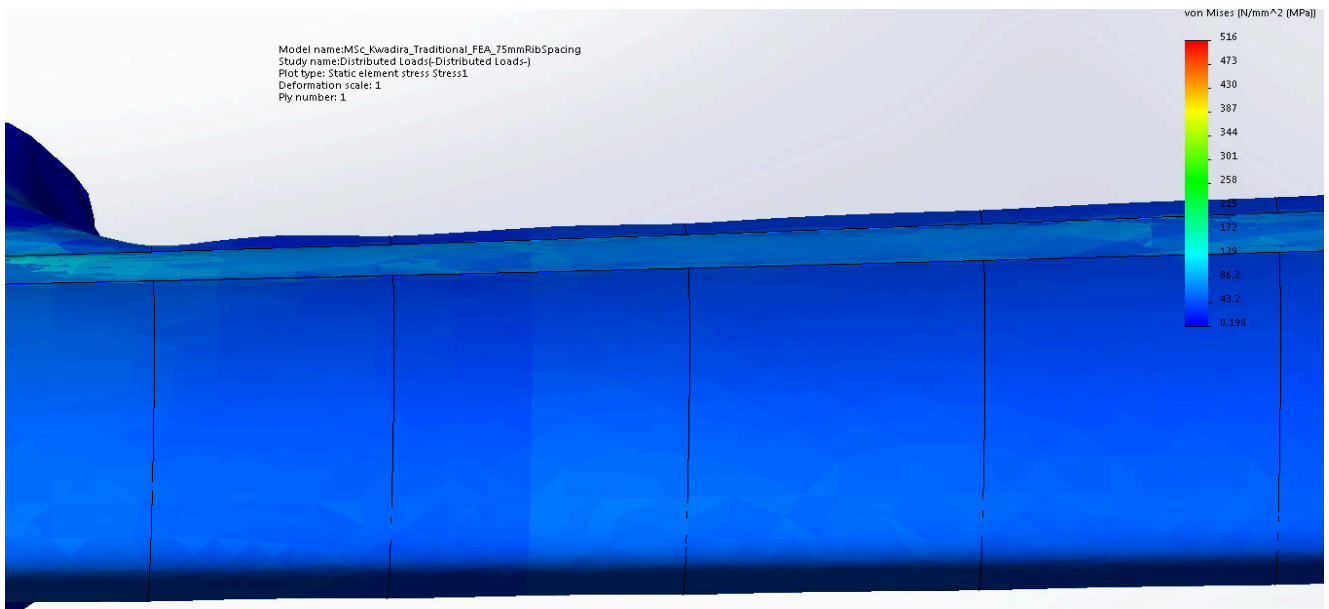
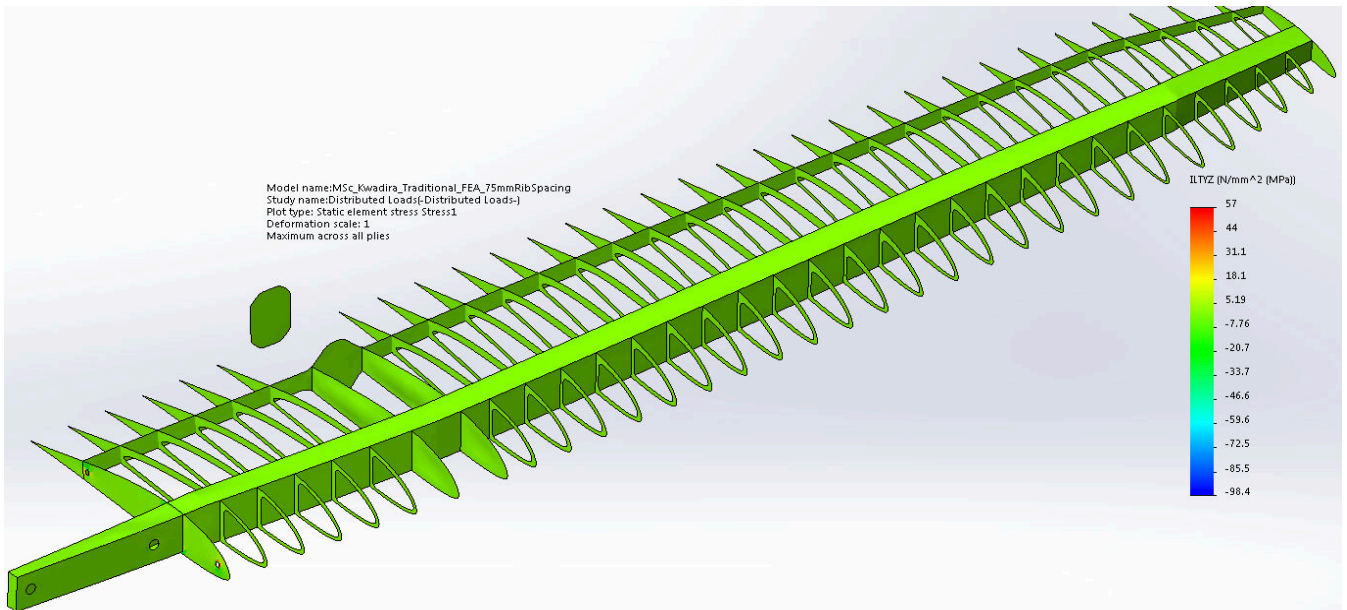
## Appendix B – Layout and Layup Iteration Results

The FEA analysis results are presented in the following order:

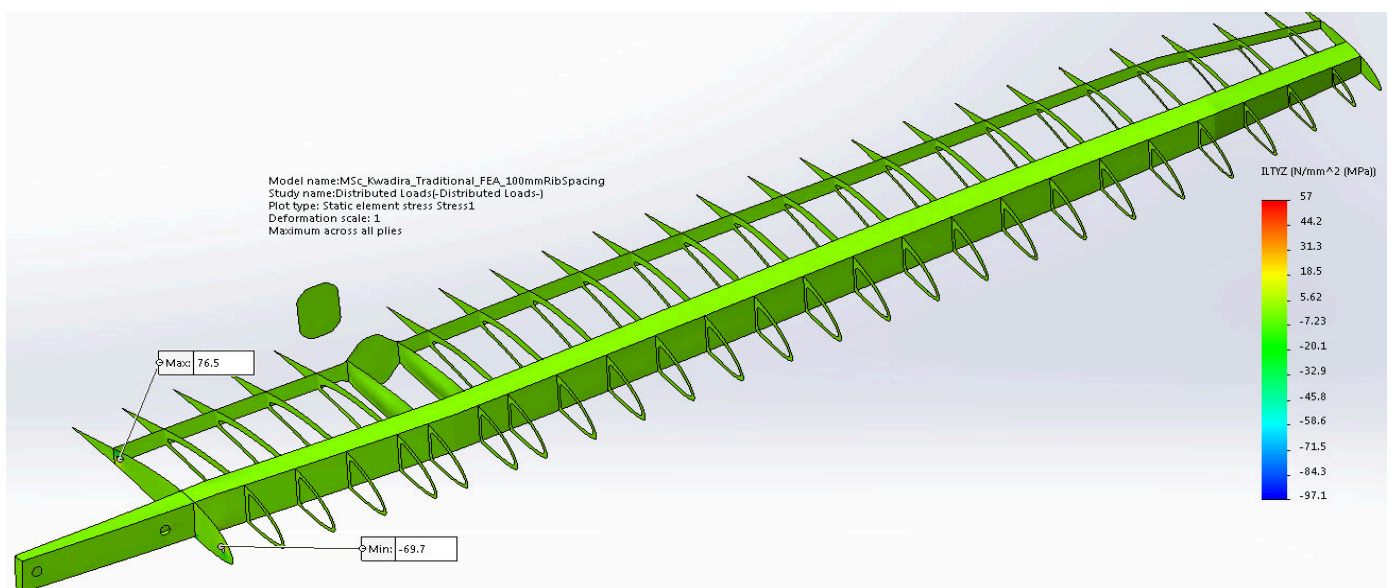
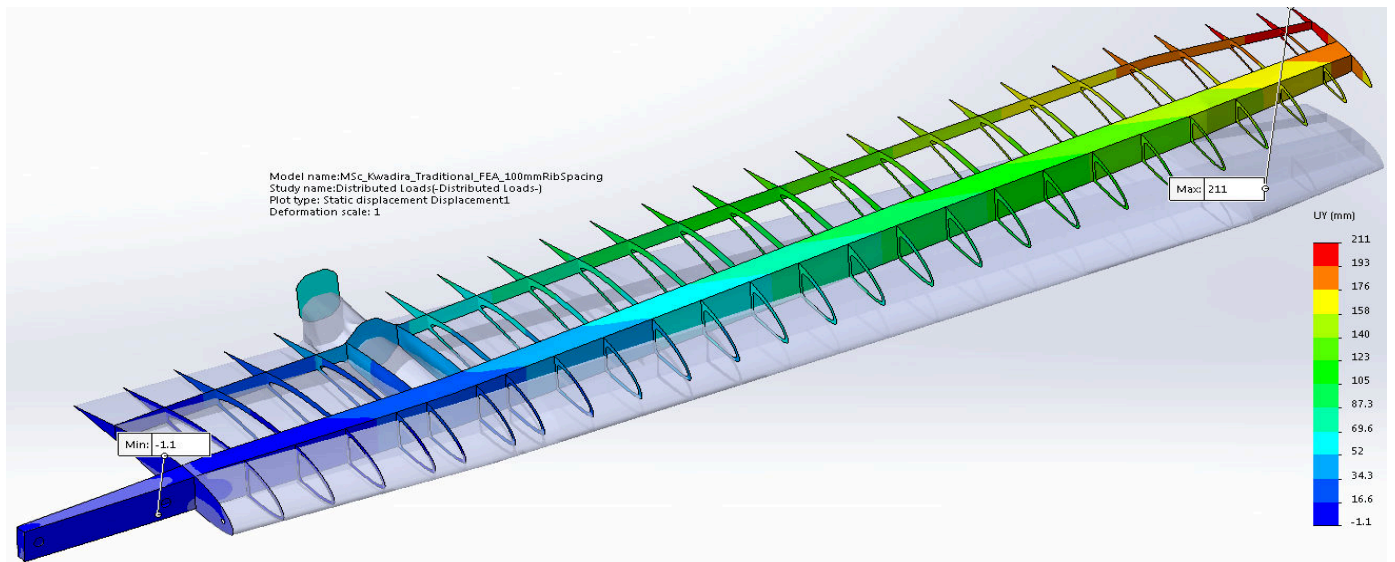
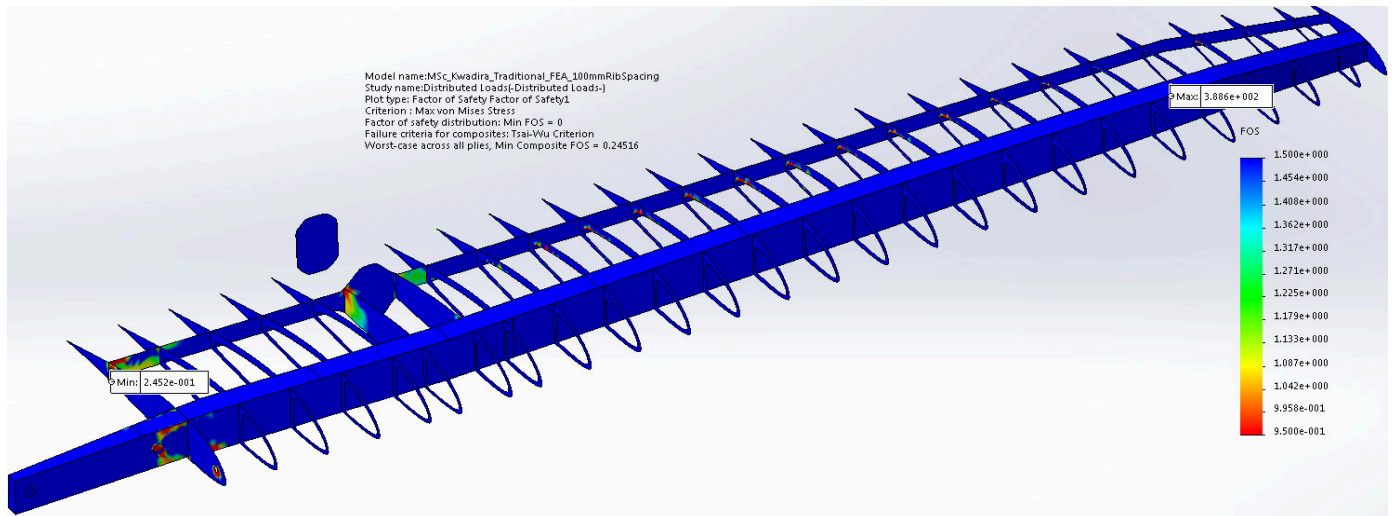
- Plot of Tsai-Wu failure index (worst case across all plies, inverted by SolidWorks Simulation to a FOS) showing the internal wing structure
- Plot of bending deflection in the Y-direction showing the internal wing structure
- Plot of inter-laminate shear stress showing the internal wing structure
- Close-up plot of the Von Mises stress distribution showing the skin deflection under load
- Plot of the Tsai-Wu failure index (worst case across all plies) showing the wing skins

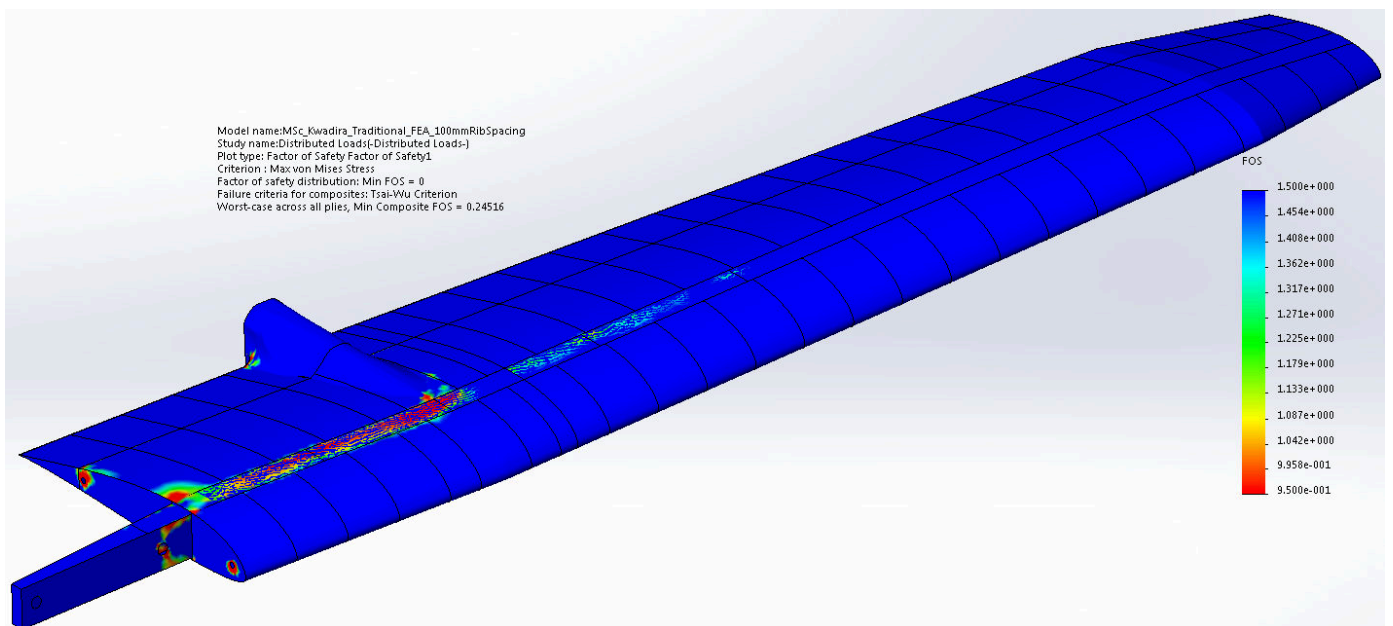
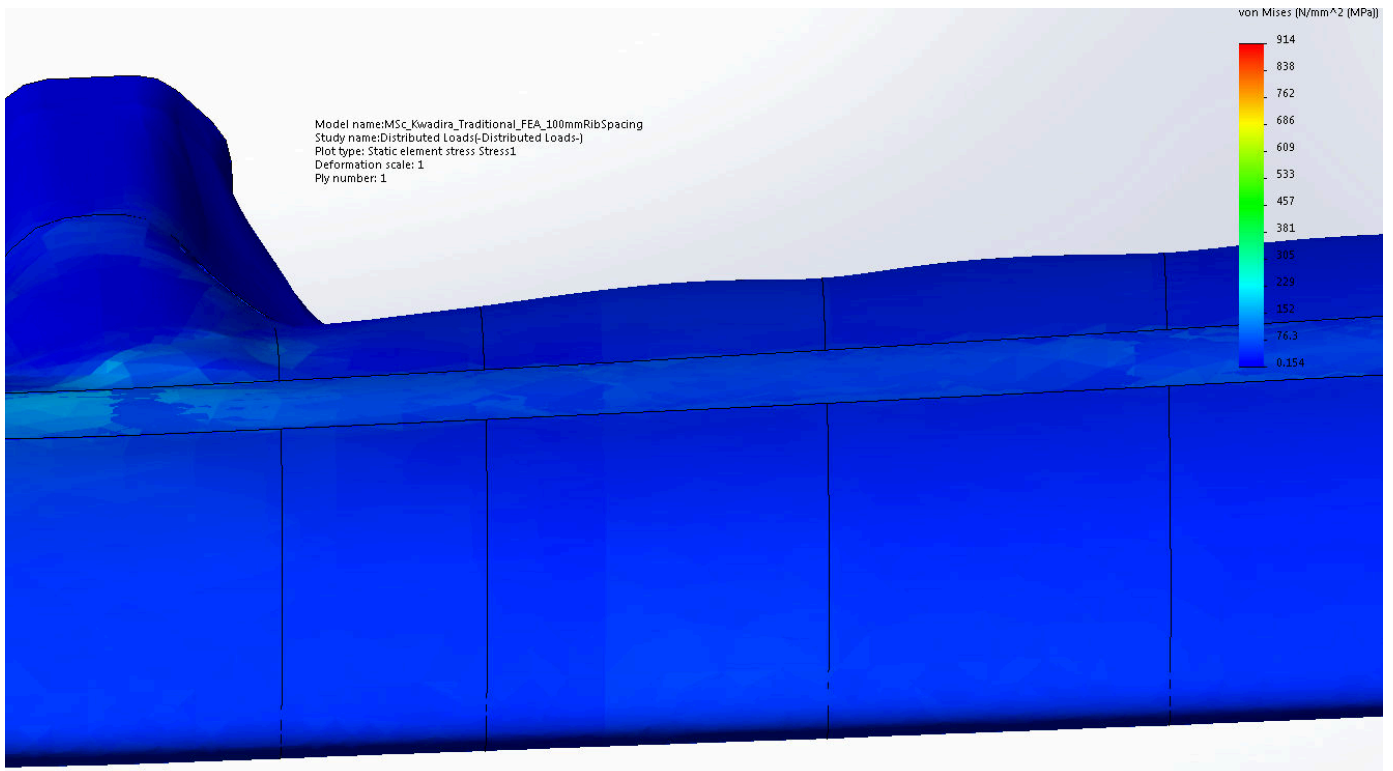
### Traditional Layout, 75mm Rib Spacing



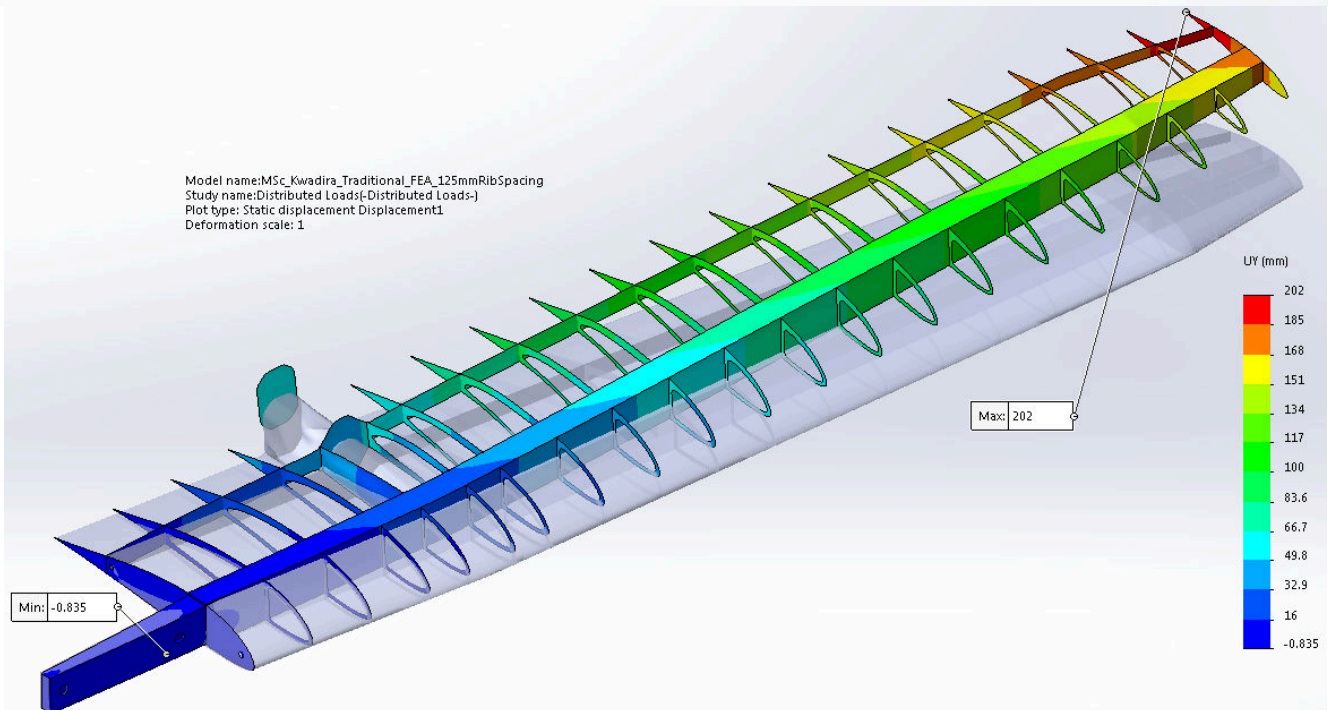
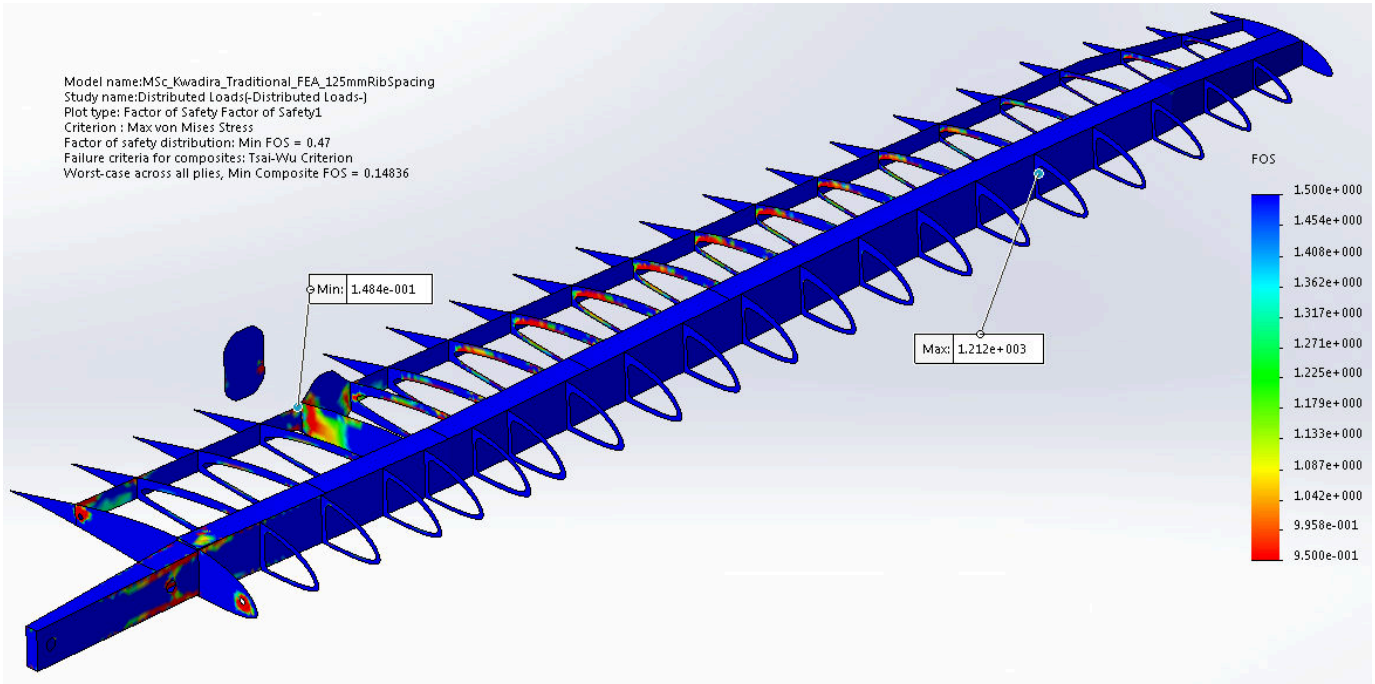


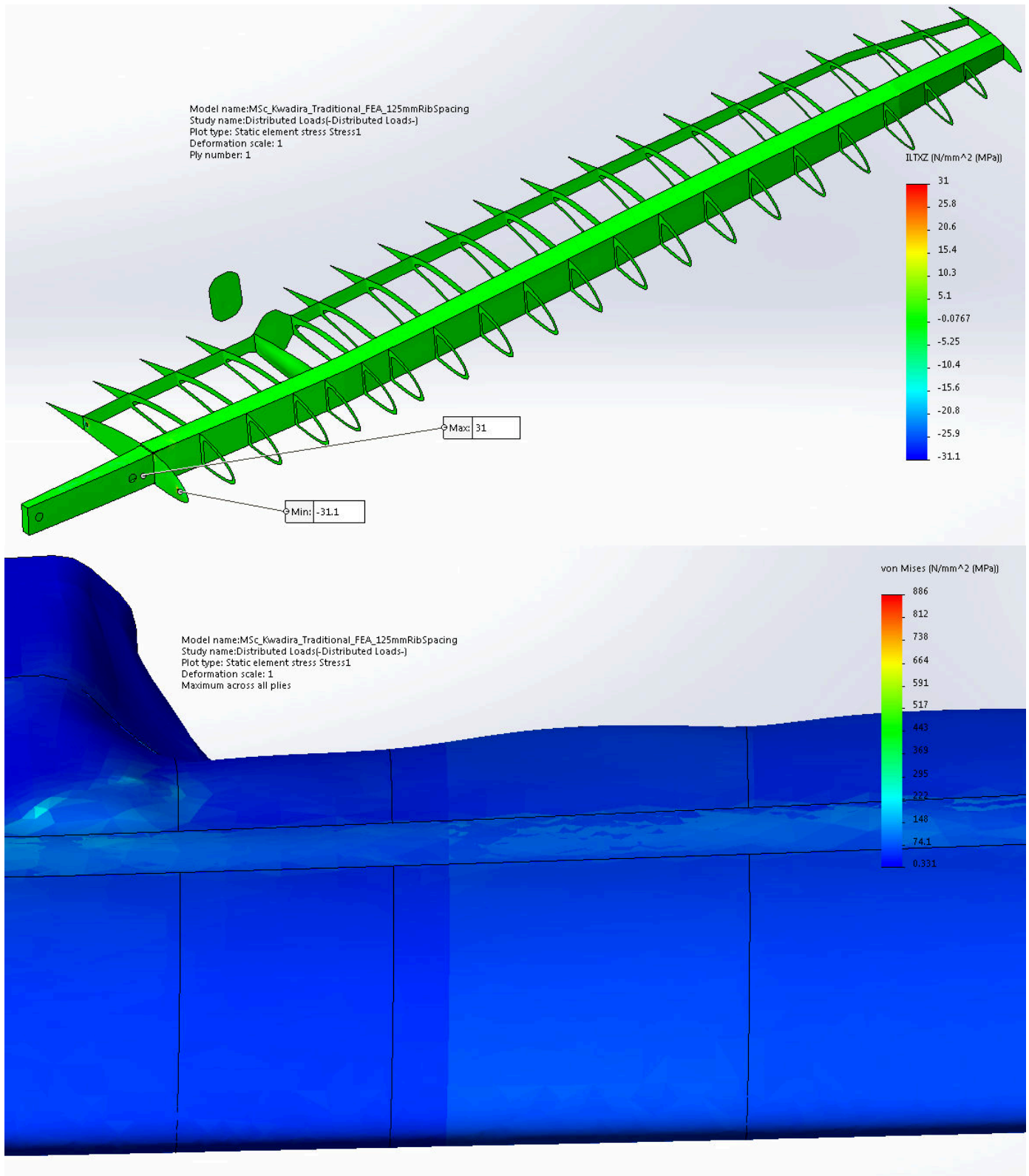
# Traditional Layout, 100mm Rib Spacing

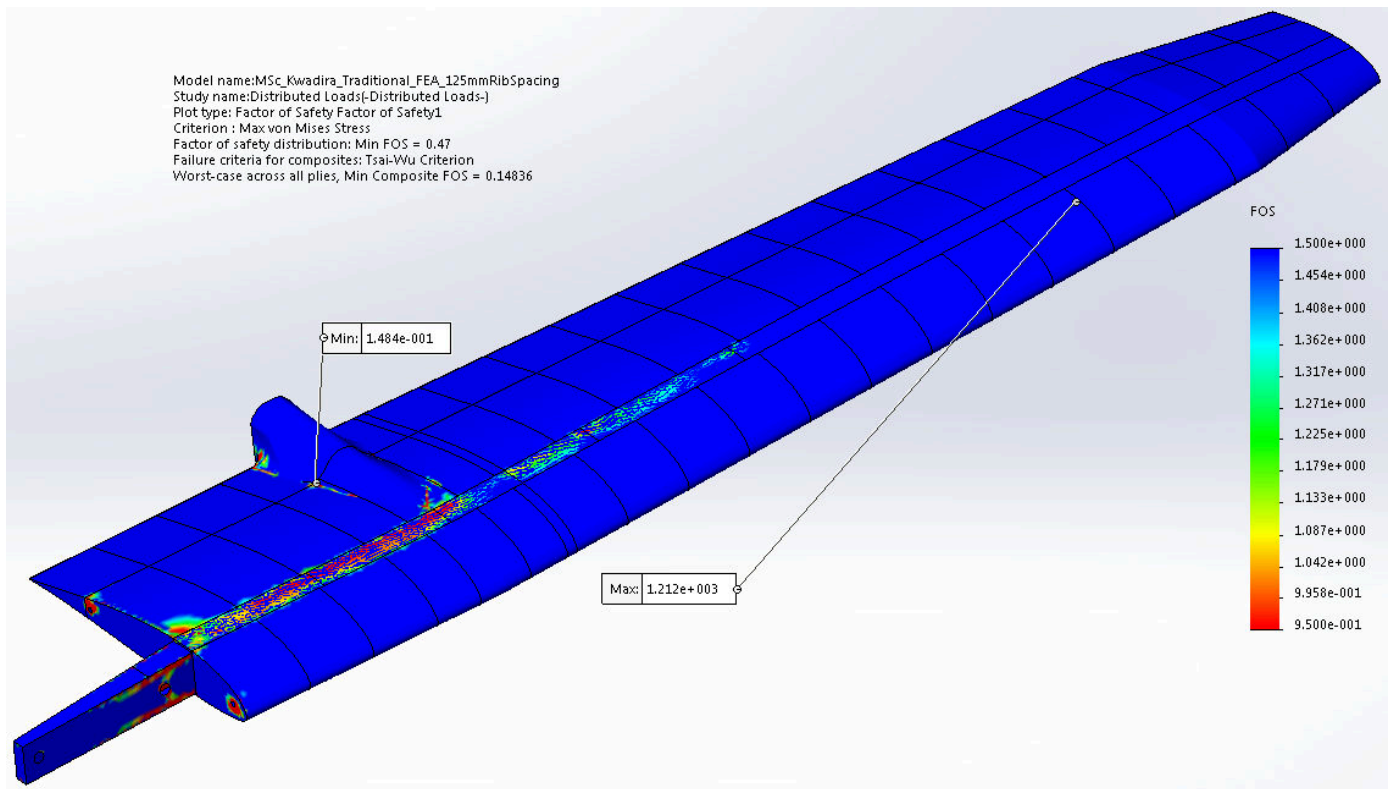




# Traditional Layout, 125mm Rib Spacing







## Appendix C – Journal Paper Submitted For Review

### LIGHTWEIGHT STRUCTURAL DESIGN OF A UAV WING THROUGH THE USE OF CORELESS COMPOSITE MATERIALS

Moore N. N.<sup>1</sup>, Bemont C. P.<sup>2</sup> and Thomson V.A.<sup>3</sup>

<sup>1</sup>Council for Scientific and Industrial Research, Aeronautic Systems Competency, Pretoria, South Africa

<sup>2</sup>University of Kwa-Zulu Natal, Pietermaritzburg, South Africa

<sup>3</sup>Craven Designs, Johannesburg, South Africa

E-Mail: nmoore@csir.co.za

Postal Address: Building 12, CSIR, Meiring Naude Drive, Brummeria, Pretoria, 0184, South Africa

#### ABSTRACT

A new structural layout was designed for an existing UAV wing with the aims of lightening the wing by eliminating the use of cored composite construction and reducing the manufacturing time of the wing by making use of waterjet-cut internal frames while satisfying strength and stiffness requirements. In order to present a valid comparison with the previous wing design the same composite materials were used in the design of the new wing layout and material tests were performed according to ASTM testing standards to obtain the mechanical properties of these materials. Load cases for the wing in flight were calculated according to FAR23 standards and the loads on the wing were found using XFLR5 vortex-lattice methods. A traditional type metal-wing layout was selected for the new structural layout. An empirical, spreadsheet-based initial sizing tool was developed to obtain preliminary layouts for an iterative FEA-based optimisation process that employed the SolidWorks Simulation Premium software package and made use of the Tsai-Wu composite material failure criterion. A full scale prototype wing was constructed in the CSIR UAS Laboratory using wet layup techniques and laser cut internal frames. The prototype wing showed a weight saving of 14% but took considerably longer to manufacture due to the necessity of constructing specialised jigs to aid in the bonding and alignment of the internal frames. The prototype wing was tested using a custom set-up whiffle tree rig up to its maximum limit load of 4.9 g and showed an average of 4% error between measured and predicted deflections thereby validating the FEA models. It was concluded that a UAV wing can be significantly lightened through a coreless structural design, but at the expense of an increase in construction time on the one-off prototype wing, not a decrease as was originally hypothesized. It is hoped that this study will contribute towards a changed design philosophy in an industry where cored construction is the norm.

**Keywords:** UAV wing, lightweight, coreless composite materials, aircraft structures, FEA

#### 1. INTRODUCTION

The CSIR's Kwadira UAV was designed and built in 2014 as an avionics demonstrator platform with a maximum take-off mass of 75 kg and the capability to carry a 15 kg payload for up to 5 hours. It was built almost entirely out of Fibre-Reinforced Plastics (FRPs) and followed the approach of using a cored layup in the construction of the wing skins, shear webs and ribs. Cored (or sandwich) composite construction has, for some time, been the industry-standard method of building UAVs in

South Africa [1] due to the advantages offered by cored construction such as greater stiffness-to-weight ratio, greater resilience to buckling and ease of manufacture when compared to stiffened skin construction [2, 3].



**Figure 73 - SolidWorks render of the CSIR Kwadira UAV.**

Practical experience with designing and building of cored composite wings led to the discovery of a number of disadvantages:

- Due to the wet laminating manufacturing processes used it is not possible to absorb excess resin using from one side of the core material when moulding a cored laminate.
- The cores tend to absorb more resin than what the core suppliers claim. Standard practice is to use closed-cell PVC foam core which invariably requires large amounts of resin to ensure that skins bond to the core properly.

Excess resin weakens the laminate, and together with resin absorbed by the foam core adds undesirable weight to the laminate and airframe. Another disadvantage found was that preparation of the core material adds significantly to the total labour costs involved in building a UAV, since particularly the thinner core materials require detailed edge trimming and finishing by hand.

It was thus decided to challenge the industry-standard approach and re-design the internal structure of the Kwadira UAV wing by using the same materials employed in the original version but making use of as little core material as possible in the construction. The objectives were:

- i. To determine if the weight of the wing could be reduced whilst maintaining adequate structural strength and stiffness.
- ii. To determine if labour time could be reduced by eliminating the preparation of core materials.

A decrease in the structural weight of an aircraft allows it to carry more payload or fuel which in turn allows it to perform more useful missions or extend its operating range. These factors, combined with a potential decrease in labour costs and construction time, provided the motivation for carrying out this research.

## 2. MATERIALS AND METHODS

### 2.1 Selected Materials

The materials selected for this project were chosen to be the same as those used in the original design in order to make a valid comparison between old and new designs. The original design made use of Ampreg 21 laminating resin and thus it was decided to continue with its use. Table 1 shows the materials used along with their mechanical properties. These properties were obtained from Perini [4], Bardella [5] and from material tests performed specifically for this project by the CSIR Materials Science and Manufacturing (MSM) unit. The tests conformed to ASTM standards D3039 [6] and D3518 [7] for composite materials.

Although it would be expected to provide a lighter and stronger layup, carbon fibre was not chosen for wing skins and ribs due to concerns of possible electro-magnetic blanking of internally mounted antennas. This was further motivated by the desire to provide a close comparison to the original wing design.

**Table 11 - Properties of the materials used in the design of the new wing structural layout. Sources: Perini [4] (Carbon fibres), Bardella [5] (Resin) and material testing (Glass fibres).**

Property →	Young's Modulus x-Direction	Young's Modulus y-Direction	Tensile Strength x-Direction	Tensile Strength y-Direction	Shear Modulus	Shear Strength	Poisson's Ratio	Nominal Thickness Per Ply
Material ↓	$E_x$	$E_y$	$\sigma_{max, Tx}$	$\sigma_{max, Ty}$	$G_{xy}$	$\tau_{Max}$	$\nu_{xy}$	$t_{Nominal}$
Property Unit	GPa	GPa	MPa	MPa	GPa	MPa	-	mm
<b>86GSM Plain Weave Glass Fibre + Ampreg 21 Resin</b>	21.39	21.39	260	260	1.57	59	0.133	0.083
<b>106GSM Plain Weave Glass Fibre + Ampreg 21 Resin</b>	21.14	21.14	347	347	1.28	64	0.088	0.09
<b>200GSM Twill Weave Carbon Fibre + Ampreg 21 Resin</b>	48.9	48.9	464.2	464.2	6.5	125	0.16	0.32
<b>343GSM UD Carbon Tape + Ampreg 21 Resin</b>	82.1	-	1073.4	-	-	-	0.28	0.3
<b>Ampreg 21 Epoxy Resin + Cotton Flock Filler</b>	32.2	32.2	561	561	1.31	57	0.389	-

### 2.2 Load Cases and Spanwise Distributions

The maximum positive and negative symmetric load cases were determined by constructing a velocity-load factor (V-n) diagram according to Federal Aviation Regulations Part 23 (FAR-23) [8] methods and were found to be: Point A (3.8 g, 35 m/s, full aileron deflection) Point B (4.9 g, 40 m/s)

and Point D (-1.75 g, 50 m/s). FAR-23 recommends a safety factor of 1.5 be applied to these limit loads to obtain ultimate loads.

A freeware subsonic aerodynamic analysis program called XFLR5 was used to combine XFOIL with an implementation of the Vortex-Lattice Method (VLM) to obtain local span-wise lift, drag and pitching moment coefficient distributions at the maximum load cases. These coefficients were converted to external loads acting on the wing using wing local wing chord and area and then integrated across the wing span to obtain load distributions using methods from Anderson [9]. Since the empennage is connected to the rear of the wing with two slender booms the lift, drag and pitching moment contributions of the empennage were added to the external loads after trim calculations were performed.

### 2.3 New Layout Design

Aircraft wings are most often constructed from thin sheets of metal or composites which, under large axial or shear loads, are prone to buckling. Cored composite laminates overcome this buckling by effectively thickening the laminate using the core material to separate plies thereby creating intrinsically stiff sheets. Traditional metal wing construction overcome the buckling problem by employing numerous webs, ribs and stringers to stiffen and support the wing skins and each other [10], all of which are typically thin sheets.

In order to lighten the structure by eliminating core material while still providing sufficient buckling resistance the traditional metal-wing semi-monocoque layout with stiffened skins was chosen for the new internal structural layout. This layout comprised the following elements as shown in figure 2:

- i. Uni-directional carbon fibre spar caps/flanges (343GSM UD carbon fibre tape)
- ii. Woven carbon fibre main shear webs (200GSM twill weave woven carbon fibre)
- iii. Woven glass fibre sub-shear webs (86GSM and 106GSM woven glass fibre)
- iv. Woven glass fibre ribs (86GSM and 106GSM woven glass fibre)
- v. Woven glass fibre skins (86GSM woven glass fibre)

In order to allow the new wing design to interface with the existing Kwadira fuselage design it was decided to make use of the same single main spar structure. This sees the spar root extension of the port wing angled forward and that of the starboard wing angled backwards in order for the spars to pass by each other while keeping the chord-wise location of each spar the same. The bending load is then transferred between wing spars via two stainless steel shear pins that also serve as wing retention pins.

### 2.4 Initial Sizing Model

Span-wise shear force, bending moment and torsion diagrams were drawn up for the wing and used in a spreadsheet-based initial sizing model. This model assumed that the spar caps resist bending moments and the combination of the wing skins, span-wise webs and chord-wise ribs resist shear and torsion loads, as recommended by Megson [11]. Classical symmetric bending equations were used to find direct stresses in the spar caps and equations for torsion and shear in thin shell members were used to obtain shear flow distributions in the wing skins, span-wise webs and chord-wise ribs. A form of netting theory demonstrated by Collins [1] was then used to obtain initial layups for each internal structural component.

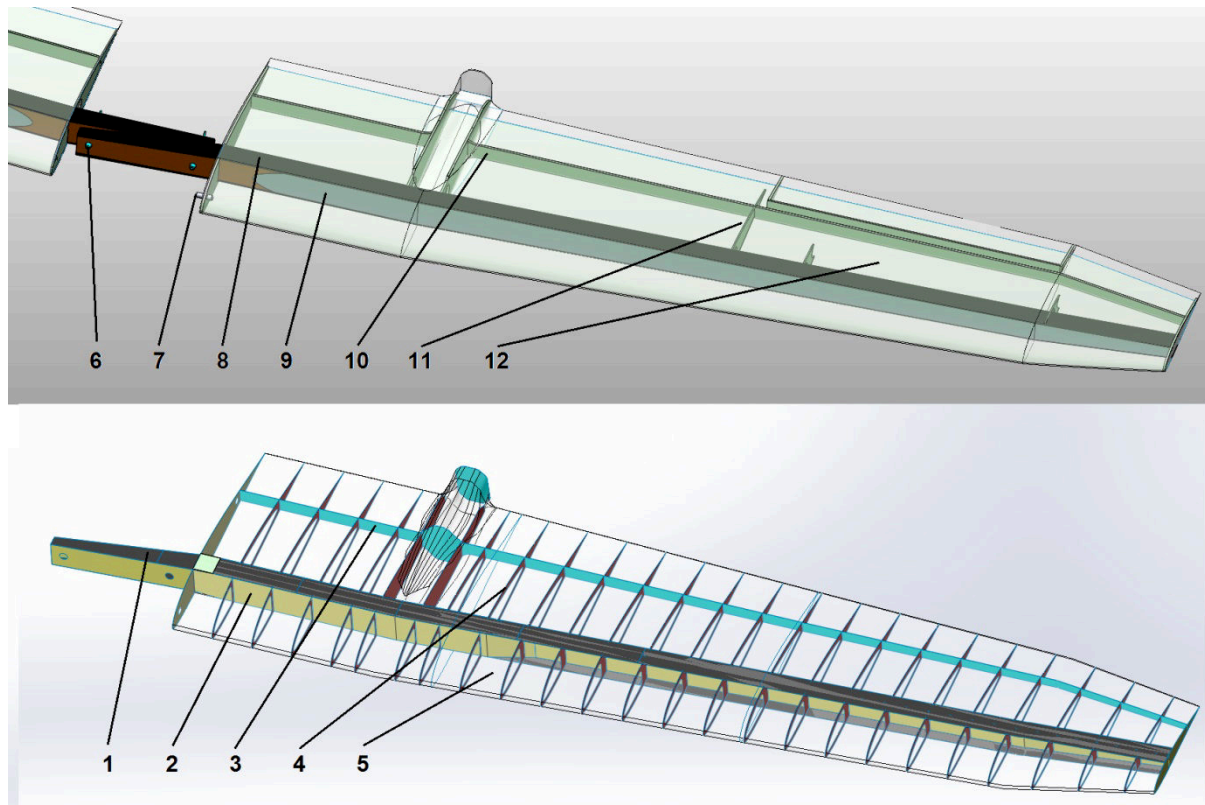


Figure 74 - SolidWorks CAD image showing the original (top) and new (bottom) layouts.

Key: 1. Uni-directional carbon fibre spar caps 2. Woven carbon fibre main shear webs 3. Woven glass fibre sub-shear webs 4. Woven glass fibre ribs 5. Woven glass fibre skins 6. Spar bending transfer shear pins 7. Fuselage attachment/shear pins 8. Uni-directional carbon fibre spar caps 9. Glass fibre sandwich main shear webs 10. Glass fibre sandwich sub shear webs 11. Glass fibre sandwich ribs 12. Glass fibre sandwich skins

### 3. FEA MODEL AND ITERATIVE OPTIMISATION

#### 3.1 Surface Model, Laminate Assignment and Mesh Generation

The wing and internal structural components were modelled in SolidWorks 2017 using surfaces. The model was then imported into SolidWorks Simulation Premium which includes a composite material analysis module. The layups obtained from the initial sizing model were assigned to each of the structural components as thin orthotropic shells. The orientation and thickness of each ply in the laminates were specified as well as the offset of the laminate from the surface.

A curvature-based mesh was selected which makes use of second-order triangular shell elements and automatically refines areas of high curvature such as at the wing leading edge. A mesh refinement study was performed which resulted in a maximum and minimum element sizes of 17.5 mm and 1 mm respectively. Further refinement was performed in areas of high curvature and thin sections of material. The internal components were modelled as being rigidly bonded to the wing skins and to each other by specifying bonded connections between components. This accurately represents the physical adhesive bonding of internal components to each other using the resin-based bonding agent as described in section 4.1, Construction. The mesh is shown in figure 3.

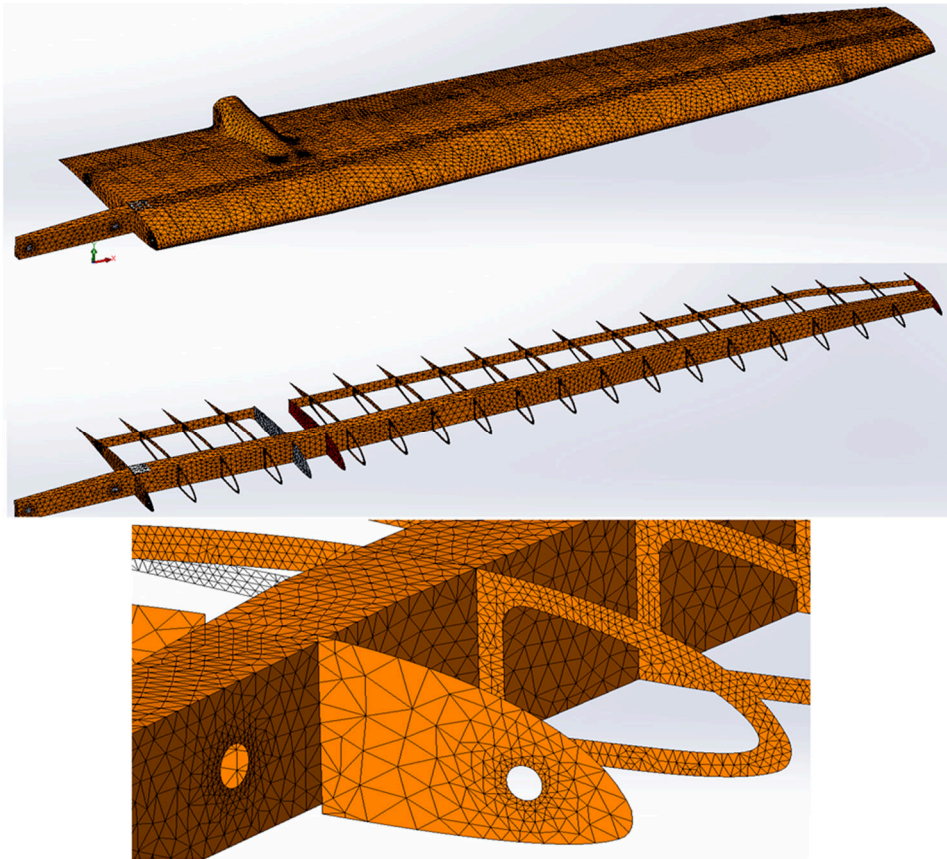


Figure 75 – SolidWorks Simulation image showing the second-order triangular shell elements employed in the mesh. Note also the refinement around areas of high curvature and thin sections.

### 3.2 Loads and Constraints

Two sets of constraints and two sets of loads were defined and separately applied to the model:

#### 3.2.1 Constraints

A set of simple constraints were applied to the wing root rib shear pins (constraining lift and drag shear loads and torsional loads) and the spar root extension (constraining lift bending loads) which were representative of the way in which the wing is held in place in the Kwadira UAV fuselage. These simple constraints were used during the iterative optimisation process due to their computational efficiency.

A second set of more complex constraints was applied to the wing root rib and spar root extension. This included the use of non-penetrating contact bodies fixed in place to replicate a) the stainless steel pins that transfer shear and torsion loads to and from the fuselage to hardpoints in the wing root rib, and b) the stainless steel pins that transfer bending loads between the port and starboard wing root extensions. These constraints were used during the final optimisation iterations and for the whiffle tree predictions in order to represent the actual fuselage connections as realistically as possible.

### 3.2.2 Loads

The first set of loads applied to the model were the maximum positive and negative distributed lift, drag and pitching moment loads obtained from the load case analysis (see section 2.2). The lift and drag loads were applied to the wing skins using distributed pressure loads and the pitching moment loads applied to the wing ribs as a distributed torsion load. These loads were used in the iterative optimisation of the wing structure and represent the limit loads that the wing is expected to see during flight.

The second set of loads applied to the wing were simple vertical loads applied to the bottom wing skin (the wing is tested inverted due to test rig constraints) which were matched to the whiffle tree loads discussed in section 4.2. These loads were used to predict the deflection of the wing during physical testing using the whiffle tree setup.

### 3.4 Failure Criterion and Buckling

The Tsai-Wu failure criterion was selected as the primary failure theory for the analyses since it takes into account differing material strengths in tension and compression [12]. SolidWorks Simulation automatically evaluates the Tsai-Wu failure criterion and reports the inverse of this as a safety factor against failure. Components were also checked for inter-laminar shear failure by evaluating the reported value against the shear strength of Ampreg 21 resin. The combined compressive and shear buckling of each component was evaluated using empirical methods from Niu [13] and by making use of compressive and shear stress values reported by the FEA model.

### 3.3 Iterative Layout and Layup Optimisation

An iterative layout optimisation was performed by varying the number of internal chord-wise ribs in the wing with the objective of minimising mass while satisfying Tsai-Wu failure, inter-laminar shear stress and buckling constraints. The mass of the complete wing was determined after each iteration by using a spreadsheet-based mass model which took into account the mass of each structural component as well the amount of bonding agent required to assemble the wing. This resulted in a rib spacing of 100 mm, with 22 ribs.

An iterative layup optimisation was then performed on the wing skins, the span-wise shear webs and chord-wise ribs with the same objective of minimising mass while satisfying strength constraints. One set of components were optimised at a time in order to avoid the skewing of iteration results by complex component interactions. Buckling of the top wing skins at the wing root and the main shear webs at the spar root dictated the layups in these areas. This resulted in the final layups for the wing being specified so as to provide adequate strength and sufficient buckling resistance at the worst load cases, while also minimising mass.

## 4. CONSTRUCTION, TESTING AND RESULTS

### 4.1 Construction

The new wing design was built in the CSIR UAS Laboratory using the same wet-layup methods used in the construction of the original wing. The wing top and bottom skins and spar caps were layed up the existing Kwadira UAV wing moulds and cured under at 25°C for 48 hours. The internal webs and ribs were cut out of sheets of the required laminates layed up on a flat surface. A laser cutter was used to cut the glass fibre laminates and a CNC router to cut the carbon fibre laminates. The webs and ribs were then bonded and cleated to the top skin using a mixture of Ampreg 21 resin and cotton flocks. The same mixture was finally used to bond the bottom skin to the top skin, webs and ribs.

This proved to be more time consuming than originally anticipated due to the large number of parts involved. The need to replicate the component bonding modelled in the FEA model required a large number of thin cleating strips to be carefully laid up between components in order to effectively bond them together. The final measured weight of the wing was 5.814 kg which is a 14% decrease from the 6.778 kg of the original wing.

#### 4.2 Whiffle Tree Setup

The new wing was tested using the CSIR Wing Structural Test Rig (WSTR) by making use of a whiffle tree assembly connected to a hydraulic cylinder. A spreadsheet was developed to convert the distributed loads determined by the shear force diagram for the Point B load case (4.9 g, 40 m/s) into 8 point loads applied to evenly spaced span-wise locations on the wing. Point B was chosen since it would produce a large, measurable deflection and represented one of the worst load cases experienced by the wing. The spreadsheet also evaluated the required length ratios of the whiffle tree beams needed to produce the 8 point loads from a single load applied by the hydraulic jack.

The point loads were applied to the wing using 100 mm –wide, custom-made polystyrene saddles cut in the shape of the wing aerofoil and supported by Aluminium brackets. Aluminium beams also formed the whiffle tree structure. The total mass of the whiffle tree and the wing saddles was taken into account when calculating the total load to be applied. A load cell was connected in series with the whiffle tree and a hydraulic cylinder to measure the total load applied to the wing using a simple Arduino-based data acquisition system. The wing was attached to the WSTR using representative fuselage geometry that was designed to replicate the representative fuselage constraints modelled in FEA.

#### 4.3 Test Results

The deflection of the wing tip was chosen as the parameter to be measured during testing since it was predicted to have the largest deflection and hence the smallest measurement error. The wing was loaded up to the limit load of 4.9 g four times without any failures or buckling occurring. The deflection of the wing tip was recorded over a range of loads in 0.5 g increments and the deflection results of the four tests averaged. Figure 5 shows the measured deflection of the wing tip vs the FEA-predicted deflection. The average error in prediction is 3.9% and it can be seen that the FEA model predicts larger deflections at higher loads.

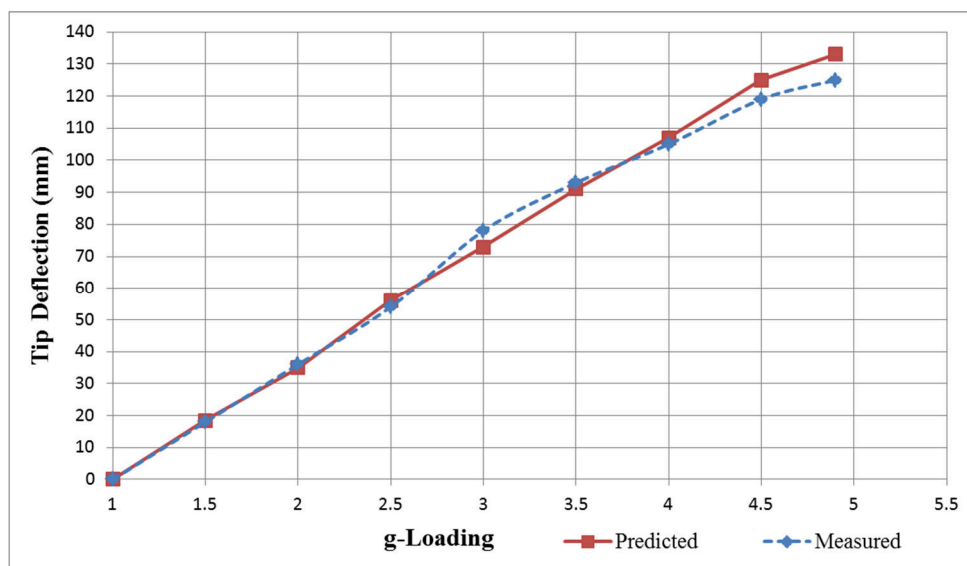


Figure 76 - Plot of predicted vs. measured wing tip deflection as a function of total g-load applied.

## 5. DISCUSSION AND CONCLUSIONS

The physical whiffle tree testing performed on the prototype wing validated the FEA model of the new wing design under whiffle tree loads, with an average error in prediction of 3.9%. Several factors are thought to be sources of error: The accuracy with which the wing saddles were located on the wing, the difference between the predicted and actual weight distribution of the whiffle tree beams, and variation in the amount of bonding agent used to join internal structural components to each other.

The validity of the FEA model with whiffle tree loads implies the validity of the FEA model with distributed loads; which was utilised to determine the final layups of the wing at its ultimate positive and negative loads. Section 4.1 details a final weight saving of 14% (0.964 kg) on the original wing design that utilised cored construction. This suggests that it is indeed possible to reduce the weight of a wing by eliminating core material from its design, while maintaining adequate strength and stiffness. Utilising this new wing design could decrease the structural weight of the Kwadira UAV by about 1.93 kg, enabling it to carry a larger payload or extend its operating range.

The construction process of laying up wing skins, cutting out webs and ribs from prepared sheets and bonding all the components together proved to be more time consuming than originally anticipated. This was due to the large number of parts involved and the necessity to construct a number of jigs and frames to accurately align the parts and keep them in place during bonding. This suggests that eliminating core material from the design does not decrease but rather increases the amount of labour involved in manufacturing a wing. This might be mitigated to an extent by, for example, utilising carefully designed jigs capable of aligning and bonding a number of ribs at once.

It is recommended that a similar study be applied to other Kwadira UAV components that currently utilise cored composite construction, for example the vertical fins, horizontal stabiliser and sections of the fuselage and tail booms, with a view to minimising the structural weight of the entire aircraft. It is also recommended that a trade-off study be conducted on the potential benefits of employing an all-carbon fibre design, in particular a decrease in structural weight and therefore increased range, be weighed against the drawbacks of mounting antennae externally, such as increased drag.

It is hoped that this research be taken into consideration by industry when designing structural layouts of future unmanned aircraft in this weight category by exploring viable alternatives to cored composite construction

## REFERENCES

- [1] Collins, V. E. (1985). *Leghorn Structural Design Report*. National Institute for Aeronautics and Systems Technology. Pretoria: CSIR.
- [2] Gagauz, P. (2013). *Composite Sandwich Panels Design and Structural-Technological Solutions*. Kharkov: National Aerospace University.
- [3] Unal, M. (2013). *Lockheed 1049 Super Constellation Aircraft Wing Structural Investigation*. Istanbul: Istanbul Technical University.
- [4] Perini, F. (2012). *Structural design, manufacturing and testing of a new wing for the CSIR's Modular UAS in composite materials*. MSc Thesis, University of Bologna, Bologna.

- [5] Bardella, L. (2000). *Mechanical Behaviour of Glass-Filled Epoxy Resins: Experiments, Homogenization Methods for Syntactic Foams, and Applications*. PhD Thesis, University of Brescia, Owensboro.
- [6] ASTM International. (2002). ASTM D3039. *Standard Test Method for Tensile Properties of Polymer Matrix Composite Materials*. West Conshohocken, United States of America.
- [7] ASTM International. (2001). ASTM D3518. *Standard Test Method for In-Plane Shear Response of Polymer Matrix Composite Materials by Tensile Test of a  $\pm 45^\circ$  Laminate*. West Conshohocken, United States of America.
- [8] United States. Department of Transport. (1965). *Part 23 - Airworthiness standards: Normal, utility, acrobatic and commuter category airplanes*. FAA.
- [9] Anderson, J. D. (2007). *Fundamentals of Aerodynamics* (5th ed.). New York: McGraw-Hill.
- [10] Ithurbure, R. P. (1999). *Design of the Wing of a Regional Airliner in Composite Material*. Memorandum, Delft University of Technology, Delft.
- [11] Megson, T. H. (2013). *Aircraft Structures for Engineering Students* (5th ed.). Oxford: Elsevier Press.
- [12] Tsai, S. W. (2008). *Theory of Composites Design* (3rd ed.). Stanford: Stanford University Press.
- [13] Niu, M. C. (1997). *Airframe Stress Analysis And Sizing*. Grenada Hills, California: Conmilit Press.